



**FACULTY
OF MATHEMATICS
AND PHYSICS**
Charles University

MASTER THESIS

Jan Střeleček

The geometry of quantum state driving

Supervisor of the master thesis: prof. RNDr. Pavel Cejnar, Dr., DSc.

Study programme: Physics

Study branch: Theoretical physics

Prague 2022

I declare that I carried out this master thesis independently, and only with the cited sources, literature and other professional sources. It has not been used to obtain another or the same degree.

I understand that my work relates to the rights and obligations under the Act No. 121/2000 Sb., the Copyright Act, as amended, in particular the fact that the Charles University has the right to conclude a license agreement on the use of this work as a school work pursuant to Section 60 subsection 1 of the Copyright Act.

In date
Author's signature

+Michal, Kuba, Martin.

Title: The geometry of quantum state driving

Author: Jan Střeleček

Institute: Institute of Particle & Nuclear Physics

Supervisor: prof. RNDr. Pavel Cejnar, Dr., DSc.

Abstract: Abstract.

Keywords: key words

Contents

Some notes to the notation	3
Introduction	4
1 Mathematical introduction	6
1.1 Fiber bundle	9
1.2 Riemannian geometry	10
1.3 Geometry in 2 dimensions	11
2 Theory behind quantum driving	12
2.1 Space of all states	12
2.2 Rays and bare states	13
2.3 Sectioning the space	13
2.4 Transporting states on state manifolds	14
2.4.1 3-dimensional parametric space	16
2.5 Fidelity	17
2.6 Metric and geometric tensor	18
2.7 General fidelity driving	21
2.7.1 APT	21
2.8 How to advantageously drive the system	22
2.8.1 Adiabatic driving	22
2.8.2 Counter-diabatic driving	23
3 Geometrization of quantum mechanics	29
3.1 From the projective Hilbert space to state manifolds	29
3.2 Restriction to eigenstate manifolds	30
4 Two level system	32
4.1 Harmonic oscillator correspondence	33
4.2 Energy variance for two level system	33
4.3 Geodesic driving	34
4.3.1 Derivation of the fidelity	35
4.3.2 Analysis of the infidelity formula	36
4.3.3 Energy variance	39
4.4 Linear driving	40
4.4.1 Dependence on time	41
4.4.2 Final fidelity	42
4.4.3 Summary	47
4.4.4 Energy variance	49
5 Lipkin-Meshkov Glick model	50
5.1 Special cases	50
5.1.1 Case $N = 3$	51
5.1.2 Case $N = 5$	57
5.1.3 Limit $N \rightarrow \infty$	61
5.2 General behavior	62

6 Driving on the ground state manifold	66
6.1 Minimizing the energy variance	67
6.2 Transport using quenches	67
Conclusion	72
Bibliography	74
List of Figures	76
A Eigenvalues for Lipkin-Meshkov Glick model	79
B Attachments	81
B.1 First Attachment	81

Some notes to the notation

Symbol	Meaning	Defining formula
\mathcal{A}	Gauge (calibrational) potential	$\mathcal{A}_\mu = i\hbar\partial_\mu$
\mathbb{N}	Natural numbers, without zero	
\mathcal{C}^k	k -times differentiable function	

Mathematical spaces will be denoted *mathcal* and operators with *hat*.

The colored text will be sometimes used during the derivations. The text can be understood without the colors, its goal is strictly pedagogical and helps reader to see some underlying connections.

Introduction

One of the unsolved problems of the quantum physics are quantum computers. There are many mathematical problems, which are solvable in exponential time on computers with classical bits, but are solvable in polynomial time on quantum computers. Essentially you prepare some initial state of qubits (these might be electron spins, or more recently, Josephson junctions are being used) and perform certain operations on them using *quantum gates*. In the end you measure the qubits, causing the collapse of wave-function, and read the result. The first main problems in this area, is holding the superposition of qubits until all operations are performed. The second great problem is the quantum noise, either spontaneous emission of excited states, or interaction with the thermal basis of the surrounding. The impact of these effects can be seen on symmetrical experiment, in which we start with some state, let's say spin up. Perform any number of operation on it and then perform their inverse, leading to the same state, spin up. In perfect quantum computer, we would get the initial state with 100 % accuracy. The problem is that due to noise we sometimes measure different state, in this case it would be spin down. The *percentage of getting the result we want* is called the *fidelity*.

This problem is of course more general. What is happening in the example above mathematically, is that we have interaction Hamiltonian between the qubits, thermal basis and quantum gates. The interaction with gates can be described by some Hamiltonian element with free parameter. Changing this parameter influences the qubit and *drives* it to some final state, which will be measured. The theory of quantum driving, as created by physicists in the second half of 20. century, uses mathematical formalism which sometimes lacks on precise definitions. It can be formalized in a language of differential geometry, which basics are reminded in Chapter 1. The theory of quantum driving itself is described in Chapter 2.

The important question in quantum computing is: "How to achieve the greatest *final fidelity*, meaning *how to prepare the state we want to prepare with the highest percentage?*" During the driving one might add some energy to the qubit, which leads to its excitation and possibly destroying the superposition. This can be avoided by many methods. There are a few methods how to avoid this excitation, described in Chapter 2.8. The surprising fact is that not every sequence of quantum gates leads to the same fidelity. For example if one starts with *spin up*, applying the X or Y gate has the same effect. Both result in *spin down*, because these gates just rotate the spin in a Bloch sphere around corresponding axis (x , resp. y).

For some special drivings, such as driving using small *quenches* (quick, but small change in driving parameter), one might get interested in *ground state manifold properties*.

To understand the general fidelity driving, a simple two level system was analyzed in Chapter 4. Some driving phenomena are noticed here, which are demonstrated on the two analytically solvable drivings. Because with the Hamiltonian complexity, the driving complicates noticeably, it is important to understand the geometry of ground state manifolds first. The ground state manifold consists of

all ground states of Hamiltonian with different driving parameter value. Until now not many implications of this structure is known. Some of them were theoreticized in previous works, some of them were developed here. In Chapter 6, there is a general introduction of driving on ground state manifold.

another motivation is in biochemistry...

1. Mathematical introduction

The modern approach to the closed system dynamics is using *differential geometry* formalism. Before we get to the quantum mechanics itself, let's introduce this formalism and recapitulate some definitions of this branch of mathematics. More detailed notes can be found for example in Loring [2017], or Fecko [2006].

Let's have a manifold \mathcal{M} and curves on it, parametrized by some real interval:

$$\gamma : \mathbb{R} \supset (P_i, P_o) \rightarrow \mathcal{M} \quad \xi \mapsto \gamma(\xi) \text{ for } \xi \in (P_i, P_o).$$

The space of functions is $\mathcal{FM} \equiv \{f : \mathcal{M} \rightarrow \mathbb{R}\}$.

To define *vectors* on \mathcal{M} , we need to make sense of the *direction*. It is defined using curves satisfying

$$\gamma_1(0) = \gamma_2(0) \equiv P$$

$$\frac{d}{dt}x^i(\gamma_1(t))\Big|_{t=0} = \frac{d}{dt}x^i(\gamma_2(t))\Big|_{t=0}.$$

Taking the equivalence class created by those two rules, sometimes noted as $[\gamma] = v$, we have element of the tangent space to \mathcal{M} . We will use standard notation for the *tangent space of \mathcal{M}* in some point P as $\mathbb{T}_P\mathcal{M}$. Cotangent space is denoted as $\mathbb{T}_P^*\mathcal{M}$. Unifying all *tangent*, resp. cotangent spaces over all x we get tangent and cotangent bundle, $\mathcal{T}\mathcal{M}$ and $\mathcal{T}^*\mathcal{M}$ respective. To generalize this notation to higher tensors, we denote $\mathbb{T}_P\mathcal{M} \in \mathcal{T}^1\mathcal{M}$, $\mathbb{T}_P^*\mathcal{M} \in \mathcal{T}_1\mathcal{M}$. This offers to increase the order to arbitrary numbers, leading to p -times *contravariant* and q -times *covariant* tensors. These are usually denoted $\mathcal{T}_q^p\mathcal{M}$. Tensor space in point $P \in \mathcal{M}$ is denoted $\mathcal{T}_q^p\mathcal{M}$. Using the congruence of curves on \mathcal{M} , the expression

$$\frac{d}{d\xi}f \circ \gamma(\xi)\Big|_{\xi=0} \tag{1.1}$$

has a good meaning, and we can define the *vector* in some $P \in \mathcal{M}$ as

$$v : \mathcal{FM} \rightarrow \mathbb{R} \quad f \mapsto v[f] \equiv \frac{d}{d\xi}f(\gamma(\xi))\Big|_P \equiv \partial_\xi\Big|_P f. \tag{1.2}$$

It holds, that $v \in \mathbb{T}_P\mathcal{M}$ and can be expressed as the *derivative in direction*,¹ which can be understood in coordinates as

$$v[f] = \frac{d}{dv}f \circ \gamma(\xi)\Big|_{\xi=0} = v^\mu \frac{d}{dx^\mu}f(x)\Big|_P. \tag{1.4}$$

The directional derivative will be denoted ∇_v and in basis $e_i \equiv \partial/\partial x^i$ we will denote

$$\nabla = (e_1, e_2, e_3).$$

¹The direction itself is usually denoted as

$$\frac{D}{d\alpha}\gamma(\xi), \tag{1.3}$$

where the "big D" notation is used to point out that it's not a classical derivative, but it maps curves to some entirely new space of directions.

During the whole thesis, the Greek indices will be *abstract* and Latin *pointer*. Abstract indices show the rank of the tensor, meaning *how many empty slots for contraction the tensor has*. Pointer indices extract specific number from the tensor. For example

$$t_{\nu\kappa}^\mu \in \mathcal{T}_2^1 \mathcal{M}, \quad \text{whilst for some } i, j, k \in \mathbb{N} : t_{jk}^i \in \mathbb{F}.$$

For *Tensor contraction*, the index notation will be used. When it is clear what type of tensors we are operating with, the object notation can be used, for example $t(\mathbf{u}, \mathbf{v}) \equiv t_{\mu\nu} \mathbf{u}^\mu \mathbf{v}^\nu$. The contraction can also be noted using contraction operator \mathbf{C} , when it is clear which indices are contracted, or when it does no matter which of them are.

Now we have the notation to define one strong structure on manifolds – *metric tensor*.

Definition 1 (Metric tensor). *If the form $g_{\mu\nu} \in \mathcal{T}_2^0 \mathcal{M}$ is*

- *linear:* $\forall \alpha, \beta \in \mathbb{F}; \mathbf{u}, \mathbf{v}, \mathbf{w} \in \mathcal{T}^1 \mathcal{M} : g(\mathbf{u}, \alpha \mathbf{v} + \beta \mathbf{w}) = \alpha g(\mathbf{u}, \mathbf{v}) + \beta g(\mathbf{u}, \mathbf{w})$
- *symmetric:* $\forall \mathbf{v}, \mathbf{w} \in \mathcal{T}^1 \mathcal{M} : g(\mathbf{v}, \mathbf{w}) = g(\mathbf{w}, \mathbf{v})$
- *non-degenerate:* $\forall \mathbf{v} \in \mathcal{T}^1 \mathcal{M}$ the function $\mathbf{w} \mapsto g(\mathbf{v}, \mathbf{w})$ is not identically zero.

we call $g_{\mu\nu}$ a metric tensor.

We will often require *differentiable metric tensor*, or at least almost everywhere differentiable². That will assure that *covariant derivatives* and *parallel transport* are well-defined almost everywhere.

Vectors of tangent space to some manifold can be compared only within one such space. To perform some tensor operations we need to transport them to some common tangent space. This can be done using the *parallel transport* which is connected to the notion of *covariant derivative*.

Definition 2 (Pseudoderivative). *\mathbf{P} is called a pseudoderivative of type p, q , if $\forall f \in \mathcal{FM}, \mathbf{A}, \mathbf{B} \in \mathcal{T}_q^p \mathcal{M}$:*

- $\mathbf{P} : \mathcal{T}_q^p \mathcal{M} \rightarrow \mathcal{T}_{q+n}^{p+m} \mathcal{M}$
- $\mathbf{P}f = 0$ (*ultralocality*)
- $\mathbf{P}(f\mathbf{A} + \mathbf{B}) = f\mathbf{PA} + \mathbf{PB}$ (*linearity*)
- $\mathbf{P}(\mathbf{AB}) = (\mathbf{PA})\mathbf{B} + \mathbf{A}(\mathbf{PB})$ (*Leibniz rule*)
- $\mathbf{MC}\mathbf{A} = \mathbf{CMA}$ (*commutation with contraction*)

Definition 3 (Covariant derivative). *$\nabla_{\mathbf{v}}$ is called covariant derivative in a direction $\mathbf{v} \in \mathbb{T}_P \mathcal{M}$, if $\forall f \in \mathcal{FM}, \mathbf{A}, \mathbf{B} \in \mathcal{T}_q^p \mathcal{M}, \alpha \in \mathbb{F}$:*

- $\nabla_{\mathbf{v}} : \mathcal{T}_q^p \mathcal{M} \rightarrow \mathcal{T}_{Pq}^p \mathcal{M}$

²Almost everywhere means *with an exception to the submanifold of zero measure*. Most often it means only a few point singularities.

- $\nabla_{f\mathbf{v}} \mathbf{A} = f \nabla_{\mathbf{v}} \mathbf{A}$ (*ultralocality in a direction*)
- $\nabla_{\mathbf{v}}(\mathbf{A} + \alpha \mathbf{B}) = \nabla_{\mathbf{v}} \mathbf{A} + \alpha \nabla_{\mathbf{v}} \mathbf{B}$ (*linearity in argument*)
- $\nabla_{\mathbf{v}}(\mathbf{AB}) = (\nabla_{\mathbf{v}} \mathbf{A})\mathbf{B} + \mathbf{A}(\nabla_{\mathbf{v}} \mathbf{B})$ (*Leibniz rule*)
- $\nabla_{\mathbf{v}}(\mathbf{CA}) = \mathbf{C}\nabla_{\mathbf{v}}(\mathbf{A})$ (*commutation with contraction*)
- $\nabla_{\mathbf{v}} f = \mathbf{v}[f] \equiv \mathbf{v}^\beta \mathbf{d}_\beta f$ (*operation on functions*)

Definition 4 (Coavariant differential). *For $\mathbf{v} \in \mathbb{T}_P \mathcal{M}$, $\mathbf{A} \in \mathcal{T}_q^p \mathcal{M}$, the covariant differential is defined as*

$$\nabla : \mathcal{T}_q^p \mathcal{M} \rightarrow \mathcal{T}_{P_{q+1}}^p \mathcal{M}, \text{ for which } \nabla_{\mathbf{v}} \mathbf{A}_{\beta\dots}^{\alpha\dots} = \mathbf{v}^\gamma \nabla_\gamma \mathbf{A}_{\beta\dots}^{\alpha\dots}$$

Definition 5 (Parallel transport). *Parallel transport of tensors in tensor field $\mathbf{A} \in \mathcal{T}_q^p \mathcal{M}$ along some path $\gamma \equiv (P_i, P_e) \subset \mathcal{M}$*

$$\begin{aligned} \text{par}_\gamma : \mathcal{T}_{P_i}^p \mathcal{M} &\rightarrow \mathcal{T}_{P_e}^p \mathcal{M} \\ A|_{P_i} &\mapsto \text{par}_\gamma A|_{P_e}. \end{aligned}$$

This means that the parallel transport takes a tensor at some $\mathcal{T}_{P_i}^p \mathcal{M}$ and transports it to $\mathcal{T}_{P_e}^p \mathcal{M}$. Those two tensors belong to the same tensor field, but are essentially different.

Definition 6 (Coordinate derivative). *Associate the derivative ∂ with coordinates x^μ on some $O \subset \mathcal{M}$ as*

$$\partial(\mathbf{d}x^j) = 0.$$

Then the coordinate derivative of any tensor can be expressed as

$$\partial_\rho \mathbf{A}_{\beta\dots}^{\alpha\dots} = \mathbf{A}_{b\dots,q}^{a\dots} \mathbf{d}_\alpha x^q \mathbf{d}_\alpha x^b \dots \frac{\partial^\beta}{\partial x^a}, \quad (1.5)$$

where on the expression on the left means *taking the covariant derivative of the tensor* and the expression on the right *multiplying the basis of the tensor space by derivative of the elements of tensor \mathbf{A}* .

Theorem 1 (Difference of covariant derivatives). *Difference of two covariant derivatives, i.e. two objects $\nabla, \tilde{\nabla}$ satisfying Def. 3,*

$$\nabla - \tilde{\nabla}$$

is a pseudoderivative from Def. 2.

Definition 7 (Connection and Christoffel symbols). *The difference of covariant and coordinate derivative*

$$\Gamma := \nabla - \partial$$

is called a Connection and its elements are Christoffel symbols.

On metric space, the Affine connection can be expressed as

$$\Gamma_{\mu\nu}^\alpha = \frac{1}{2}g^{\alpha\beta}(g_{\beta\mu,\nu} + g_{\nu\beta,\mu} - g_{\mu\nu,\beta}), \quad (1.6)$$

where we used comma notation for the coordinate derivative. The covariant derivative of $a \in \mathbb{T}_P\mathcal{M}$ can then be expressed as

$$\frac{D a^\mu}{d x^\nu} = a_{,\nu}^\mu - \Gamma_{\alpha\beta}^\mu x^\alpha a^\beta \quad (1.7)$$

and for $\alpha \in \mathbb{T}_P^*\mathcal{M}$ it is

$$\frac{D \alpha_\mu}{d x^\nu} = \alpha_{\mu,\nu} - \Gamma_{\mu\beta}^\alpha x^\beta \alpha_\alpha \quad (1.8)$$

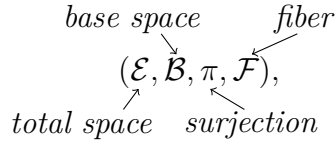
The vector $v \in \mathbb{T}_P\mathcal{M}$ is said to be parallel transported along curve $\gamma(\lambda)$, if its covariant derivative vanishes along $\gamma(\xi)$

$$\frac{D v^\mu}{d \xi} = 0. \quad (1.9)$$

1.1 Fiber bundle

At every point of manifold we introduced a tensor space. This creates rather complicated structure, which can be simplified using so-called *fiber bundles*. From classical mechanics one might recognize the space of all vectors, *vector bundle*, as a union of all vectors from the phase space $\cup_x \mathbb{T}_x\mathcal{M}$.

Definition 8 (Fiber bundle). *Structure*



for topological spaces \mathcal{E} , \mathcal{B} , \mathcal{F} and continuous surjection $\pi : \mathcal{E} \rightarrow \mathcal{B}$ satisfying a local triviality is called a Fiber bundle. The local triviality means that \mathcal{B} is connected³ and for every $x \in \mathcal{B}$, there is an open neighborhood $\mathcal{U} \subset \mathcal{B}$ (trivializing neighborhood) such that there exists a homeomorphism from \mathcal{U} to so-called product space

$$\phi : \pi^{-1}(\mathcal{U}) \rightarrow \mathcal{U} \times \mathcal{F},$$

such that $\pi^{-1} \circ \pi(\mathcal{U}) = \mathcal{U}$. The structure is as follows:

$$\begin{array}{ccc}
 \pi^{-1}(U) & \xrightarrow{\varphi} & U \times \mathcal{F} \\
 \pi \downarrow & & \swarrow \text{proj}_1 \\
 U & &
 \end{array}$$

Figure 1.1: stolen from wiki, redraw in tikz

Because projections of products are open maps, $\pi : \mathcal{E} \rightarrow \mathcal{B}$ must be open map. The manifolds at every point $x \in \mathcal{F}$ are all locally diffeomorphic to each other.

³Connected mean, it can't be represented as a union of two and more disjoint sets

1.2 Riemannian geometry

Let's briefly mention some definitions and theorems from Riemannian geometry, which will be used later on.

Definition 9 (Riemannian manifold). *Manifold is called Riemannian, iff it's equipped with positive definite metric tensor.*

Definition 10 (Connected manifold). *Manifold is connected, iff the distance between two points is infimum of the lengths of curves joining the two points.*

Definition 11 (Compact manifold). *Manifold is said to be compact if its every open cover has a finite subcover.*

Definition 12 (Geodesical completeness). *A manifold is said to be geodesically complete if its every geodesic can be extended to infinite values of their affine parameter.*

This condition holds if the space does not contain any singularities and its coordinate-independent notion.

Definition 13 (Geodesic maximality). *A manifold is said to be geodesically maximal if it's either geodesically complete, or every non-complete geodesic (such that cannot be extended to infinite values of their affine parameter) ends in a singularity.*

Geodesic maximality is coordinate dependent notion, only if the manifold is geodesically complete.

Theorem 2 (Von Neumann-Wigner). (*Von Neumann J, Wigner E. 1929. Physikalische Zeitschrift 30:467-470 can't find this anywhere*) This, sometimes called the Non-Crossing Theorem states, that the eigenvalues of Hermitian matrix driven by N continuous real parameters forms at maximum $(N - 2)$ -dimensional submanifold.

Theorem 3 (Hopf-Rinow Theorem). *For connected Riemannian manifold \mathcal{M} with the metric g , following are equivalent:*

- (\mathcal{M}, g) is geodesically complete, i.e. all geodesics are infinite
- (\mathcal{M}, g) is geodesically complete at some point P , i.e. geodesics going through P are infinite
- (\mathcal{M}, g) satisfies the Heine-Borel property, i.e. every closed bounded set is compact
- (\mathcal{M}, g) is complete as a metric space.

See Petersen [1998]/[p.125].

Theorem 4 (Modified Hopf-Rinow Theorem). *For connected Riemannian manifold \mathcal{M} with the metric g , any two points of \mathcal{M} can be joined with a minimizing geodesic. See Gorodski [2012]/[Chapter 3].*

This generally means, that in a space with singularity exists such points, which cannot be connected with the rest of the manifold using geodesics. In General relativity, this area is below event horizon.

Theorem 5. *A compact Riemannian manifold is geodesically complete. See Gorodski [2012]/[Chapter 3].*

1.3 Geometry in 2 dimensions

Most general object to start with is the *Riemann tensor*

$$R^\alpha_{\beta\gamma\delta} := \Gamma^\alpha_{\beta\delta,\gamma} - \Gamma^\alpha_{\beta\gamma,\delta} + \Gamma^\mu_{\beta\delta}\Gamma^\alpha_{\mu\gamma} - \Gamma^\mu_{\beta\gamma}\Gamma^\alpha_{\mu\delta}. \quad (1.10)$$

Ricci tensor can be defined as its contraction

$$R_{\alpha\gamma} := R^\mu_{\alpha\mu\gamma}, \quad (1.11)$$

which is second order symmetric tensor. *Ricci scalar* is defined as contraction of Ricci tensor

$$R := R^\mu_\mu. \quad (1.12)$$

This can be simplified for 2-dimensional manifold as

$$R = \frac{2}{g_{22}} \left(\Gamma^1_{22,1} - \Gamma^1_{12,2} + \Gamma^1_{11}\Gamma^1_{22} + \Gamma^1_{12}\Gamma^2_{22} - \Gamma^1_{21}\Gamma^1_{12} - \Gamma^1_{22}\Gamma^2_{12} \right). \quad (1.13)$$

Another possibility to express Ricci tensor, see Gutiérrez-Ruiz et al. [2021, eq. 6,7], is

$$R = \frac{1}{\sqrt{|g|}} (\mathcal{A} + \mathcal{B}) \quad (1.14)$$

for

$$\mathcal{A} := \left(\frac{g_{12}}{g_{11}\sqrt{|g|}} g_{11,2} - \frac{1}{\sqrt{|g|}} g_{22,1} \right)_{,1} \quad (1.15)$$

$$\mathcal{B} := \left(\frac{2}{\sqrt{|g|}} g_{12,1} - \frac{1}{\sqrt{|g|}} g_{11,2} - \frac{g_{12}}{g_{11}\sqrt{|g|}} g_{11,1} \right)_{,2}. \quad (1.16)$$

This equation turned out to give bigger numerical error, therefore Eq. 1.13 will be user later on.

2. Theory behind quantum driving

This chapter heavily depends on the mathematical formalism developed in Chapter 1 and basic knowledge of quantum mechanics is required.

Most parts of this chapter are inspired by Kolodrubetz et al. [2017] and original notes by Berry [1984], Berry [1989], Berry [2009] with attempt to give them more rigorous meaning in the language of differential geometry. We will see, that the structure of the space of states on which the driving will occur is quite complicated. The reason is its fiber structure, where every fiber is another fiber bundle. Luckily what we will be using later on are sections of this space, which will be much easier Riemannian manifolds.

From now on we will use natural units, so $\hbar = 1$.

2.1 Space of all states

Assume parameter $\lambda \in \mathcal{U} \subset \mathbb{R}^d$ for \mathcal{U} open set. This parameter controls some finite-dimensional Hamiltonian $\hat{H}(\lambda)$, which is bounded from below and has discrete spectrum. From this we can construct the fiber bundle, such that at every point of the base manifold $\lambda \in \mathcal{U}$, we construct fiber spanning all possible states of $\mathcal{H}(\lambda)$, thus the fiber structure can be according to Def. 8 written as

$$\left(\mathcal{H}_{full} := \bigcup_{\lambda \in \mathcal{U}} \mathcal{H}(\lambda), \quad \mathcal{U} \subset \mathbb{R}^d, \quad \pi, \quad \mathcal{H}(\lambda) := \bigcup_{states} |\psi(\lambda)\rangle \right).$$

The projection is defined as $\pi(\lambda) : |\psi(\lambda)\rangle \mapsto \lambda$ and $\mathcal{H}(\lambda)$ is Hilbert space for all pure states of $\mathcal{H}(\lambda)$. Note that some states in the \mathcal{H}_{full} space are physically identical. Geometric intuition is displayed in fig. 2.1.

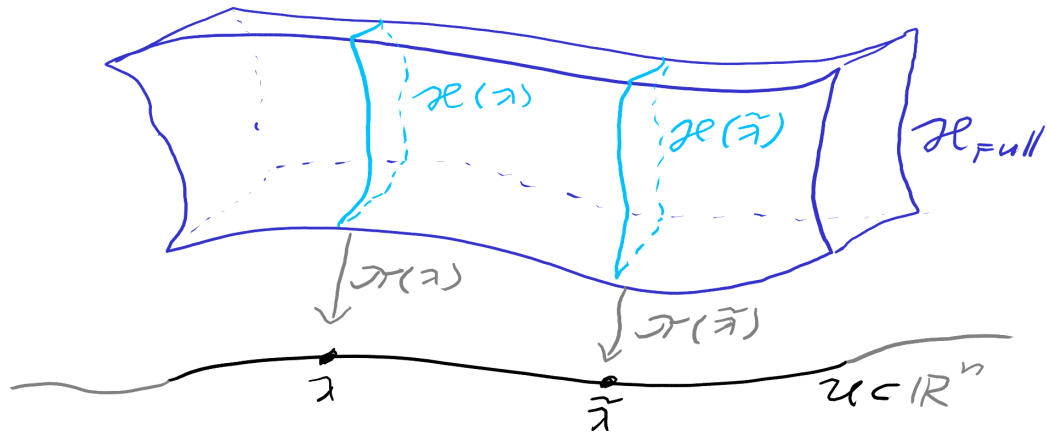


Figure 2.1: Base manifold $\mathcal{U} \subset \mathbb{R}^d$ is visualized as a line. From every point λ there is constructed one Hilbert space $\mathcal{H}(\lambda)$ as a fiber. The union of all these fibers is full Hilbert space \mathcal{H}_{full} .

2.2 Rays and bare states

In quantum mechanics, physical observables are related to the *space of rays*, defined as $\mathcal{PH} := \mathcal{H}/U(1)$, where elements of $U(1)$ are unitary transformations $e^{i\varphi}$ for $\varphi \in \mathbb{R}$. This defines the gauge symmetry between quantum states. The phase φ is chosen the same for every vector and can be chosen arbitrarily. We cannot alter the phase of individual vectors. The geometrical intuition is drawn for any λ on fig. 2.2.

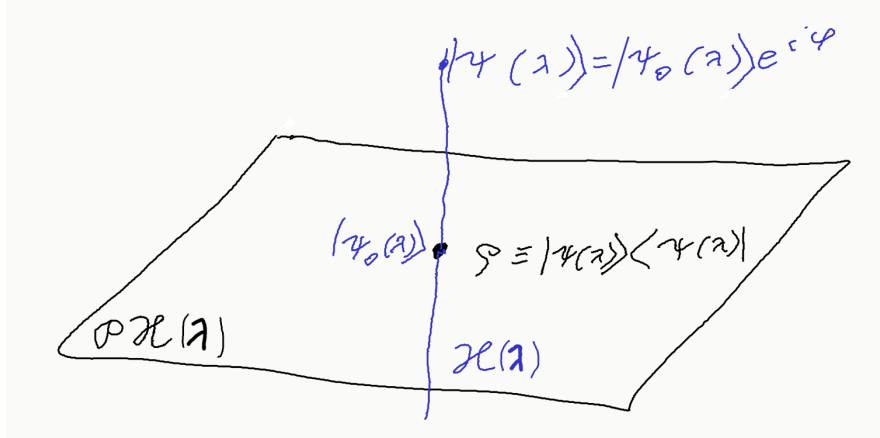


Figure 2.2: For every λ we have the Hilbert space $\mathcal{H}(\lambda)$ containing all states $e^{i\varphi} |\psi(\lambda)\rangle$. Choosing the phase φ fixes some projective Hilbert space \mathcal{PH} .

This resembles the fiber structure

$$(\mathcal{H}, \mathcal{PH}, \pi_{rays}, \{e^{i\varphi} | \varphi \in \mathbb{R}\}),$$

where π_{rays} is just rule setting phase φ to arbitrary value, which we will fix to $\varphi = 0$.

2.3 Sectioning the space

Assume one begins with the state $|\psi_0\rangle$. The state then evolves along some path $\gamma := \{\lambda(t) | t \in (0, T)\} \subset \mathcal{U}$ parametrized by time, for which the Schrödinger equation

$$i\hbar \frac{d}{dt} |\psi(\lambda(t))\rangle = \hat{H}(\lambda) |\psi(\lambda(t))\rangle \quad (2.1)$$

holds. For eigenstates of instantaneous Hamiltonian it reads as energy Schrödinger equation

$$\hat{H}(\lambda) |s(\lambda)\rangle = E_s(\lambda) |s(\lambda)\rangle. \quad (2.2)$$

Notice that these states are independent on the trajectory γ_t . For every $\hat{H}(\lambda)$ its energies can be sorted from the lowest, defining the set $\sigma(\hat{H}(\lambda)) := \{E_0, \dots, E_n\}$, which will be called *spectrum of the Hamiltonian*. In this set, degeneracies are not unified into one element, therefore every $\sigma(\lambda)$ has n elements. From this there exists an isomorphism between all σ -sets, and we can define *section*

$$\text{sec}_s : |s(\lambda)\rangle \mapsto \mathcal{U} \subset \mathbb{R}^d, \quad \text{for } s \in \{0, \dots, n-1\}.$$

This maps eigenstates corresponding to energy E_s to the base manifold. This mapping is similar to previously introduced π , except it chooses one point from the infinite dimensional Hilbert space and maps it to the base manifold. From this the \sec_s is an isomorphism.

Now we have constructed n sections of the full Hilbert space, which are isomorphic to the base manifold. Because \mathcal{U} is a Riemannian manifold, these so-called *projective energy manifolds* \mathcal{PM}_s , must be also Riemannian. Special importance of the *projective ground state manifold* \mathcal{PM}_0 , which will be used later on for adiabatic transports of ground states. Geometrical intuition is drawn on fig. 2.3.

The reason for calling these manifolds *projective* is the gauge symmetry of the Schrödinger equation. We can change the phase of vector $|\psi\rangle \mapsto e^{i\varphi} |\psi\rangle$ by any φ . Unifying over all phases, we get *energy manifolds*

$$\mathcal{M}_s := \left\{ \bigcup_{\varphi \in \mathbb{R}} \bigcup_{\lambda \in \mathcal{U}} e^{i\varphi} |\psi(\lambda)\rangle \right\} \quad (2.3)$$

Because these manifolds were created by sectioning, they are considered to be vector spaces in a geometrical sense. This was expected, because they contain quantum states, which themselves are vectors. **Elaborate here, construction of basis should be enough.**

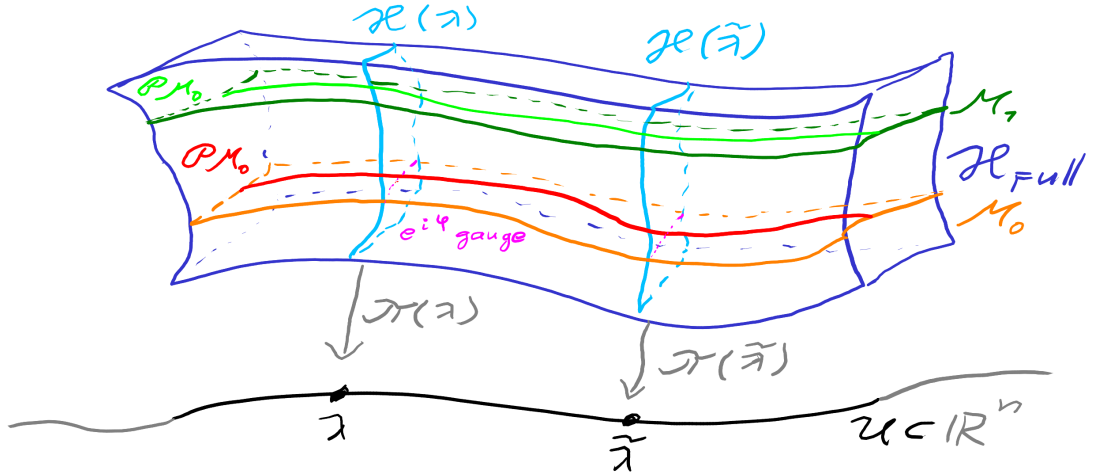


Figure 2.3: From the full Hilbert space we identified eigenstates. First was caused by the fiber structure and separates different Hilbert spaces $\hat{H}(\lambda)$. Newly introduced sectioning correspond to eigenstates of individual Hamiltonians and creates Riemannian manifolds \mathcal{M}_s .

2.4 Transporting states on state manifolds

Let's now focus on decomposition of \mathcal{H}_{full} to different state manifolds \mathcal{M}_s , as displayed on figure 2.4.

Changing the state from eigenstate $|s(\lambda)\rangle \in \mathcal{M}_s$ to $|\psi(\tilde{\lambda})\rangle \in \mathcal{M}_s$ during some time period is unitary transformation and can be thought of as *parallel transport on fiber bundle* between two states. Assuming the transport goes along curve parametrized by time $\gamma := \{\lambda(t) | t \in (0, T)\} \subset \mathcal{U}$. The transported state can be

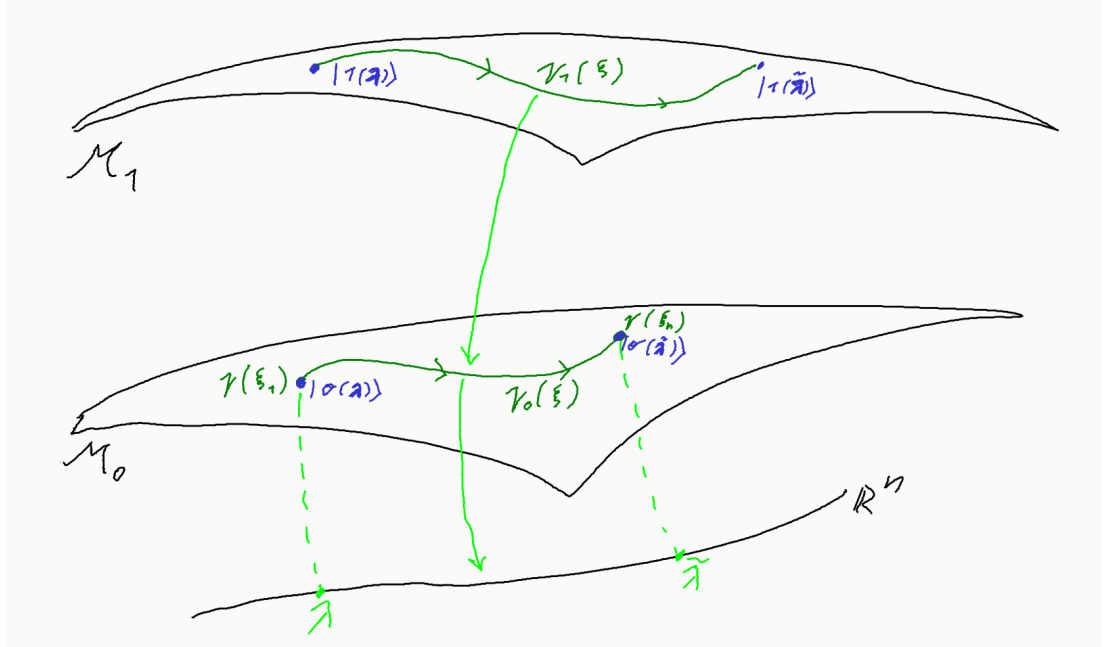


Figure 2.4: Geometrical intuition to transport on fiber manifold sections \mathcal{M}_s .

written at any time as

$$|\psi(t)\rangle = \text{par}_{\gamma_s(t)} |s(\boldsymbol{\lambda}(t))\rangle = \exp\left(-i \int_0^t E_s(\tau) d\tau\right) \exp(i\gamma_s(t)) |s(\boldsymbol{\lambda}(t))\rangle. \quad (2.4)$$

Let's describe the meaning of two exponentials in this transport.

Dynamical phase

The first exponential in Eq. 2.4, the *dynamical phase*, is well known solution to energy Schrödinger equation 2.2 and depends only on time and energy spectrum during the transport. This dynamical phase changes the states only within the projective state manifold \mathcal{PM}_s .

Geometrical phase

The complication arises with the fact that our playground is a state manifold \mathcal{M}_s and some element $e^{i\varphi} = e^{i\gamma_s(t)}$, called *geometrical phase* needs to be included.¹ This phase is generally non-integrable, meaning it depends on the whole path and cannot be written simply as $\gamma_s(\boldsymbol{\lambda})$. For some closed curve on

$$C = \{\boldsymbol{\lambda}(t) | t \in [0, T], \text{ such that } \boldsymbol{\lambda}(0) = \boldsymbol{\lambda}(T)\} \subset \mathcal{U} \quad (2.5)$$

we generally get $\text{par}_C |\psi(\boldsymbol{\lambda})\rangle \neq |\psi(\boldsymbol{\lambda})\rangle$. This property is sometimes more generally called an *anholonomy* and geometric intuition can be seen on fig. 2.5.

¹The usage of φ as a geometrical phase is no coincidence, because it corresponds its to previous usage in gauge symmetry of quantum states.

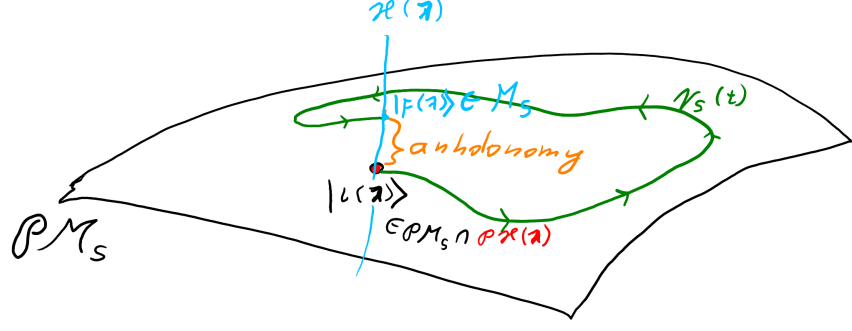


Figure 2.5: Parallel transport around some **closed curve** C . The **eigenstate** from \mathcal{PM}_s can be transported to another eigenstate in \mathcal{M}_s . The **anholonomy** represents their difference in a **gauge** direction.

Substituting general solution 2.4 to Eq. 2.1 yields²

$$\hat{H}(\boldsymbol{\lambda}(t)) |\psi(t)\rangle = i \frac{d}{dt} |\psi(t)\rangle \quad (2.6)$$

$$E_s(\boldsymbol{\lambda}(t)) |s(\boldsymbol{\lambda}(t))\rangle = E_s(\boldsymbol{\lambda}(t)) |s(\boldsymbol{\lambda}(t))\rangle - \frac{d\gamma(t)}{dt} |s(\boldsymbol{\lambda}(t))\rangle + \frac{d}{dt} |s(\boldsymbol{\lambda}(t))\rangle \quad (2.7)$$

$$\frac{d\gamma(t)}{dt} = i \langle s(\boldsymbol{\lambda}(t)) | \frac{d}{dt} |s(\boldsymbol{\lambda}(t))\rangle. \quad (2.8)$$

Separating the dependence of vectors on driving parameter and time, we get

$$\frac{d\gamma(\boldsymbol{\lambda}(t))}{dt} = i \langle s(\boldsymbol{\lambda}(t)) | \partial_j s(\boldsymbol{\lambda}) \rangle \frac{d\boldsymbol{\lambda}^j(\lambda)}{dt}. \quad (2.9)$$

Integrating this equation around some closed curve C and assuming the dynamical phase to be zero, we get

$$\gamma_s(C) = i \oint_C \langle s(\boldsymbol{\lambda}) | \partial_j s(\boldsymbol{\lambda}) \rangle d\boldsymbol{\lambda}^j. \quad (2.10)$$

We see, that the geometric phase does not depend on energy or time, only on the sequence of Hamiltonians, which means it depends only on the path itself.

2.4.1 3-dimensional parametric space

The problem of calculating Eq. 2.10 lies in the element $\partial_{\lambda} s(\boldsymbol{\lambda})$, which locally requires knowledge of single-valued basis $\{|0\rangle, \dots, |n\rangle\}$. This can be avoided in 3-dimensions using Stokes's theorem for S as the surface with boundary $\partial S = C$, for coordinate gradient ∇

$$\begin{aligned} \gamma_s(C) &= -\text{Im} \iint_C \mathbf{d}S \cdot \nabla \times \langle s(\boldsymbol{\lambda}) | \nabla n(\boldsymbol{\lambda}) \rangle \\ &= -\text{Im} \iint_C \mathbf{d}S \cdot \langle \nabla s(\boldsymbol{\lambda}) | \times | \nabla s(\boldsymbol{\lambda}) \rangle \\ &= -\text{Im} \iint_C \mathbf{d}S \cdot \sum_{m \neq s} \langle \nabla s(\boldsymbol{\lambda}) | m(\boldsymbol{\lambda}) \rangle \times \langle m(\boldsymbol{\lambda}) | \nabla s(\boldsymbol{\lambda}) \rangle \\ &= -\iint_C \mathbf{d}S \cdot \mathbf{V}_s(\boldsymbol{\lambda}) \end{aligned} \quad (2.11)$$

²Here the derivation along upper bound $F(x) := \int_0^{g(x)} f(t) dt \Rightarrow F'(x) = f(g(x))g'(x)$ for $f(t) \in L^1(0, g(x))$ and differentiable function g , is used.

for

$$\mathbf{V}_s(\boldsymbol{\lambda}) = \sum_{m \neq s} \text{Im} \frac{\langle s(\boldsymbol{\lambda}) \nabla_{\boldsymbol{\lambda}} \hat{H}(\boldsymbol{\lambda}) | m(\boldsymbol{\lambda}) \rangle \times \langle m(\boldsymbol{\lambda}) | \nabla_{\boldsymbol{\lambda}} \hat{H}(\boldsymbol{\lambda}) | s(\boldsymbol{\lambda}) \rangle}{(E_m(\boldsymbol{\lambda}) - E_s(\boldsymbol{\lambda}))^2}. \quad (2.12)$$

The element of summation $m = s$ in third step of derivation 2.11 is real, therefore has no influence on γ_s and can be omitted. The last equivalence holds, because if we differentiate the Schrödinger equation 2.2, we get for any $|s\rangle := |s(\boldsymbol{\lambda})\rangle \in \mathcal{M}_m$, $|m\rangle := |m(\boldsymbol{\lambda})\rangle \in \mathcal{M}_m$

$$\begin{aligned} \overbrace{\nabla(\hat{H}(\boldsymbol{\lambda})|s\rangle)}^{E_s(\boldsymbol{\lambda})|s\rangle} &= (\nabla \hat{H}(\boldsymbol{\lambda})) |\nabla s\rangle + \hat{H}(\boldsymbol{\lambda}) |\nabla s\rangle \\ \langle m | E_s(\boldsymbol{\lambda}) | s \rangle &= \langle m | \nabla \hat{H}(\boldsymbol{\lambda}) | s \rangle + \underbrace{\langle m | \hat{H}(\boldsymbol{\lambda})}_{\langle m | E_m(\boldsymbol{\lambda})} |\nabla s\rangle \\ \langle m | \nabla s \rangle &= \frac{\langle m | \nabla \hat{H}(\boldsymbol{\lambda}) | s \rangle}{E_s(\boldsymbol{\lambda}) - E_m(\boldsymbol{\lambda})}, \quad s \neq m, \end{aligned} \quad (2.13)$$

where we used $|\nabla s\rangle \equiv \nabla |s\rangle$.

Comparing the first expression in Eq. 2.11 with its last one and extending it to real numbers, we get

$$\mathbf{V}_s(\boldsymbol{\lambda}) = \nabla \times \langle s(\boldsymbol{\lambda}) | \nabla m(\boldsymbol{\lambda}) \rangle, \quad (2.14)$$

defining *vector potential* of $\mathbf{V}_s(\boldsymbol{\lambda})$. In addition, it extends our definition from single valued basis to any solution of 2.2, thus instead of ground state manifold, we can use any \mathcal{M}_s .

As was mentioned, the above procedure from Eq. 2.10 was performed only for three-dimensional space. Proper generalization to k-dimensional space would yield, see Berry [1984],

$$\gamma_s(C) = - \iint_C (\mathbf{d}S)^{\alpha\beta} \cdot \text{Im} \frac{\overbrace{\langle s(\boldsymbol{\lambda}) \mathbf{d}_\alpha \hat{H}(\boldsymbol{\lambda}) | m(\boldsymbol{\lambda}) \rangle}^{\in \mathcal{T}_1 \mathcal{M}} \wedge \overbrace{\langle m(\boldsymbol{\lambda}) | \mathbf{d}_\beta \hat{H}(\boldsymbol{\lambda}) | s(\boldsymbol{\lambda}) \rangle}^{\in \mathcal{T}_1 \mathcal{M}}}{(E_m(\boldsymbol{\lambda}) - E_s(\boldsymbol{\lambda}))^2}. \quad (2.15)$$

2.5 Fidelity

The *fidelity* measures "closeness" of two quantum states. It is generally defined for two density operators $\hat{\rho}, \hat{\sigma}$ as

$$\begin{aligned} \mathcal{F} : \text{End}(\mathcal{H}) \times \text{End}(\mathcal{H}) &\mapsto \mathbb{C}, \\ \mathcal{F}(\hat{\rho}, \hat{\sigma}) &:= \left(\text{Tr} \sqrt{\sqrt{\rho} \sigma \sqrt{\rho}} \right)^2. \end{aligned} \quad (2.16)$$

For pure states $\hat{\rho} =: |\rho\rangle\langle\rho|$, $\hat{\sigma} =: |\sigma\rangle\langle\sigma|$, this reduces to

$$\begin{aligned} F : \mathcal{H} \times \mathcal{H} &\mapsto \mathbb{C}, \\ F(|\rho\rangle, |\sigma\rangle) &\equiv \mathcal{F}(\hat{\rho}, \hat{\sigma}) |\langle \rho | \sigma \rangle|^2. \end{aligned} \quad (2.17)$$

We can see it's physical meaning on the state manifolds, imagining *quantum quench* (rapid change of some Hamiltonian parameters). In this case F is the probability that system will remain in the new ground state and $1 - F$ is the probability of exciting the system during this quench.

2.6 Metric and geometric tensor

As a playground for this chapter, we will choose the projective ground state manifold $\mathcal{PM}_0 \equiv \cup_{\lambda \in \mathbb{R}^d} \{|o(\lambda)\rangle\}$, but it can be easily generalized to any projective state manifold \mathcal{PM}_s . This means the geometrical phase will be neglected, because the states are the physical states from the projective Hilbert space.

Let's first look at \mathcal{PM}_0 , which is needed to be *gauge independent* in a sense, that the change in phase factor φ of some state $|o(\lambda)\rangle \in \mathcal{PM}_0 \cap \mathcal{H}(\lambda)$ induces the change

$$\begin{aligned} |o(\lambda)\rangle &\mapsto e^{i\varphi(\lambda)} |o(\lambda)\rangle \\ &\Downarrow \\ \langle o(\lambda) | \nabla o(\lambda) \rangle &\mapsto \langle o(\lambda) | \nabla o(\lambda) \rangle + i \nabla \varphi(\lambda) \end{aligned} \quad (2.18)$$

For $\varphi(\lambda) \in \mathcal{C}^2$, the gauge independent choice would be for infinitesimal change for example

$$f = \langle o(\lambda + \delta\lambda) | o(\lambda) \rangle, \quad (2.19)$$

sometimes referred to as the *fidelity amplitude of a ground state*. The meaning of fidelity as a probability transition between the states during some quench, leads to the definition of *distance on \mathcal{M}_0* ³

$$ds^2 \equiv 1 - F(|o(\lambda + \delta\lambda)\rangle, |o(\lambda)\rangle) = 1 - |\langle o(\lambda + \delta\lambda) | o(\lambda) \rangle|^2. \quad (2.20)$$

We can easily check, that the axioms for metric distance holds:

- identity of indiscernibles $s(|\psi\rangle, e^{i\alpha}|\psi\rangle) = 0 \Leftrightarrow |\psi\rangle = |\phi\rangle, \alpha \in \mathbb{R}$,
- symmetry for any two states $|\psi\rangle, |\phi\rangle$ is implied by $|\langle \psi | \varphi \rangle| = |\langle \varphi | \psi \rangle|$
- triangle inequality: $s(|\psi\rangle, |\psi_2\rangle) < s(|\psi\rangle, |\psi_1\rangle) + s(|\psi_1\rangle, |\psi_2\rangle)$ for any $|\psi_1\rangle$.

From this, $g^{\mu\nu}$ is a metric tensor.

Because $1 - f^2 > 0$, the first term of Taylor expansion is zero, thus we can use it for the metric tensor definition.

Definition 14 (Metric tensor on projective state manifolds). *Because the projective state manifolds \mathcal{PM}_s are isomorphic to base manifold \mathbb{R}^n , we can define*

$$\begin{aligned} g_{\mu\nu} : \mathbb{T}\mathcal{U} \times \mathbb{T}\mathcal{U} &\rightarrow \mathbb{R} \\ g_{jk} d\lambda^j d\lambda^k + \mathcal{O}(\lambda^3) &\equiv ds^2 := 1 - |\langle o(\lambda + \delta\lambda) | o(\lambda) \rangle|^2. \end{aligned} \quad (2.21)$$

Even though we call $g_{\mu\nu}$ the metric tensor *on projective state manifolds*, it takes forms from $\mathbb{T}\mathcal{U}$. Using abstract indices this means

$$g^{\mu\nu} d_\mu \lambda d_\nu \lambda. \quad (2.22)$$

This whole procedure can be made more rigorous using so-called *vector bundles*, see Loring [2017][Chap. 7]. In our case we can use the bijection $\mathbb{T}\mathcal{U} \times \mathbb{T}\mathcal{U} \rightarrow \mathbb{T}\mathcal{M} \times \mathbb{T}\mathcal{M}$ and simply write

$$g_{jk} d\lambda^j d\lambda^k = g_{jk} \frac{d\lambda^j}{d\mathbf{v}^l} \frac{d\lambda^k}{d\mathbf{v}^m} d\mathbf{v}^l d\mathbf{v}^m =: G_{lm} d\mathbf{v}^l d\mathbf{v}^m. \quad (2.23)$$

³Reminder for d notation: It is assumed to be an exterior differential. On functions, it acts as $d : \mathcal{F}\mathcal{M} \rightarrow \mathbb{T}\mathcal{M}$ and intuitively corresponds to total differential from functional analysis.

In calculations only $g_{\mu\nu}$ is used, thus what should have been called *the metric tensor on state manifolds* $G_{\mu\nu}$ leaves without proper name. "And some things that should not have been forgotten were lost." [Tolkien, 1977]

Complex tensor generalization

Because the metric tensor is an analytical real function of coordinates, we can make an analytical continuation and say that it is in fact a real part of a more general *Geometric tensor*, defined as

$$\chi_{\mu\nu} := \langle \partial_\mu o | \partial_\nu o \rangle_c \equiv \langle \partial_\mu o | \partial_\nu o \rangle - \langle \partial_\mu o | o \rangle \langle o | \partial_\nu o \rangle, \quad (2.24)$$

where shortened notation $\partial_\nu := \frac{\partial}{\partial \lambda^\nu}$ was used. The subscript c means *connected* and is defined by the formula.

The Geometric tensor can be decomposed to real and imaginary part as

$$\chi_{\mu\nu} \equiv g_{\mu\nu} - i \frac{1}{2} \nu_{\mu\nu}, \quad (2.25)$$

where the Real part is our well-known metric, sometimes called the *Fubini-Study tensor*⁴. It can also be expressed as

$$g_{\mu\nu} = \frac{\chi_{\mu\nu} + \chi_{\nu\mu}}{2} = \text{Re} \langle \partial_\mu o | \partial_\nu o \rangle_c = \text{Re} \sum_{o \neq j} \frac{\langle o | \frac{\partial \mathcal{H}}{\partial \lambda^\mu} | j \rangle \langle j | \frac{\partial \mathcal{H}}{\partial \lambda^\nu} | o \rangle}{(E_o - E_j)^2}. \quad (2.26)$$

The second newly introduced tensor $\nu_{\mu\nu}$ is called the *curvature tensor*, or *Berry curvature*. It can be expressed as

$$\nu_{\mu\nu} = i(\chi_{\mu\nu} - \chi_{\nu\mu}) = \text{Im} \langle o | [\overset{\leftrightarrow}{\partial}_\nu, \partial_\mu] | o \rangle_c = -2\text{Im} \sum_{o \neq j} \frac{\langle o | \frac{\partial \mathcal{H}}{\partial \lambda^\mu} | j \rangle \langle j | \frac{\partial \mathcal{H}}{\partial \lambda^\nu} | o \rangle}{(E_o - E_j)^2}, \quad (2.27)$$

where $\overset{\leftrightarrow}{\partial}_\nu$ affects the covector on the left.

Proof of the metric tensor definitions correspondence.

To prove the correspondence of geometric tensor, described by Eq. 2.24, to distance on \mathcal{M}_0 in Eq. 2.20, we start with eigenstate $|o(\boldsymbol{\lambda})\rangle \in \mathcal{M}_0 \cap \mathcal{H}(\boldsymbol{\lambda})$. Changing parameters $\boldsymbol{\lambda}$ to $\boldsymbol{\lambda} + \delta\boldsymbol{\lambda}$ results in Hamiltonian \hat{H}_f with eigenstates $|s(\boldsymbol{\lambda} + \delta\boldsymbol{\lambda})\rangle \in \mathcal{M}_s \cap \mathcal{H}(\boldsymbol{\lambda} + \delta\boldsymbol{\lambda})$, meaning it can be excited. Probability amplitude of going to such state is

$$\begin{aligned} a_s &= \langle s(\boldsymbol{\lambda} + \delta\boldsymbol{\lambda}) | o(\boldsymbol{\lambda}) \rangle \approx \delta\lambda^\mu \langle \partial_\mu s(\boldsymbol{\lambda}) | o(\boldsymbol{\lambda}) \rangle \\ &= -\delta\lambda^\mu \langle s(\boldsymbol{\lambda}) | \partial_\mu | o(\boldsymbol{\lambda}) \rangle. \end{aligned} \quad (2.28)$$

If we introduce the *gauge potential*, aka *calibration potential*, as⁵

$$\hat{\mathcal{A}}_\mu := i\partial_\mu, \quad (2.29)$$

the probability amplitude can be expressed as

$$a = i \langle s(\boldsymbol{\lambda}) | \hat{\mathcal{A}}_\mu | o(\boldsymbol{\lambda}) \rangle \delta\lambda^\mu, \quad (2.30)$$

⁴In some literature, this is called the Geometric tensor

⁵In SI units, the gauge potential is $\hat{\mathcal{A}}_\mu := i\hbar\partial_\mu$

which has meaning of matrix elements of the gauge potential. Probability of the excitation i.e. transition to any state $s > 0$ from ground state is then (omitting the λ dependence in notation)

$$\begin{aligned} \sum_{s \neq 0} |a_s|^2 &= \sum_{s \neq 0} \delta\lambda^\mu \delta\lambda^\nu \langle o | \hat{\mathcal{A}}_\mu | s \rangle \langle s | \hat{\mathcal{A}}_\nu | o \rangle + \mathcal{O}(|\delta\lambda^3|) \\ &= \delta\lambda^\mu \delta\lambda^\nu \langle o | \hat{\mathcal{A}}_\mu \hat{\mathcal{A}}_\nu | o \rangle_c =: \delta\lambda^\mu \delta\lambda^\nu \chi_{\mu\nu} + \mathcal{O}(|\delta\lambda^3|), \end{aligned} \quad (2.31)$$

where last term defines the geometric tensor. \square

Definition 15 (Berry connection). *On the ground state manifold \mathcal{M}_0 , the Berry connection is defined as the mean value of calibration potential*

$$A_j(\lambda) := \langle o(\lambda) | \hat{\mathcal{A}}_j | o(\lambda) \rangle = -i \langle o(\lambda) | \partial_j | o(\lambda) \rangle = -i \frac{d\lambda^j}{dx^i} \langle o(\lambda) | \frac{\partial}{\partial \lambda^j} | o(\lambda) \rangle, \quad (2.32)$$

which uses the decomposition of λ to some orthogonal basis $\{x_i\}_{i=1}^n$ of the base manifold \mathbb{R}^n .

This empowers us to take derivatives in any direction and the expression for geometric tensor

$$\chi_{\mu\nu}(\lambda) = \partial_\mu A_\nu(\lambda) - \partial_\nu A_\mu(\lambda) \quad (2.33)$$

has a good meaning. This formula can be directly proven by comparing with 2.24.

Definition 16 (Berry phase). *The Berry phase, as an integral of the Berry connection along some closed curve \mathcal{C} ⁶*

$$\varphi_B \equiv - \oint_{\mathcal{C}} A_\mu(\lambda) d\lambda^\mu = \int_{\mathcal{S}} \chi_{\mu\nu}(\lambda) d\lambda^\mu \wedge d\lambda^\nu, \quad (2.36)$$

where we used the Stokes theorem for some area \mathcal{S} with boundary $\partial\mathcal{S} = \mathcal{C}$.

Berry phase is zero, when the curve does not go around some geometric tensor singularity. This can be formally written using the *winding number*, which counts *how many times the curve goes counterclockwise around some point of interest*. In our case the points of interest are singularities a , and we say:

$$\varphi_B = 0 \Leftarrow \text{Ind}_a \gamma(\lambda) = 0.$$

Those singularities appear in the system due to energy spectrum degeneracies, in the case of ground state manifold, when $E_1 - E_0 = 0$. Those points are called *diabolic*, because of their shape in the (λ, χ) parameter space.⁷

⁶The reasonability of this definition can be seen, if we assume the ground state of a free particle $\langle \mathbf{x} | i(\lambda) \rangle \equiv i(\mathbf{x}, \lambda) = |i(\mathbf{x})| e^{i\varphi(\lambda)}$, then the Berry connection is

$$A_\mu = - \int d\mathbf{x} |i(\mathbf{x}, \lambda)|^2 \partial_\mu \varphi(\lambda) = - \partial_\mu \varphi(\lambda) \quad (2.34)$$

and Berry phase

$$\varphi_B = \oint_{\mathcal{C}} \partial_\mu \varphi d\lambda^\mu, \quad (2.35)$$

which represents total phase accumulated by the wave function. It is really the analogy for Berry phase in classical mechanics, which for example in the case Foucault pendulum on one trip around the Sun makes $\varphi_B = 2\pi$

⁷<https://en.wikipedia.org/wiki/Diabolo>

2.7 General fidelity driving

Until now, our interest was mostly in projective state manifolds \mathcal{PM}_s . If every state during the driving belongs to \mathcal{PM}_s , the fidelity $F = 1$ all the time, and we are talking about *unit fidelity driving*. But how to calculate the case when the fidelity is "almost one"?

2.7.1 APT

Following the article from Rigolin [2008], we approximate the wave-function by series. Because every element will then be decomposed into another series, we will bear in mind is the *locality of variables*. Let's call variable $V(s)$ *local* if it depends only on infinitesimal surrounding of s . These variables will be in shades of blue and *non-local* variables in shades of red.

We will be interested in some driving along path $\{\gamma(t)|t \in [0, T]\}$ with an initial condition

$$|\psi(0)\rangle = |\psi_0\rangle \in \mathcal{PM}_0. \quad (2.37)$$

One might directly solve the Schrödinger equation here, but we would like to find more simple solution, which holds for $F \approx 1$.

The power series will be derived using a small parameter $v := 1/T$

$$|\Psi(s)\rangle = \sum_{p=0}^{\infty} v^p |\Psi^{(p)}(s)\rangle, \quad (2.38)$$

for

$$|\Psi^{(p)}(s)\rangle = \sum_{n=0} e^{-\frac{i}{v}\omega_n(s)} e^{i\gamma_n(s)} b_n^{(p)}(s) |n(s)\rangle. \quad (2.39)$$

Here we have

$$\text{dynamical phase } \omega_n(s) := \frac{1}{\hbar} \int_0^s E_n(s') ds', \quad (2.40)$$

$$\text{Berry phase } \gamma_n(s) := i \int_0^s \langle n(s') | \frac{d}{ds'} n(s') \rangle ds' \equiv i \int_0^s M_{nn}(s') ds' \quad (2.41)$$

and $|n(s)\rangle$ are solution to

$$\hat{H}(s) |n(s)\rangle = E_n(s) |n(s)\rangle. \quad (2.42)$$

Variables $\omega_n(s)$ and $\gamma_n(s)$ are defined using integration over the whole protocol, therefore there are *non-local variables*. The problem now lies in determining $b_n^{(p)}(s)$, which is also *non-local*. Because it depends on its relative *geometric* and *dynamical phase* to other *energy levels*, let's write it as a series

$$b_n^{(p)}(s) = \sum_{m=0} e^{\frac{i}{v}\omega_{nm}(s)} e^{-i\gamma_{nm}(s)} b_{nm}^{(p)}(s), \quad (2.43)$$

where $\omega_{nm} := \omega_m - \omega_n$, $\gamma_{nm} := \gamma_m - \gamma_n$. The reason for *locality* of $b_{nm}^{(p)}(s)$ will be clear soon.

Inserting all to original series 2.38, we get

$$|\Psi(s)\rangle = \sum_{n,m=0} \sum_{p=0}^{\infty} v^p e^{-\frac{i}{v}\omega_m(s)} e^{i\gamma_m(s)} b_{nm}^{(p)}(s) |n(s)\rangle. \quad (2.44)$$

Because the initial state is eigenstate, we get initial conditions $b_{nm}^{(0)}(s) = 0$. In addition, one can rewrite equation 2.44 to the iteratively solvable form

$$\frac{i}{\hbar} \Delta_{nm}(s) b_{nm}^{(p+1)}(s) + \dot{b}_{nm}^{(p)}(s) + W_{nm}(s) b_{nm}^{(p)}(s) + \sum_{k=0, k \neq n} M_{nk}(s) b_{km}^{(p)}(s) = 0, \quad (2.45)$$

for $\Delta_{nm}(s) := E_m - E_n$, $W_{nm}(s) := M_{nn}(s) - M_{mm}(s)$, where M_{mn} is defined in Eq. 2.41. We can see that $b_{mn}^{(p)}$, as a solution to Eq. 2.45, only depends on difference between energy levels, eigenstates during the path and their directional derivatives. Not on the path itself. All of those are easily obtained, once the driving path is prescribed.

2.8 How to advantageously drive the system

In many experimental settings, one needs to achieve as high fidelity as possible. If $F = 1$ we speak about *unit fidelity protocols*. If the driving is slow enough that $F = 1$, we say the driving is *adiabatic*. The fidelity can be practically improved by many methods, three of them in which we will be interested are⁸:

- close adiabatic driving - changing the driving parameters slowly, so the system has plenty of time to collapse into the ground state,
- path variation - varying the driving trajectory, avoiding the topological defects on manifolds,
- counter-diabatic driving - countering the excitation by adding some element to the Hamiltonian, making the fidelity precisely 1.

2.8.1 Adiabatic driving

Adiabatic transformation is such transformation from \mathcal{PM}_0 to \mathcal{PM}_0 , which does not excite the system, meaning the fidelity $F = 1$. Generally it can be achieved by two methods – *infinitely slow transformation of states*, or adding some *counter-diabatic element* to the Hamiltonian.

In this chapter, we will be dealing with the system described by the finite-dimensional Hamiltonian $\hat{H}(\lambda)$ which drives the system according to Schrödinger equation from some initial state $|s(\lambda)\rangle$ to $|s(\tilde{\lambda})\rangle$ along the path $\gamma(\lambda)$. Before going throw the details of adiabatic transformations, let's define its meaning properly.

Definition 17 (Adibaticity). *Slow change of the driving parameters of the Hamiltonian $H(\lambda)$ in a sense, that it does not excite the system and allows the system to return to the same energetic state after circulation around any closed path on the ground state manifold with fidelity $F = 1$.*

⁸There is a nice analogy with driving a toy car (a quantum state) in a curved terrain (a Hilbert space). To avoid the car jumping on the hills (the state excitation), you can either drive slowly (close adiabatic driving), or you can go around the hills (vary the path), or you can have a friend (a counter-diabatic element), who will push the car against the ground every time it is supposed to jump.

Slow transports

As was mentioned in the introduction of this chapter, one way to change the system parameters without exciting it is to change the driving parameter slowly enough. The meaning of the word "slow" clears up next theorem.

Theorem 6 (Adiabatic theorem). *For slowly varying Hamiltonian \hat{H} in the time range $(0, T_f)$, the solution of the Schrödinger equation*

$$\hat{H}(\lambda) |\psi_n(\lambda)\rangle = E_n(\lambda) |\psi_n(\lambda)\rangle$$

with initial condition in x -representation $\langle x|\psi(t=0)\rangle = \psi(x, 0)$ can be approximated as

$$||\psi(\lambda) - \psi_{ad}(\lambda)|| \approx o\left(\frac{1}{T_f}\right) \quad (2.46)$$

for adiabatic state

$$|\psi_{ad}\rangle = e^{\omega_n(\lambda)} e^{\gamma_n(\lambda)} |\psi(\lambda)\rangle, \quad (2.47)$$

where we define dynamical phase induced by energy transitions,

$$\omega_n(\lambda) \equiv - \int_0^t E_n(\tau) d\tau$$

and geometrical phase, also called Berry phase

$$\gamma_n(\lambda) \equiv \int_0^t i \langle \psi_n(\tau) | \partial_t \psi_n(\tau) \rangle d\tau.$$

Proof. TBD (is on wikipedia :), it will give a sense to the theorem)

□

2.8.2 Counter-diabatic driving

Assume differentiable and non-singular Hamiltonian $\hat{H}(\boldsymbol{\lambda})$ with non-degenerate basis $\{|m, \boldsymbol{\lambda}\rangle\}_m$ called the *adiabatic basis*. This is generally the family of adiabatically connected eigenstates⁹ The transition amplitude between states for adiabatic change is

$$0 = \langle m(\boldsymbol{\lambda}) | \hat{H} | n(\tilde{\boldsymbol{\lambda}}) \rangle \quad \text{for } n \neq m, \forall \boldsymbol{\lambda}, \forall \tilde{\boldsymbol{\lambda}}. \quad (2.48)$$

This can be driven along some curve $\gamma(\lambda)$, i.e. differentiated by ∂_t :

$$\begin{aligned} 0 &= \langle \partial_t m(\boldsymbol{\lambda}) | \hat{H}(\tilde{\boldsymbol{\lambda}}) | n(\tilde{\boldsymbol{\lambda}}) \rangle + \langle m(\boldsymbol{\lambda}) | \underbrace{\partial_t \hat{H}(\tilde{\boldsymbol{\lambda}})}_{\approx \partial_t \hat{H}(\lambda)} | n(\tilde{\boldsymbol{\lambda}}) \rangle + \langle m(\boldsymbol{\lambda}) | \hat{H}(\tilde{\boldsymbol{\lambda}}) | \partial_t n(\tilde{\boldsymbol{\lambda}}) \rangle \\ &= E_n(\lambda) \langle \partial_t m(\boldsymbol{\lambda}) | n(\tilde{\boldsymbol{\lambda}}) \rangle + E_m(\lambda) \langle m(\boldsymbol{\lambda}) | \partial_t n(\tilde{\boldsymbol{\lambda}}) \rangle + \langle m(\boldsymbol{\lambda}) | \partial_t \hat{H}(\tilde{\boldsymbol{\lambda}}) | n(\tilde{\boldsymbol{\lambda}}) \rangle \\ &= (E_m(\lambda) - E_n(\lambda)) \underbrace{\langle m | \partial_t (\tilde{\boldsymbol{\lambda}}) \rangle}_{-\frac{i}{\hbar} \langle m | \hat{\mathcal{A}}_t | n(\tilde{\boldsymbol{\lambda}}) \rangle} + \langle m | \partial_t \hat{H} | n(\tilde{\boldsymbol{\lambda}}) \rangle, \end{aligned} \quad (2.49)$$

⁹In the case of energy level crossing, the eigenstates are not unified, because transition between them is not adiabatic.

which can be rewritten in matrix form as

$$i\hbar\partial_t\hat{H} = [\hat{\mathcal{A}}_t, \hat{H}] - i\hbar\hat{M}_t \quad \text{for } \hat{M}_t \equiv -\sum_n \frac{\partial E_n(\lambda)}{\partial t} |n(\lambda)\rangle \langle n(\lambda)|. \quad (2.50)$$

\hat{M} is diagonal in energetic basis and its elements has meaning of *generalized force*. We can easily see that $[\hat{H}, \hat{M}] = 0$, implying

$$[\hat{H}, i\hbar\partial_t\hat{H} - [\hat{\mathcal{A}}_t, \hat{H}]] = 0. \quad (2.51)$$

This can be used as the definition for *counter-diabatic potential* $\hat{\mathcal{A}}_t$, because it was obtained from only one assumption – adiabaticity. The strength of this equation lies in fact, that it finds counter-diabatic potential without the need of Hamiltonian diagonalization. For more, see Kolodrubetz et al. [2017][chap. 2.3].

Gauge potentials

In section 2.6 we introduced the gauge potential without proving its gauge meaning, but only stating its correspondence to transition probability, see Eq. 2.30. *Gauge transformations*, in classical mechanics called *canonical*, can be defined such, that they *preserve Lagrangian of the system under local transformations from some Lie group*. This implies, that gauge transformed Hamiltonian $\hat{H}(\boldsymbol{\lambda})$ and $\hat{H}(\boldsymbol{\lambda} + d\boldsymbol{\lambda})$ commutes with its canonically transformed version¹⁰

$$[\hat{H}(\boldsymbol{\lambda}), \hat{H}(\boldsymbol{\lambda} + \delta\boldsymbol{\lambda})] = 0. \quad (2.52)$$

To understand the meaning of gauge symmetries, let's first consider classical system and then move to quantum mechanics.

Classical gauge potential

In the Hamiltonian classical mechanics, we assume the manifold \mathcal{M} as subset of the phase space defined by Hamiltonian $H = H(p_i, q_i)$, where momentum p_i and position q_i are assumed to form the orthogonal basis of the phase space

$$\{q^i, p_j\} = \delta_j^i, \quad (2.53)$$

which also defines *calibrational freedom* in their choice. *Canonical transformations* then by definition preserve this formula. Using the *Poisson bracket*, defined as

$$\{A, B\} := \frac{\partial A}{\partial q^j} \frac{\partial B}{\partial p_j} - \frac{\partial B}{\partial q^j} \frac{\partial A}{\partial p_j}, \quad (2.54)$$

we will examine continuous canonical transformations generated by gauge potential \mathcal{A}_λ

$$q^j(\lambda + \delta\lambda) = q^j(\lambda) - \frac{\partial \mathcal{A}_\lambda(\mathbf{p}, \mathbf{q})}{\partial p_j} \delta\lambda \Rightarrow \frac{\partial q^j}{\partial \lambda} = -\frac{\partial \mathcal{A}_\lambda}{\partial p_j} = \{\mathcal{A}_\lambda, q^j\} \quad (2.55)$$

$$p_j(\lambda + \delta\lambda) = p_j(\lambda) - \frac{\partial \mathcal{A}_\lambda(\mathbf{p}, \mathbf{q})}{\partial q^j} \delta\lambda \Rightarrow \frac{\partial p_j}{\partial \lambda} = -\frac{\partial \mathcal{A}_\lambda}{\partial q^j} = \{\mathcal{A}_\lambda, p_j\}. \quad (2.56)$$

¹⁰This can be easily reformulated to the world of classical physics, where the commutator is replaced by Poisson bracket.

Substituting this to relations of orthogonality 2.53, we get

$$\{q^j(\lambda + \delta\lambda), p_j(\lambda + \delta\lambda)\} = \delta_j^i + \mathcal{O}(\delta\lambda^2). \quad (2.57)$$

If λ is time parameter and $\mathcal{A}_t = -H$, equations 2.55, 2.56 are identical to the Hamilton equations

$$\begin{aligned}\dot{q}^j &= -\{H, q^j\} = \frac{\partial H}{\partial p_j} \\ \dot{p}_j &= -\{H, p_j\} = -\frac{\partial H}{\partial q^j}.\end{aligned}\quad (2.58)$$

Because the Hamiltonian is generator of the movement in the phase space (\mathbf{q}, \mathbf{p}) , we can interpret \mathcal{A}_t as the generators of the movement on \mathcal{M} . Other specific choice might be $\lambda = X^i$, which gives us the momentum components $\mathcal{A}_{X^i} = p_i$.

Generally every gauge symmetry is generated by its gauge potential and corresponds to some conserved property, as theorem of Emma Nöether states.

Quantum gauge potential

[Kolodrubetz et al., 2017][chap. 2.2] The role of Poisson brackets in quantum mechanics is taken by commutators, canonical transformations are called *unitary transformations* and calibration freedom is hidden in the choice of basis. Now let's find some special basis transformations \hat{U} between initial system S and the transformed \tilde{S} . Both of them describe the system with Hamiltonian $\hat{H}(\boldsymbol{\lambda})$ with eigenstates $|n(\boldsymbol{\lambda})\rangle$ and eigenstate manifolds $\mathcal{M}_n \equiv \cup_{\boldsymbol{\lambda}} \{|n(\boldsymbol{\lambda})\rangle\}$.

From fiber structure goes¹¹, that any state of $\hat{H}(\boldsymbol{\lambda})$ for $\forall \boldsymbol{\lambda} \in U \subset \mathbb{R}^d$ can be decomposed as

$$|\psi(\boldsymbol{\lambda})\rangle \equiv \sum_n \psi_n(\boldsymbol{\lambda}) |n\rangle \quad (2.59)$$

for some coordinate independent basis $\{|n\rangle\}_n$. Then there exist unitary transformation

$$\hat{U}(\boldsymbol{\lambda}) : \tilde{S} \rightarrow S, \quad \hat{U}(\boldsymbol{\lambda}) |m(\boldsymbol{\lambda})\rangle = |n\rangle. \quad (2.60)$$

where scalar parameter t is assumed to be changing along the path $\gamma(t)$, corresponding to situation on fig. 2.4. This satisfies

$$i\hbar \partial_t \hat{U}(t) = \hat{H}(t) \hat{U}(t) \quad (2.61)$$

for \hat{H} the full Hamiltonian of the system and any point on $\tilde{\gamma}(t)$, along which the partial derivative is taken.

The wave function $|\psi\rangle$ in S can be decomposed using Schmidt decomposition¹²

$$|\psi(\boldsymbol{\lambda})\rangle = \sum_{m,n} \psi_n(\boldsymbol{\lambda}) |m(\boldsymbol{\lambda})\rangle \underbrace{\langle m(\boldsymbol{\lambda})|n\rangle}_{U_{mn}(\boldsymbol{\lambda})} = \sum_m \underbrace{\tilde{\psi}_m(\boldsymbol{\lambda})}_{\langle m(\boldsymbol{\lambda})|\psi_n|n\rangle} |m(\boldsymbol{\lambda})\rangle, \quad (2.62)$$

where $U_{mn}(\boldsymbol{\lambda})$ are matrix elements of unitary transformation $\hat{U}(\boldsymbol{\lambda})$. In this work, we will be interested only in the gauge transformations preserving energy of the system.

¹¹especially from the fact, that all spaces $\hat{H}(\boldsymbol{\lambda})$ are isomorphic to each other

¹²The Schmidt decomposition can be performed in finite dimension, or if the Hamiltonian is compact, which is not automatic in quantum mechanics. What's more, the Hamiltonian is usually not even bounded. Anyway, for simple systems with bounded energy we can assume so.

Adiabatic gauge potential

Adiabatic gauge potentials, sometimes just *adiabatic potentials*, are generators of unitary transformations, so we can define them analogically to the classical case

$$i\hbar\partial_\lambda |\tilde{\psi}(\boldsymbol{\lambda})\rangle = i\hbar\partial_\lambda \left(\hat{U}^+(\boldsymbol{\lambda}) |\psi\rangle \right) = \underbrace{i\hbar \left(\partial_\lambda \hat{U}^+(\boldsymbol{\lambda}) \right)}_{-\hat{\mathcal{A}}_\lambda} \hat{U}(\boldsymbol{\lambda}) |\tilde{\psi}(\boldsymbol{\lambda})\rangle. \quad (2.63)$$

The adiabatic potential $\hat{\mathcal{A}}_\lambda$ can be transformed to non-tilde system as

$$\begin{aligned} \hat{\mathcal{A}}_\lambda &= \hat{U}(\boldsymbol{\lambda}) \tilde{\hat{\mathcal{A}}}_\lambda \hat{U}^+(\boldsymbol{\lambda}) = -i\hbar \hat{U}(\boldsymbol{\lambda}) \left(\partial_\lambda \hat{U}^+(\boldsymbol{\lambda}) \right) = \\ &= -i\hbar \partial_\lambda \left(\underbrace{U^+(\boldsymbol{\lambda}) U(\boldsymbol{\lambda})}_1 \right) - \left(\partial_\lambda U(\boldsymbol{\lambda}) \right) U^+(\boldsymbol{\lambda}) = i\hbar \left(\partial_\lambda U(\boldsymbol{\lambda}) \right) U^+(\boldsymbol{\lambda}). \end{aligned} \quad (2.64)$$

From this we get the equations for adiabatic potential in two systems

$$\hat{\mathcal{A}}_\lambda = i\hbar \left(\partial_\lambda U(\boldsymbol{\lambda}) \right) U^+(\boldsymbol{\lambda}) \quad (2.65)$$

$$\tilde{\hat{\mathcal{A}}}_\lambda = -i\hbar \left(\partial_\lambda \hat{U}^+(\boldsymbol{\lambda}) \right) \hat{U}(\boldsymbol{\lambda}) \quad (2.66)$$

which can be shown to be Hermitian

$$\tilde{\hat{\mathcal{A}}}_\lambda^+ = i\hbar U(\boldsymbol{\lambda})^+ \left(\partial_\lambda \hat{U}(\boldsymbol{\lambda}) \right) = -i\hbar \left(\partial_\lambda \hat{U}(\boldsymbol{\lambda})^+ \right) \hat{U}(\boldsymbol{\lambda}) = \tilde{\hat{\mathcal{A}}}_\lambda, \quad (2.67)$$

analogically for non-tilde potential. Using the eigenbasis of \hat{H} , the matrix elements are

$$\langle n | \tilde{\hat{\mathcal{A}}}_\lambda | m \rangle = i\hbar \langle n | \hat{U}(\boldsymbol{\lambda})^+ \partial_\lambda \hat{U}(\boldsymbol{\lambda}) | m \rangle = i\hbar \langle n(\boldsymbol{\lambda}) | \partial_\lambda | m(\boldsymbol{\lambda}) \rangle. \quad (2.68)$$

and because

$$\langle n(\boldsymbol{\lambda}) | \hat{\mathcal{A}}_\lambda | m(\boldsymbol{\lambda}) \rangle = \langle n | \tilde{\hat{\mathcal{A}}}_\lambda | m \rangle, \quad (2.69)$$

we get

$$\hat{\mathcal{A}}_\lambda = i\hbar\partial_\lambda. \quad (2.70)$$

Adiabatic gauge transformations are class of gauge transformations with fidelity $f = 1$. This means, that if the system is driven by Hamiltonian $\hat{H}(\boldsymbol{\lambda})$ with fidelity $f < 1$, there exists such adiabatic potential \mathcal{A}_λ , that driving of the same system using $\hat{H} - \mathcal{A}_\lambda$ has fidelity $f = 1$.

The adiabatic gauge potentials can then be understood as affine connections defining the parallel transport on fiber bundle, if we define covariant derivative as

$$D_\mu = \partial_\mu + i\hat{\mathcal{A}}_\mu, \quad (2.71)$$

which yields $D_\mu |\psi_n\rangle = 0$ for every eigenstate, which yields, that the transport of eigenvalues on \mathcal{M}_0 is parallel. $\hat{\mathcal{A}}_\mu$ is generally defined 2.65, which generally gives non-zero covariant derivative for states not belonging to \mathcal{M}_0 .

Finding of those potentials has many practical applications, so let's introduce one analytical procedure of finding them.

Performing counter-diabatic driving

[Kolodrubetz et al., 2017][page 15–17] The main idea of a counter-diabatic driving is, that any excitation of the system can be countered by adding so called *counter-diabatic potential* to the Hamiltonian. Consider again any eigenstate $|\psi(t)\rangle$ of the Hamiltonian $\hat{H} = \hat{H}(\lambda)$ driven along the curve $\gamma(\lambda(t))$ on \mathcal{M}_0 depending on time t , during which the fidelity $f \neq 0$. Because the system is not measured during the trip, it can't be stated if or if not it was excited, but the main goal here is to make fidelity zero, which is iff \tilde{H} is diagonal. For diagonalizable Hamiltonian, there exist a transformation, see eq. 2.60, for which the fidelity will be zero. Such a transformation does not have to be unique, but we can choose any one of them. This can be seen more clearly from direct transformation of the Schrödinger equation.

The Schrödinger equation

$$i\hbar \frac{d}{dt} |\psi(\lambda)\rangle = \hat{H}(\lambda) |\psi(\lambda)\rangle \quad (2.72)$$

can be transformed using

$$\hat{U}(\lambda)^+ |\psi(\lambda)\rangle = |\tilde{\psi}(\tilde{\lambda})\rangle, \quad (2.73)$$

for which $\tilde{H} := \hat{U}^+ \hat{H} \hat{U}$ is diagonal, leading to

$$i\hbar \frac{d}{dt} (\hat{U}(\tilde{\lambda}) |\tilde{\psi}(\tilde{\lambda})\rangle) = \hat{H}(\lambda) \hat{U}(\tilde{\lambda}) |\tilde{\psi}(\tilde{\lambda})\rangle \quad (2.74)$$

$$i\hbar \frac{d\lambda}{dt} \partial_\lambda \hat{U}(\tilde{\lambda}) |\tilde{\psi}(\tilde{\lambda})\rangle + i\hbar \hat{U}(\tilde{\lambda}) \frac{d}{dt} |\tilde{\psi}(\tilde{\lambda})\rangle = \hat{H}(\lambda) \hat{U}(\tilde{\lambda}) |\tilde{\psi}(\tilde{\lambda})\rangle. \quad (2.75)$$

This can be rewritten using adiabatic potential from Eq. 2.70, using *dot* notation for time derivatives and omitting the points in which the objects are evaluated, as

$$i\hbar \frac{d}{dt} |\tilde{\psi}\rangle = \left[\hat{U}^+ \hat{H} \hat{U} - \dot{\lambda} \tilde{\mathcal{A}}_\lambda \right] |\tilde{\psi}\rangle = \left[\tilde{H} - \dot{\lambda} \tilde{\mathcal{A}}_\lambda \right] |\tilde{\psi}\rangle =: \tilde{H}_m |\tilde{\psi}\rangle, \quad (2.76)$$

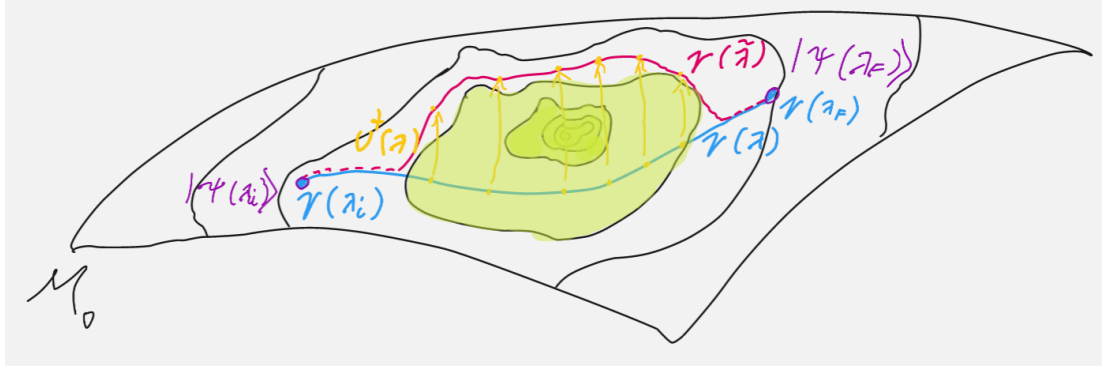
where the term $-\dot{\lambda} \tilde{\mathcal{A}}_\lambda$ is called *Galilean* and \tilde{H}_m is the Hamiltonian in transformed system. Because \tilde{H} is diagonal, it drives $|\tilde{\psi}\rangle$ with fidelity $f = 1$. This means that for any driving defined by $\hat{H}(\lambda(t))$, which defines the unitary transformation \hat{U} , there exists such *counter-diabatic potential* $\tilde{\mathcal{A}}_\lambda$, that $\tilde{H}_m + \dot{\lambda} \tilde{\mathcal{A}}_\lambda$ has $f = 1$.

This procedure does not directly tell us how to calculate the counter-diabatic potential, only states its existence. For many simple cases the calculation can be done analytically, but most often some approximation methods are needed.

Explicit form

If we now consider the parametrization with time $t := t$, \hat{U} can be explicitly expressed according to **ansatz** in eq. 2.4 as

$$\hat{U}(t) = \sum_n \exp \left(\frac{i}{\hbar} E_n(\tau) d\tau - \int_0^t \langle s(\tau) | \partial_\tau n(\tau) \rangle d\tau \right) |s(t)\rangle \langle s(0)|. \quad (2.77)$$



Inserting to eq. 2.61, we get explicit form of the Hamiltonian, which can be decomposed into the diagonal form of the original Hamiltonian and a counter-diabatic potential

$$\hat{H}(t) = \sum_n |n\rangle E_n \langle n| + i\hbar \sum_n |\partial_\lambda n\rangle \langle n| - \langle n|\partial_\lambda n\rangle |n\rangle \langle n| =: \hat{H}_0(t) + \hat{H}_1(t), \quad (2.78)$$

for shortened notation $|n\rangle \equiv |n(t)\rangle$, analogically for bras. Using

$$\hat{H}_0(t) |n\rangle = E_n |n\rangle \quad \Rightarrow \quad \langle m|\partial_\lambda n\rangle = \frac{\langle m|\partial_\lambda \hat{H}_0|n\rangle}{E_n - E_m} \quad (2.79)$$

we have explicit formula

$$\hat{H}_1(t) = i\hbar \sum_{m \neq n} \frac{|m\rangle \langle m|\partial_\lambda \hat{H}_0|n\rangle \langle n|}{E_n - E_m} \quad (2.80)$$

3. Geometrization of quantum mechanics

Differential geometry is believed to be the modern language of physics and there is a strong urge to reformulate theories in this language. As introduction to the problem, see Ashtekar and Schilling [1997], Ashtekar and Schilling [1995], or more mathematical work by Molitor [2013].

In the previous chapter, we have used classical formulation of quantum mechanics with some parts described using differential geometry. Here, the complete reformulation of quantum mechanics and the bridge between this theory and the one we have already formulated will be build. Reformulating the whole theory of quantum driving into the language of differential geometry might give some new insights, but it is beyond the scope of this thesis.

3.1 From the projective Hilbert space to state manifolds

Consider the Hilbert space \mathcal{H} to be a space of *bare states* and \mathcal{S} to be the space of *normalized bare states*. Physical observables are related to the *space of rays*, defined as $\mathcal{PH} := \mathcal{H}/U(1)$, for the factorization by elements of one-dimensional unitary group $U(1)$. This group consists of unitary transformations $e^{i\varphi}$ for $\varphi \in \mathbb{R}$, defining gauge symmetry between quantum states. \mathcal{PH} is then considered to be the *space of pure states*. We will consider the states to be normalized, leading to the *space of normalized pure physical states*.

It can be shown, that \mathcal{PH} is of a Kähler structure, meaning it has two non-degenerate sesquilinear¹ 2-forms embedded along with complex unit operator

$$(J, G, \Omega),$$

such that

$$J^2 = \mathbb{1} \tag{3.1}$$

and any bracket of $|\psi_1\rangle, |\psi_2\rangle \in \mathcal{PH}$ can be decomposed into real and imaginary part[Ashtekar and Schilling, 1997]

$$\langle \psi_1 | \psi_2 \rangle \equiv Q(\psi_1, \psi_2) = \frac{1}{2}G(\psi_1, \psi_2) - \frac{i}{2}\Omega(\psi_1, \psi_2). \tag{3.2}$$

From braket sesquilinearity goes that G is symmetric and Ω antisymmetric form, thus they can be uniquely written into one 2-form called *Fubini-Study metric* with property

$$G = \text{Re}Q; \quad \Omega = \text{Im}Q. \tag{3.3}$$

Because $\langle \psi_1 | \psi_2 \rangle \in [0, 1]$ we say, that the metric is measuring the geodesic distance on the Bloch sphere. Here if we define

$$| \langle \psi_1 | \psi_2 \rangle | = \cos^2 \frac{\theta}{2}, \tag{3.4}$$

¹We are in physics, so complex conjugated is the first input of the 2-form.

we get $d\theta = 2ds = 2\sqrt{|g_{\mu\nu}d\lambda^\mu d\lambda^\nu|}$, see Cheng [2013].

To write the metric in a standard form, we need to realize how our space looks like. For finite $(n+1)$ -dimensional Hilbert space, one dimension is lost in the gauge transformation, leaving us with n -dimensional \mathcal{PH} . Another dimension is lost due to normalization, which is usually done by mapping to an n -dimensional complex sphere

$$CP^n = \left\{ \mathbf{Z} = (Z_0, Z_1, \dots, Z_n) \in \mathbb{C}^{n+1}/\{0\} \right\} / \{\mathbf{Z} \sim c\mathbf{Z} \text{ for } c \in \mathbb{C}\}.$$

Natural property of such complex spaces is splitting of its tangent space to holonomic and anholonomic part²

$$\mathcal{T}_0^1 \mathcal{M} = \text{Span} \left\{ \frac{\partial}{\partial Z_i} \right\}; \quad \mathcal{T}_1^0 \mathcal{M} = \text{Span} \left\{ \frac{\partial}{\partial \bar{Z}_i} \right\}.$$

Distance on \mathbb{C}^{n+1} is usually defined using Hermitian metric³

$$ds^2 = d\bar{Z} \otimes dZ. \quad (3.5)$$

For *normalized states* in quantum mechanics is $dZ = ??????$, which plugged into Eq. 3.5 yields

$$ds^2 = 1 - |\langle \psi + \delta\psi | \psi \rangle|^2. \quad (3.6)$$

3.2 Restriction to eigenstate manifolds

In quantum mechanics, one can examine a Hamiltonian $\hat{H}(\boldsymbol{\lambda})$, for some parameter $\boldsymbol{\lambda} \in \mathbb{R}^n$. At every point $\boldsymbol{\lambda}$ we get projective Hilbert space $\mathcal{PH}(\boldsymbol{\lambda})$. This creates a fiber structure space, in which there are some sections with interesting physical applications. Some of these sections are *eigenstate manifolds*, defined by setting only one non-zero coefficient Z_k in eigenbasis $|\psi\rangle = \sum_{k=0}^n Z_k |k\rangle$. From normalization goes automatically $Z_k = 1$. The distance on these manifolds is, as derived in Eq. 2.20,

$$\begin{aligned} ds^2 &= 1 - \langle k + \delta k | k \rangle \langle k | k + \delta k \rangle = 1 - \langle k + \delta k | \left(1 - \sum_{j \neq k} |j\rangle \langle j| \right) |k + \delta k \rangle \\ &= \sum_{j \neq k} \langle k + \delta k | j \rangle \langle j | k + \delta k \rangle. \end{aligned} \quad (3.7)$$

Using the Schrödinger equation $\hat{H} |k\rangle = E_k |k\rangle$, distributivity of derivative and projection to some state $\langle j |$, we get

$$\begin{aligned} \hat{H} |k\rangle &= E_k |k\rangle \\ (\delta \hat{H}) |k\rangle + \hat{H} |k + \delta k\rangle &= (\delta E_k) |k\rangle + E_k |k + \delta k\rangle \\ \langle j | (\delta \hat{H} - \delta E_k) |k\rangle &= \langle j | (E_k - \hat{H}) |k + \delta k\rangle = \langle j | (E_k - E_j) |k + \delta k\rangle. \end{aligned} \quad (3.8)$$

²The line over index means complex conjugation.

³Hermitian metric is by definition sesquilinear, as one would expect in quantum mechanics later on.

We can set⁴ $\delta E_k = 0$, leading for $j \neq k$ to

$$\frac{\langle j | \delta \hat{H} | k \rangle}{(E_k - E_j)^2} = \langle j | k + \delta k \rangle. \quad (3.9)$$

Plugging to Equation 3.7 and considering $\hat{H} = \hat{H}(\boldsymbol{\lambda})$, we get metric on a ground state manifold

$$ds^2 = \operatorname{Re} \sum_{j \neq k} \frac{\langle 0 | \partial_\mu \hat{H} | j \rangle \langle j | \partial_\nu \hat{H} | 0 \rangle}{(E_k - E_j)^2} d\boldsymbol{\lambda}^\mu d\boldsymbol{\lambda}^\nu \quad (3.10)$$

Definition of the k -state manifold is then

$$g_{\mu\nu}^{(k)} = \operatorname{Re} \sum_{j \neq k} \frac{\langle k | \frac{\partial \hat{H}(\boldsymbol{\lambda})}{\partial \lambda^\mu} | j \rangle \langle j | \frac{\partial \hat{H}(\boldsymbol{\lambda})}{\partial \lambda^\nu} | k \rangle}{(E_k - E_j)^2}. \quad (3.11)$$

The Fubini-Study metric on the eigenstate manifold is sometimes called *Geometric tensor*.

⁴Can it be done only for E_0 ? It does not make sense generally, because $E = E(\boldsymbol{\lambda})$, even $E_0 = E_0(\boldsymbol{\lambda})$

4. Two level system

Let's have a Hamiltonian

$$\hat{H}(t) = \begin{pmatrix} \Omega(t) & \Delta(t) \\ \Delta(t) & -\Omega(t) \end{pmatrix} \quad (4.1)$$

for $\Omega : \mathbb{R}^+ \rightarrow \mathbb{R}$, $\Delta : \mathbb{R}^+ \rightarrow \mathbb{R}$. Its spectrum is

$$E_1(t) = -E_0(t) = \sqrt{\Omega^2(t) + \Delta^2(t)} \quad (4.2)$$

and using the eigenbasis

$$\mathcal{B} := \left\{ |0\rangle \equiv \begin{pmatrix} 1 \\ 0 \end{pmatrix}, |1\rangle \equiv \begin{pmatrix} 0 \\ 1 \end{pmatrix} \right\}, \quad (4.3)$$

we get the eigenvectors

$$|0(t)\rangle = N_+ \begin{pmatrix} 1 \\ \frac{E_0(t)+\Omega(t)}{\Delta(t)} \end{pmatrix}, \quad |1(t)\rangle = N_- \begin{pmatrix} 1 \\ \frac{E_1(t)+\Omega(t)}{\Delta(t)} \end{pmatrix} \quad (4.4)$$

for normalization constants $N_{\pm} := \left(\left(\frac{\pm E_0(t) + \Omega(t)}{\Delta(t)} \right)^2 + 1 \right)^{-1/2}$. One needs to realize that at any time t the eigenbases differ. The basis \mathcal{B} forms an eigenbasis at time $t = 0$.

The goal will be to find *fidelity* $F := |\langle 0(t) | \psi(t) \rangle|^2$ of different driving protocols. For this we need to solve time Schrödinger equation

$$\hat{H}(t) |\psi(t)\rangle = i \frac{d}{dt} |\psi(t)\rangle \quad (4.5)$$

with time varying Hamiltonian. For 2-dimentional system with

$$|\psi(t)\rangle =: \begin{pmatrix} a(t) \\ b(t) \end{pmatrix}, \quad (4.6)$$

we get the system of *two coupled differentials equations of the first order with non-constant coefficients*

$$\Omega(t)a(t) + \Delta(t)b(t) = i\dot{a}(t) \quad (4.7)$$

$$\Delta(t)a(t) - \Omega(t)b(t) = i\dot{b}(t) \quad (4.8)$$

with normalization

$$a^2(t) + b^2(t) = 1, \quad \forall t \in [0, T_f]. \quad (4.9)$$

and initial value

$$\begin{pmatrix} a(0) \\ b(0) \end{pmatrix} = |0(0)\rangle. \quad (4.10)$$

4.1 Harmonic oscillator correspondence

The Equations 4.7, 4.8 have no general analytical solution, with an exception to a few easy protocols $\hat{H}(t)$. Before moving to some of these special cases, let's analyze this coupled system of equations generally.

N-dimensional Schrödinger equation can be rewritten to *one differential equation of N^{th} order with non-constant coefficients*. In our two-dimensional case, this equation corresponds to *damped harmonic oscillator without external force*

$$0 = \ddot{a}(t) + \gamma(t)\dot{a}(t) + \omega^2(t)a(t) \quad (4.11)$$

$$\gamma(t) := -\frac{\dot{\Delta}(t)}{\Delta(t)} \quad (4.12)$$

$$\omega^2(t) := i \left(\dot{\Omega}(t) - \frac{\dot{\Delta}(t)}{\Delta(t)} \Omega(t) \right) + \Delta^2(t) + \Omega^2(t). \quad (4.13)$$

Along with normalization condition 4.9 and initial condition

$$\begin{pmatrix} a(0) \\ b(0) \end{pmatrix} = |0(0)\rangle; \quad \dot{a}(0) = -i(\Omega(0)a(0) + \Delta(0)b(0)). \quad (4.14)$$

Note that we used the condition $\Delta \neq 0$. Because the energy spectrum has $\Delta \leftrightarrow \Omega$ symmetry, we can change the driving by interchanging Δ and Ω on any intervals, where the parameters 4.12, 4.13 would diverge.

Classical mechanics correspondence

When solving differential equations, it might be useful to know some analogy to classical mechanics Lagrangian. Even though it will not be used any further, let's quickly find it.

From the perspective of classical mechanics, meaning $x(t) := a(t)$ is a position in a phase space (x, p) , we can write classical Lagrangian from Eq. 4.11 as

$$\mathcal{L} = \frac{1}{2} \exp \left(\int_0^t \gamma(s) ds \right) (\dot{x}^2 - \omega^2(t)x^2) \quad (4.15)$$

Proof. The correspondence of Lagrangian 4.15 with Eq. 4.11 can be shown by direct evaluation of Euler-Lagrange equations

$$\begin{aligned} \frac{\partial \mathcal{L}}{\partial x} - \frac{d}{dt} \frac{\partial \mathcal{L}}{\partial \dot{x}} &= 0 \\ \frac{1}{2} \exp \left(\int_0^t \gamma(s) ds \right) (-2\omega^2(t)x) - \frac{d}{dt} \left(\exp \left(\int_0^t \gamma(s) ds \right) \dot{x} \right) &= 0 \\ -\omega^2(t)x - \gamma(t)\dot{x} - \ddot{x} &= 0. \end{aligned} \quad (4.16)$$

□

4.2 Energy variance for two level system

For two level system, the variance

$$\delta E^2(t) := \langle \psi(t) | \hat{H}^2 | \psi(t) \rangle - \langle \psi(t) | \hat{H} | \psi(t) \rangle^2 \quad (4.17)$$

can be rewritten inserting identity $\mathbb{1} = |0\rangle\langle 0| + |1\rangle\langle 1|$ around Hamiltonian. Omitting the time dependence of every element we get

$$\begin{aligned}\delta E^2 &= \langle\psi|\hat{H}^2\mathbb{1}|\psi\rangle - \langle\psi|\mathbb{1}\hat{H}\mathbb{1}|\psi\rangle^2 \\ &= \langle\psi|0\rangle\langle 0|\hat{H}^2|0\rangle\langle 0|\psi\rangle + \langle\psi|1\rangle\langle 1|\hat{H}^2|1\rangle\langle 1|\psi\rangle \\ &\quad + \langle\psi|0\rangle\langle 0|\hat{H}^2|1\rangle\langle 1|\psi\rangle + \langle\psi|1\rangle\langle 1|\hat{H}^2|0\rangle\langle 0|\psi\rangle \\ &\quad - \left(\langle\psi|0\rangle\langle 0|\hat{H}|0\rangle\langle 0|\psi\rangle + \langle\psi|1\rangle\langle 1|\hat{H}|1\rangle\langle 1|\psi\rangle \right. \\ &\quad \left. + \underbrace{\langle\psi|0\rangle\langle 0|\hat{H}|1\rangle\langle 1|\psi\rangle}_{\propto\langle 0|1\rangle=0} + \underbrace{\langle\psi|1\rangle\langle 1|\hat{H}|0\rangle\langle 0|\psi\rangle}_{\propto\langle 0|1\rangle=0} \right)^2.\end{aligned}\tag{4.18}$$

Using Fidelity definition $F(t) = |\langle 0(t)|\psi(t)\rangle|^2$ and Schrödinger equation $\hat{H}|k\rangle = E_k|k\rangle$ we have

$$\delta E^2 = FE_0^2 + (1-F)E_1^2 - (FE_0 + (1-F)E_1)^2 = F(1-F)(E_0 - E_1)^2.\tag{4.19}$$

For three level system we have $\mathbb{1} = |0\rangle\langle 0| + |1\rangle\langle 1| + |2\rangle\langle 2|$ and

$$\delta E^2 = \sum_{k=1}^3 E_k^2 F_k (1 - F_k) - 4 \prod_{k=1}^3 E_k F_k - 2F_0 F_1 E_0 E_1 - 2F_0 F_2 E_0 E_2 - 2F_1 F_2 E_1 E_2,\tag{4.20}$$

for $F_k := \langle k|\psi\rangle$, which has no practical simplification.

4.3 Geodesic driving

Some analytically solvable driving protocols are the *Geodesics* of the projective ground state manifold.

Define driving in 3-dimensional space

$$d(t) \equiv \begin{pmatrix} \Omega(t) \\ \Xi(t) \\ \Delta(t) \end{pmatrix} := \begin{pmatrix} -s \cos(\omega(T_f)t) \\ 0 \\ s \sin(\omega(T_f)t) \end{pmatrix}\tag{4.21}$$

parametrized by time $t \in [0, 1]$ and with use of *speed regulating function* $\omega(T_f) := \pi/T_f$. The reason for 3-dimensional driving will be the usage of $\hat{\sigma}$ matrix formalism. Such defined drivings are half-spheres in the parametric space, see Fig. 4.1. Note that the driving velocity is constant on the parametric space and on the manifold.

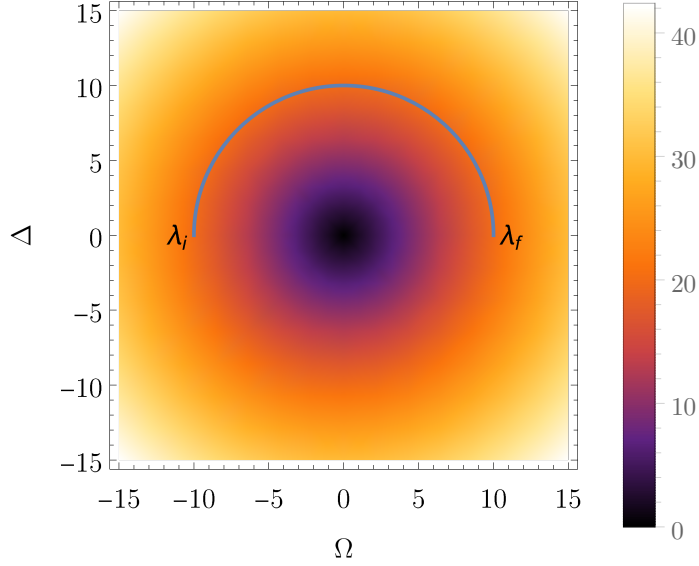


Figure 4.1: Driving along the geodesic. λ_i and λ_f are initial resp. final parameters. Density plot shows the difference between Hamiltonian eigenvalues.

4.3.1 Derivation of the fidelity

Because the Hamiltonian can be rewritten using Pauli matrices

$$\hat{H}(t) = \begin{pmatrix} -s \cos(t\omega) & s \sin(t\omega) \\ s \sin(t\omega) & s \cos(t\omega) \end{pmatrix} = \Delta(t)\sigma_x + \Omega(t)\sigma_z = d(t).\hat{\sigma}, \quad (4.22)$$

for vector $\hat{\sigma} := (\hat{\sigma}_1, \hat{\sigma}_2, \hat{\sigma}_3)^T$.

One can see that changing from the [original frame](#) with function $|\psi\rangle$ to [moving frame of reference](#), with $|\tilde{\psi}\rangle$ (let's omit the final time dependence $\omega = \omega(T_f)$ for a while) is described as

$$\psi(t) =: e^{\frac{i\omega}{2}\hat{\sigma}_y t} \tilde{\psi}(t). \quad (4.23)$$

This reflects the rotational symmetry of the system. The change of reference frame transforms Schrödinger equation as

$$\begin{aligned} \hat{H}(t)\psi(t) &= i\psi'(t) \\ \hat{H}(t)e^{\frac{i\omega}{2}\hat{\sigma}_y t}\tilde{\psi}(t) &= ie^{\frac{i\omega}{2}\hat{\sigma}_y t} \left(\frac{i\omega\hat{\sigma}_y}{2} \right) \tilde{\psi}(t) + ie^{\frac{i\omega}{2}\hat{\sigma}_y t} \tilde{\psi}'(t) \\ \underbrace{\left(e^{-\frac{i\omega}{2}\hat{\sigma}_y t} \hat{H}(t) e^{\frac{i\omega}{2}\hat{\sigma}_y t} + \frac{\omega}{2} \hat{\sigma}_y \right)}_{\tilde{H}(t)} \tilde{\psi}(t) &= i\tilde{\psi}'(t). \end{aligned} \quad (4.24)$$

From this one can equivalently solve the Fidelity problem in this new coordinate system.

Hamiltonian in the moving frame is

$$\tilde{H} = \begin{pmatrix} -s & -i\omega(T_f)/2 \\ i\omega(T_f)/2 & s \end{pmatrix}, \quad (4.25)$$

which is time independent. The Schrödinger equation can now be easily solved using evolution operator

$$\hat{U}(t) = e^{-i\hat{H}t} = \begin{pmatrix} \cos\left(\frac{t}{2}q(T_f)\right) + \frac{2is\sin\left(\frac{t}{2}q(T_f)\right)}{q(T_f)} & -\frac{\omega(T_f)\sin\left(\frac{t}{2}q(T_f)\right)}{q(T_f)} \\ \frac{\omega(T_f)\sin\left(\frac{t}{2}q(T_f)\right)}{q(T_f)} & \cos\left(\frac{t}{2}q(T_f)\right) - \frac{2is\sin\left(\frac{t}{2}q(T_f)\right)}{q(T_f)} \end{pmatrix}, \quad (4.26)$$

for $q(T_f) = \sqrt{4s^2 + \omega(T_f)^2}$.

In the original frame we get the evolution of the state $\psi(0)$

$$\psi(t) = e^{\frac{i\omega}{2}\hat{\sigma}_y t} \hat{U}(t) \tilde{\psi}(0) = \underbrace{e^{\frac{i\omega}{2}\hat{\sigma}_y t} \hat{U}}_{\hat{U}(t)} \underbrace{e^{-\frac{i\omega}{2}\hat{\sigma}_y t} \tilde{\psi}(0)}_{\psi(0)}. \quad (4.27)$$

The evolved wave-function the reads as

$$|\psi(t)\rangle = \begin{pmatrix} \cos\left(\frac{t}{2}q(T_f)\right) + \frac{2is\cos(t\omega(T_f))\sin\left(\frac{t}{2}q(T_f)\right)}{q(T_f)} \\ \frac{(\omega(T_f) - 2is\sin(t\omega(T_f)))\sin\left(\frac{t}{2}q(T_f)\right)}{q(T_f)} \end{pmatrix} \quad (4.28)$$

and the ground state

$$|0(t)\rangle = \mathcal{N} \begin{pmatrix} -\cot\left(\frac{t}{2}\omega(T_f)\right) \\ 1 \end{pmatrix}, \quad (4.29)$$

for a normalization constant $\mathcal{N} := |\langle 0(t)|0(t)\rangle|^{-1}$. Fidelity during the transport is then¹

$$F = |\langle 0(t)|\psi(t)\rangle|^2. \quad (4.30)$$

An explicit formula for fidelity in time t and geodesic driving with final time T_f is

$$F(t, T_f) = \frac{\pi^2 \left(\cos\left(t\sqrt{\frac{\pi^2}{T_f^2} + 4s^2}\right) + 1 \right) + 8s^2 T_f^2}{2 \sin^4\left(\frac{\pi t}{2T_f}\right) \left(4s^2 T_f^2 + \pi^2\right) \left(\left|\cot\left(\frac{\pi t}{2T_f}\right)\right|^2 + 1\right)^2}. \quad (4.31)$$

The domain can be extended from $t \in (0, T_f)$ to $[0, T_f]$ for any $T_f \in [0, \infty]$, because

$$\lim_{t \rightarrow 0} F = 1, \quad \lim_{T_f \rightarrow 0} F = 0.$$

Sometimes the *Infidelity*, defined as $F^* := 1 - F$, will be used. Its meaning is *the probability of excitation of the state*.

4.3.2 Analysis of the infidelity formula

Infidelity can be calculated by numerical evolution of Schrödinger equation, or from Eq. 4.31. Sometimes both solutions are plotted for comparison between numerical precision.

For some fixed final time, the infidelity is an oscillating curve with values close to 0. For $T_f = 10$ it can be seen on Fig. 4.2. The *final infidelity* (at $t = T_f$) dependence on final time T_f can be seen on Fig. 4.3 and 4.4.

¹If we calculated the fidelity in the [comoving frame](#), we would get exactly one. This realization leads to the counter-diabatic driving.

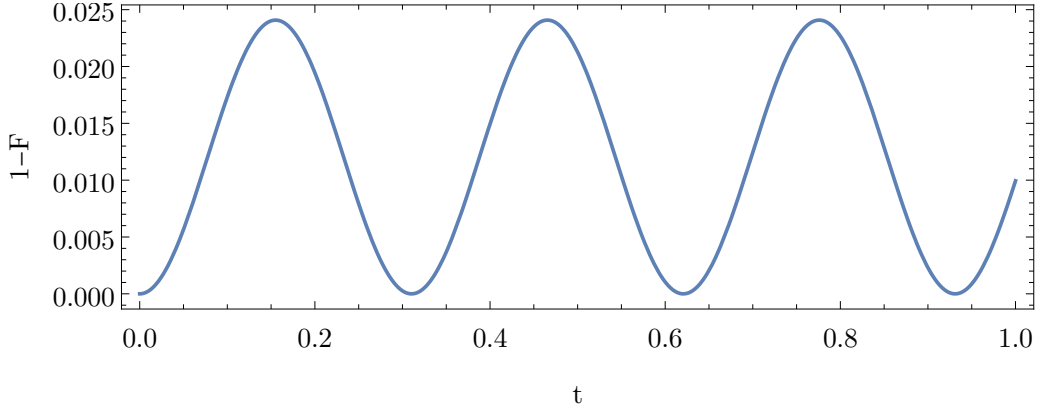


Figure 4.2: Infidelity in time for final time $T_f = 1$ for geodesical driving.

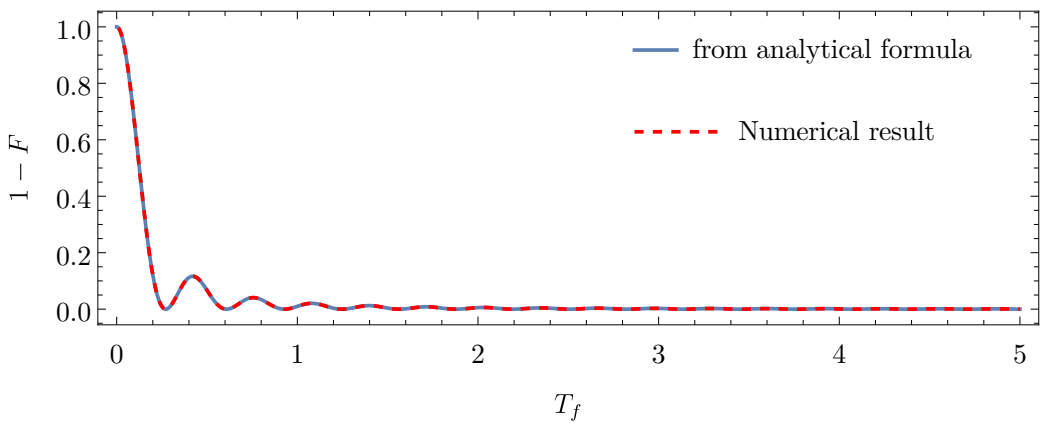


Figure 4.3: Final infidelity dependence on final time T_f for geodesical driving.

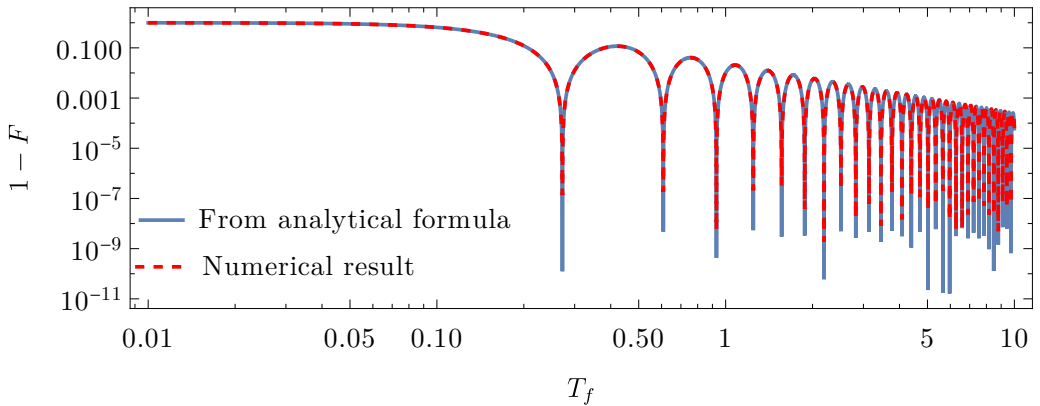


Figure 4.4: Infidelity dependence on final time in logarithmic scale. We can observe difference in numerical precision of both methods in the height of spikes. As we will see later, the spikes should go to zero, thus analytical formula has better numerical precision.

From the fidelity formula 4.31 goes that $F = 1$ is equivalent to

$$\cos \left(\sqrt{T_s^2 + \pi^2} \right) = 1, \quad (4.32)$$

for $T_s := 2sT_f$. The solution to this equation is

$$T_s = \sqrt{(2\pi k)^2 - \pi^2} \text{ for } k \in \mathbb{N}, \quad (4.33)$$

see Fig. 4.5. Because $F = 1$ has solutions 4.33, its dependence on final time in logarithmic scale has spikes going to 0, see Fig. 4.4, and their density is linear in T_f .

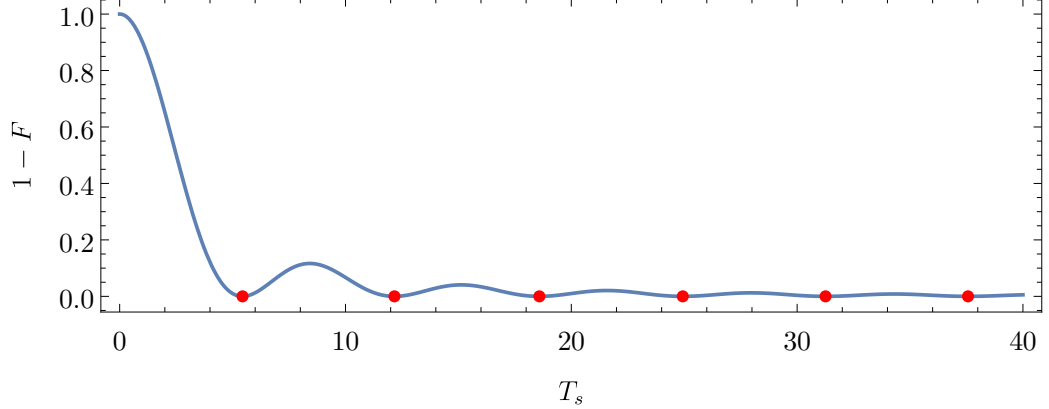


Figure 4.5: Rescaled final infidelity $T_s := 2sT_f$ dependence on final time. Red points mark the condition $F = 1$.

Fidelity as a function of time and final time can be seen in Figures 4.6. Note that only $t < T_f$ has physical meaning.

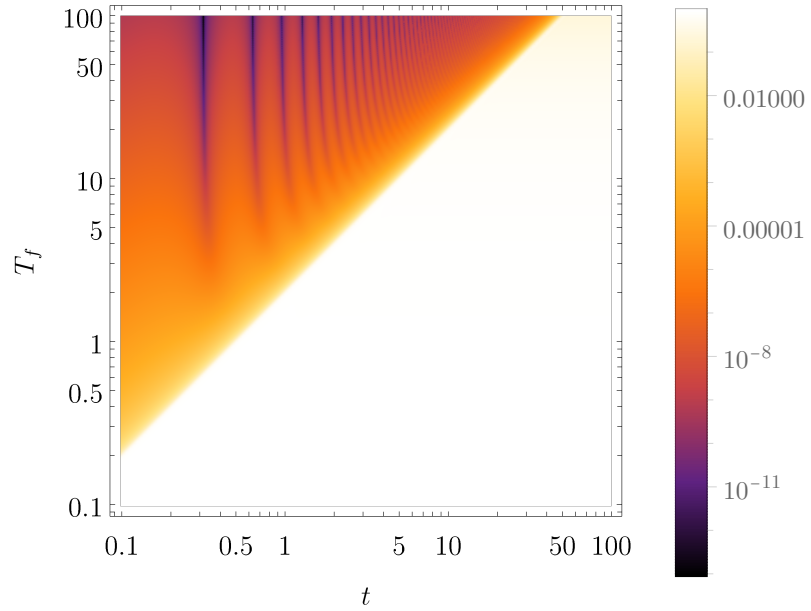


Figure 4.6: Fidelity dependence on time and final time in log-log scale. Note that only $t < T_f$ has physical meaning.

4.3.3 Energy variance

Another interesting quantity is the energy variance. It will be important later on in Theorem 8. For now, let's just mention that there the energy variance is smaller than the geometrical distance, if some conditions are fulfilled.

Evaluating the fidelity for geodesical driving gives a function of time t and final time T_f

$$\begin{aligned} \delta E^2 = & \frac{s^2}{2q^2} \left[\left[16s^4 + 2s^2 \left((\omega^2 - 8s^2) \cos(2t\omega) - 8\omega^2 \cos^2(t\omega) \cos(t\sqrt{q}) \right) \right. \right. \\ & + 14s^2\omega^2 + \omega^4 \Big] - \omega^2 \left((2s^2 + \omega^2) \cos(2t\omega) - 2s^2 \right) \cos(2tq) \\ & \left. \left. + 8s^2\omega q \sin(2t\omega) \sin(tq) + \omega^3 q \sin(2t\omega) \sin(2tq) \right], \right] \end{aligned} \quad (4.34)$$

see the definition of q under Eq. 4.26. Its value can be seen on Fig. 4.7. Note that only $t < T_f$ has a physical meaning, therefore the dependence is smooth along the whole geodesical driving protocols.

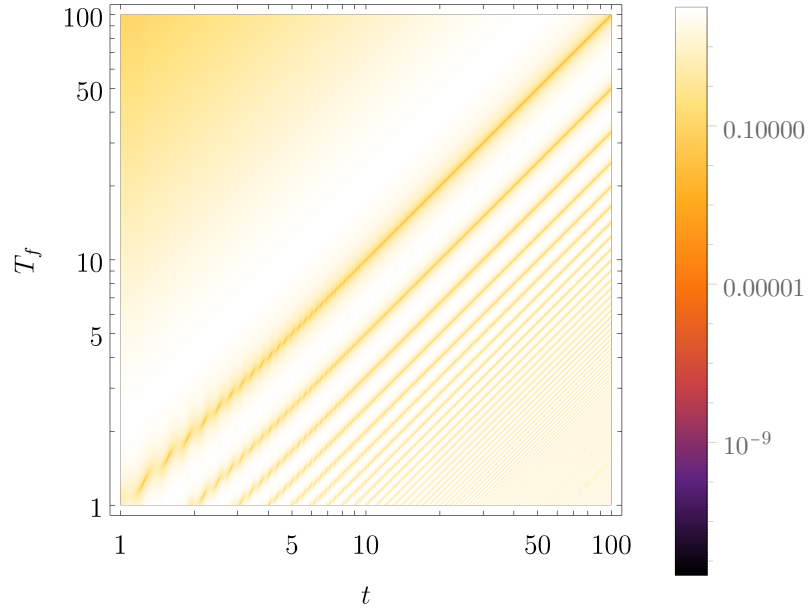


Figure 4.7: Energy variance for geodesical driving protocol.

4.4 Linear driving

Another analytically solvable driving is defined with two scaling parameters as

$$\Omega(t) = \Omega_{sc} \left(\frac{2t}{T_f} - 1 \right), \quad \Delta(t) = \Delta_{sc}, \quad \text{for } \Omega_{sc} = 10, \Delta_{sc} = 1, \quad (4.35)$$

see Fig. 4.8.

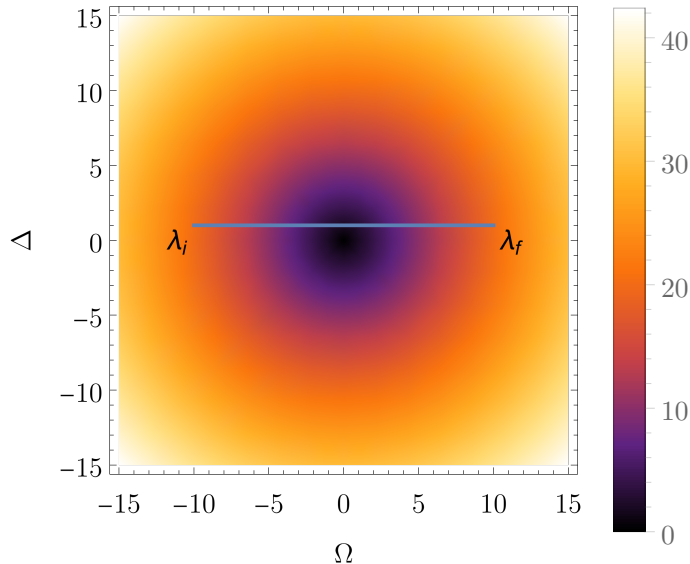


Figure 4.8: Driving along the linear path. $\lambda_i = (-10; 1)$ and $\lambda_f = (10; 1)$ are initial resp. final parameters. Density plot shows the difference between Hamiltonian eigenvalues.

From linear driving definition 4.35 and energy dependence 4.2 we have

$$\dot{\Delta}(t) = 0; \quad \Delta(t) \stackrel{\Delta(t) > 0}{=} \sqrt{\frac{E_{dif}^2(t)}{4} - \Omega^2(t)}; \quad E_{dif} := E_1 - E_0. \quad (4.36)$$

Substituting to functions from the Harmonic oscillator (Eq. 4.12, 4.13) we get

$$\gamma(t) = 0 \quad (4.37)$$

$$\omega^2(t) = i \frac{2\Omega_{sc}}{T_f} + \frac{\Omega_{sc}}{4} \left(\frac{2t}{T_f} - 1 \right)^2 + \frac{\Delta_{sc}^2}{4} = i \frac{2\Omega_{sc}}{T_f} + \frac{E_{dif}^2(t)}{4}. \quad (4.38)$$

Corresponding differential equation of second order is

$$a''(t) + \omega^2(t)a(t) = 0, \quad (4.39)$$

which is of *Weber type*² with Parabolic Cylinder functions³ as a solution, see report or publication from Felipe.

²<https://mathworld.wolfram.com/WeberDifferentialEquations.html>

³<https://mathworld.wolfram.com/ParabolicCylinderFunction.html>

4.4.1 Dependence on time

The fidelity in time can be seen on Fig. 4.9. For $t \approx T_f/2$ Hamiltonian parameters change quickly which leads to fast state excitation. Then the Harmonic oscillator damping gets involved and oscillations are quickly going to zero, never disappearing entirely.

We can see that the final fidelity decreases with longer final time, which correctly leads to adiabatic driving, where $\lim_{T_f \rightarrow \infty} F^* = 0$. For short final times we can observe so called quench, $\lim_{T_f \rightarrow 0} F^* = 1$. The interesting phenomenon on this image are the oscillations around $t = T_f/2$, which frequency increases with longer final time.

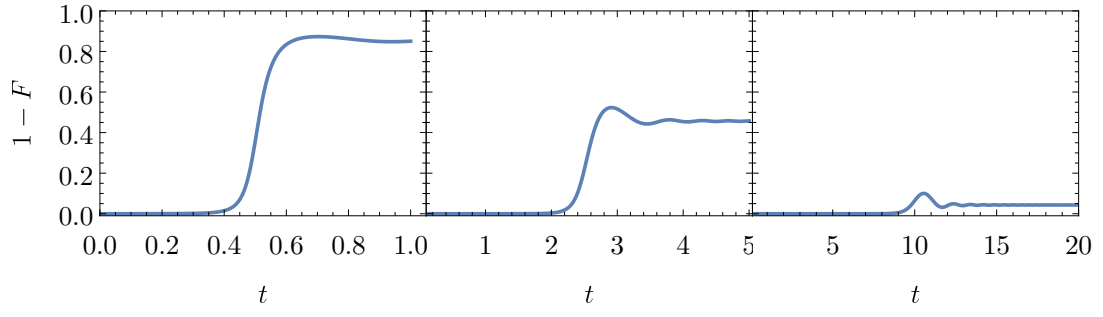


Figure 4.9: Infidelity in time for three final times $T_f \in \{1, 5, 20\}$ for the linear driving defined in 4.35.

Because in the Harmonic oscillator $\gamma(t) = 0$, the oscillations of $a(t)$ are not damped. What we are observing is infidelity

$$F^*(t) := 1 - |\langle 0(t)|\psi(t)\rangle|^2 = 1 - |\alpha(t)a(t) + \beta(t)b(t)|^2,$$

where the $|\psi(t)\rangle =: (a, b)^T$ represents the evolved state and $|0(t)\rangle =: (\alpha, \beta)^T$ evolved ground state in the initial eigenbasis \mathcal{B} . Realize that the ground state is not generally constant. In our case, the ground state described by Eq. 4.4 and is slowly changing its value from the first element α to the second element β , see Fig. 4.10. This means that at the beginning of driving, the projection to the ground state selects $b(t)$. Then it's getting more influenced by $a(t)$ until almost only $a(t)$ influences the fidelity.

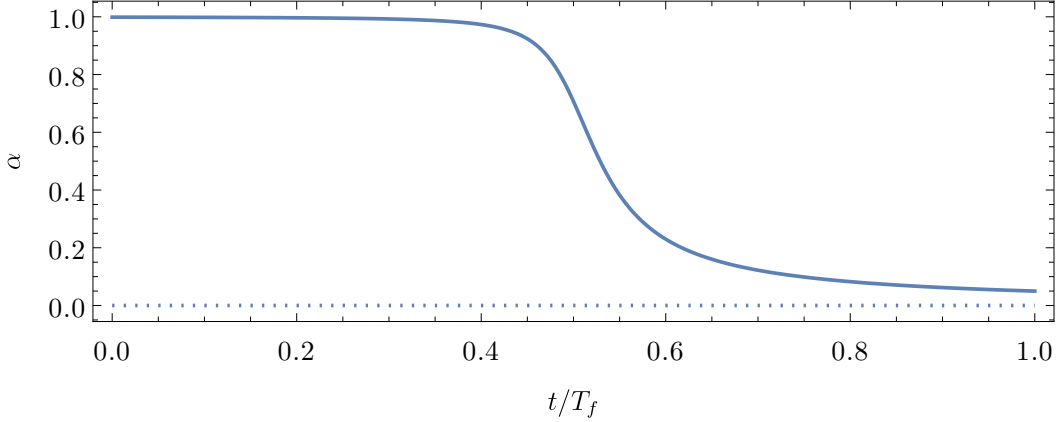


Figure 4.10: Value of first element of the ground state vector $\alpha \equiv |0(t)\rangle^1$ during linear driving.

Because of varying ground state during the transport, the oscillations cannot be analyzed only from $\omega^2(t)$ described by Eq. 4.38. At the end of the driving we have

$$\frac{1}{N_+} |0(t)\rangle^1 = \frac{E_0(t) + \Omega(t)}{\Delta(t)} \gg 1 = \frac{1}{N_+} |0(t)\rangle^2, \quad (4.40)$$

leading to *fidelity at the end of the driving*

$$F_{end} = \left| N_+ \left(\frac{E_0(t) + \Omega(t)}{\Delta(t)} a(t) + b(t) \right) \right|^2 \approx b^2(t), \quad (4.41)$$

therefore when t is getting close to T_f the fidelity is oscillating with frequency 4.13.

4.4.2 Final fidelity

Because the oscillations after fast parameter change in the Hamiltonian never disappear entirely, we must observe these oscillations even at the final time. *Final fidelity* (meaning the fidelity at $t = T_f$) has dependence on T_f as can be seen in Fig. 4.11. Because after the final time $T_f^{\Delta_{sc}=1} \approx 120$ the values are so small, we can observe some fine structure of the fidelity, along with numerical error artifacts.

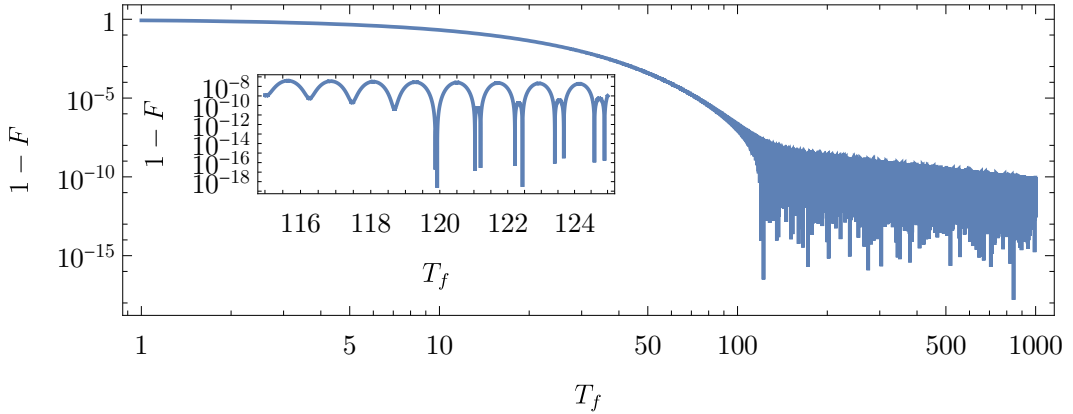


Figure 4.11: Final infidelity as a function of T_f with zoom on transitional part.

First, the numerical precision of this calculation was found to be around 10^{-13} . This means that the oscillations we see on Fig. 4.11 are of physical origin with some additional numerical error. In fact these small oscillations are the remnants of the fast excitation during close approach of energy levels, see Fig. 4.9.

Averaged final fidelity

We can eliminate the effect of oscillations by averaging over time. For that we define the *average final infidelity*

$$\langle F^* \rangle_p(T_f) := \frac{1}{(1-p)T_f} \int_{pT_f}^{T_f} F^*(t) dt. \quad (4.42)$$

It turned out that averaging over 1 % or 10 % of the driving (i.e. taking $t = 0.1$, resp. $p = 0.01$) gave approximately the same results for long enough drivings. The same result can be obtained from analytical continuation of the fidelity formula to $t \rightarrow \infty$. Even though this has no physical meaning, the analytical continuation of the harmonic oscillator solution leads to the Fidelity value around which the oscillations occur. The result of averaging can be seen on Fig. 4.12.

Using this we can describe the driving using three regimes⁴:

- *exponential/fast-driving regime* – $\langle F^* \rangle_p = \exp(-\xi T_f)$, $\xi \in \mathbb{R}^+$
- *transitional regime* – happens around *critical time* T_c .
- *polynomial/close-adiabatic regime* – $\langle F^* \rangle_p \propto T_f^{-\kappa}$ for $\kappa \in \mathbb{R}^+$.

⁴The coefficient p is assumed to be small enough not to cover the biggest oscillations after $t = T_f/2$ and big enough to average over sufficient number of oscillations. Approximately $p \in [0.6T_f, 0.999T_f]$

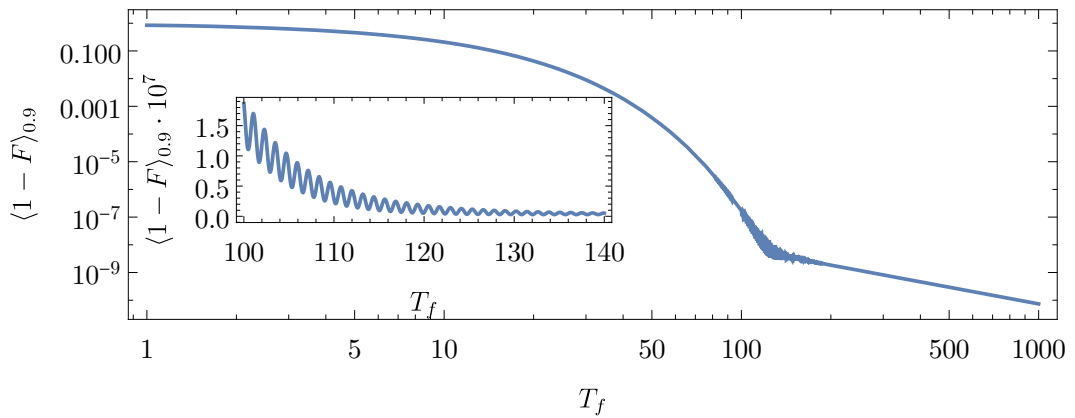


Figure 4.12: Final infidelity as a function of T_f in log-log scale with linear scaled plot inserted.

The boundary between exponential and linear regime is not strict and can be seen on Fig. 4.13, as the transition between *smooth* and *chaotic* regimes. This happens at $t = T_c$. The fine structure, see Fig. 4.14, is caused by the oscillatory character of the final fidelity. This would be smoothed out using the averaged final fidelity. The approximated dependence is

$$T_c \propto \Delta_{sc}^{-2}. \quad (4.43)$$

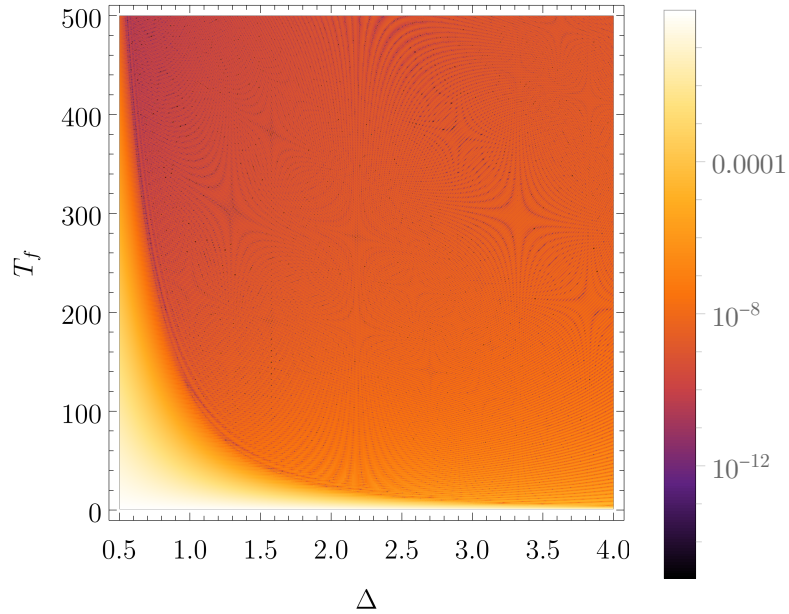


Figure 4.13: Final infidelity as a function of Δ and T_f and its three regimes. Zoomed boundary between them can be seen on 4.14.

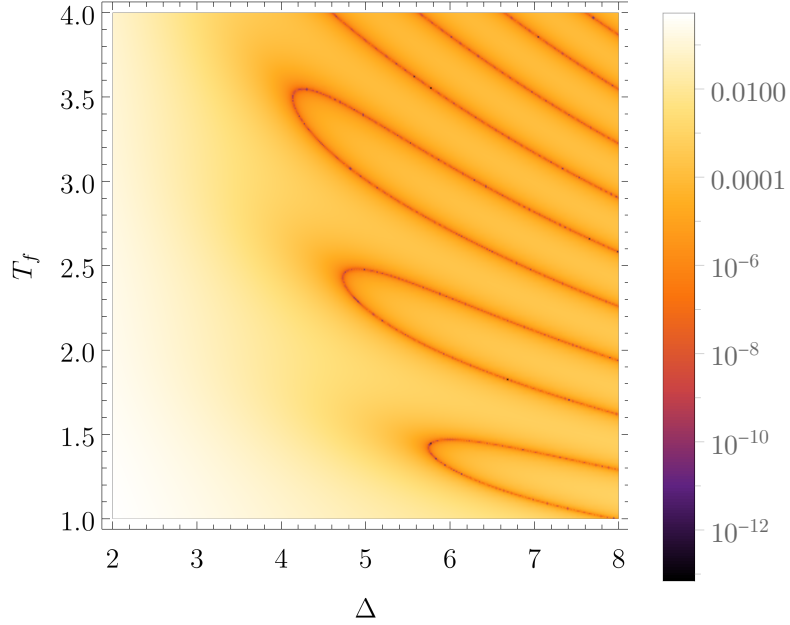


Figure 4.14: Fine structure of the boundary between fast-driving and adiabatic regimes of final infidelity.

To understand the infidelity oscillations, compare Fig. 4.15 with 4.16. Here we see two regimes, one for $t < T_c$ and on for $T > T_c$. The important observation is that in the first case it holds $F^* \neq 0$ anywhere and in the second case it touches zero periodically. The fidelity can be decomposed into a sum of two elements. Small oscillatory part, which can be explained by the theory of APT, and exponentially decreasing fidelity with final time, describable by Landau-Zener formula.

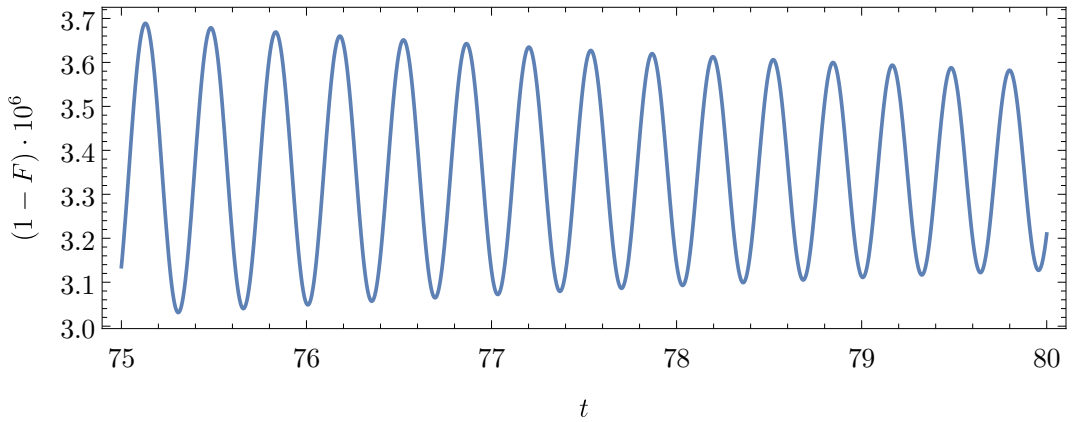


Figure 4.15: Final infidelity as a function of t for fast-driving regime, $T_f = 80 < T_c$.

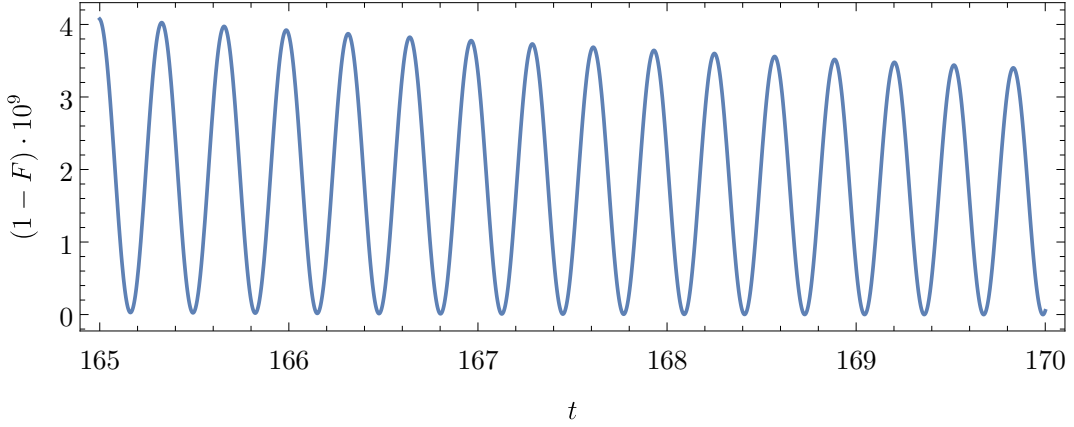


Figure 4.16: Final infidelity as a function of t for close-adiabatic regime. $T_f = 170 > T_c$

Exponential and polynomial part using Landau-Zener and APT

Landau-Zener-Stueckelberg theory provides the WKB approximation formula for the fidelity during some transport. Full form can be seen in Nakamura [2012]. In our case, only simplified theorem is needed. First let's review some definitions.

Definition 18 (Diabatic coupling). *Diabatic coupling functions are off-diagonal elements of two level Hamiltonian. At avoided crossing, it is half of Hamiltonian eigenvalue difference,*

$$A = \frac{E_2 - E_1}{2}. \quad (4.44)$$

Definition 19 (Diabatic potential). *Difference between Hamiltonian eigenvalues can be approximated by lines*

$$\Delta E \equiv E_1 - E_0 =: \alpha t \quad (4.45)$$

Diabatic potential difference is the ratio

$$|\Delta F| := \left| \frac{\alpha}{t} \right|. \quad (4.46)$$

Theorem 7 (Landau-Zener-Stueckelberg for linear driving). *For*

- *two level Hamiltonian*
- *with degeneracy in only one point,*
- *on the linear driving path in a parametric space*

the fidelity can be described for times $t \in (0, T_c)$ as

$$F = \exp \left(-\frac{2\pi A^2}{v |\Delta F|} \right), \quad (4.47)$$

for a diabatic coupling A , and diabatic potential difference $|\Delta F|$.

In our case, we have constant speed $v = 1/T_f$, off-diagonal elements are also constant $A = \Delta_{sc}$, and the driving path is symmetric along $\Omega = 0$ axis, leading to $|\Delta F| = 2\Omega_i$.

The polynomial, or chaotic regime, can be explained using APT. It holds that

$$\log(1 - F) = \log(T_f^{-2}) + \log \left(\sum_{i=1}^n |b_n^{(1)}(T_f)|^2 \right), \quad (4.48)$$

for functions $b_n^{(1)}$ from Eq. 2.43. For more detail, see [Felipe unpublished report](#).

The Equations 4.47, 4.48 can be seen in 4.17. We see that they intersect at time T_c and give the leading order in both regimes, if one omits the oscillations. In fact these two parts are not only the good approximation on both intervals, but if added together, they represent the whole fidelity curve with very high precision. It might not give a good mathematical meaning to add these two solutions together. But because the APT gives the infidelity of order 10^{-9} , it creates negligible error. The advantage is that by this process one gets an approximation for the transitional regime.

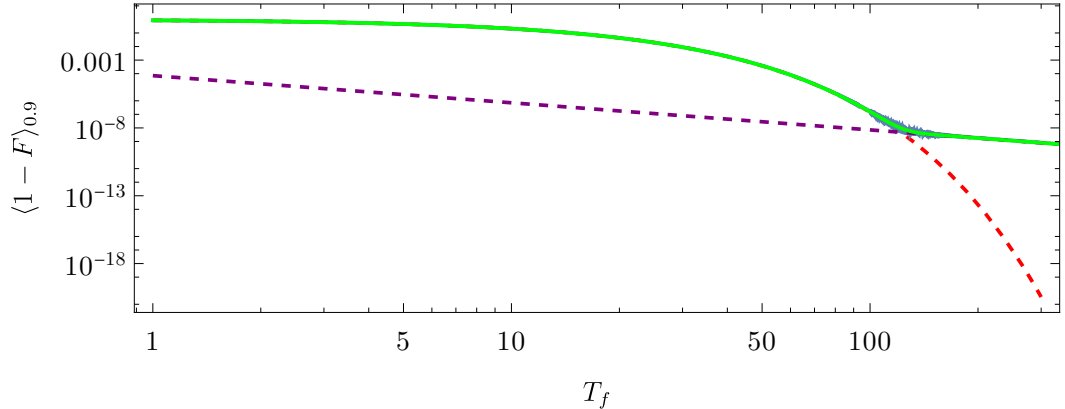


Figure 4.17: Fidelity as a function of driving final time, approximated by the **sum** (green) of **Landau-Zener** (red, dashed) and **APT** (purple, dashed)

4.4.3 Summary

Now we should understand all results separately, let's put it all together. On Fig. 4.18 we see some of the most important results.

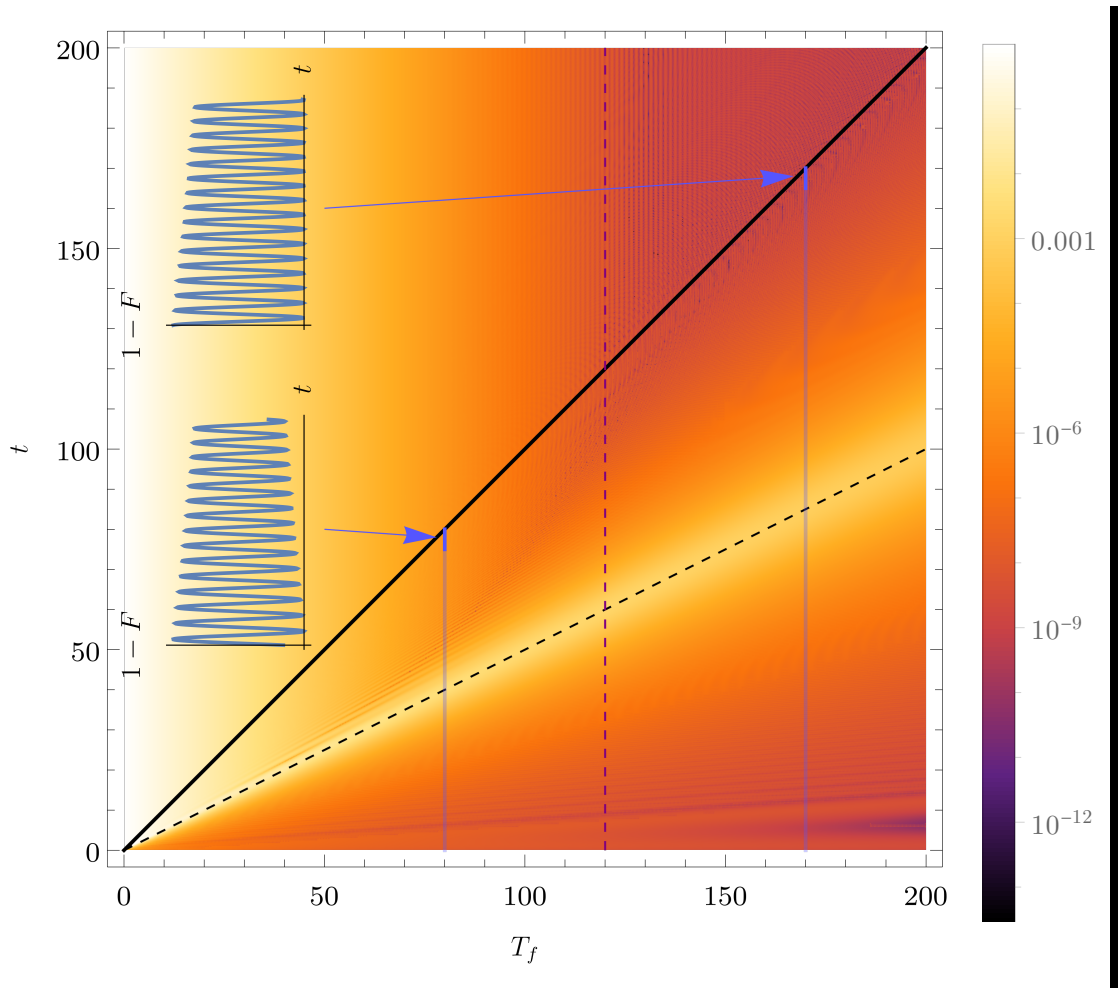


Figure 4.18: Fidelity dependence for linear driving with $\Delta = 1$. Black line marks $t = T_f$, dashed black line $t = T_f/2$ and **purple** dashed line is the approximate value of T_c . **Blue** lines marks driving from Fig. 4.15, 4.16, visualizing the final times of the driving.

4.4.4 Energy variance

Energy variance for the linear driving case can be seen on Fig 4.19, as a function of time and final time. Ω and final time. Why is it almost the same as fidelity of geodesical driving???

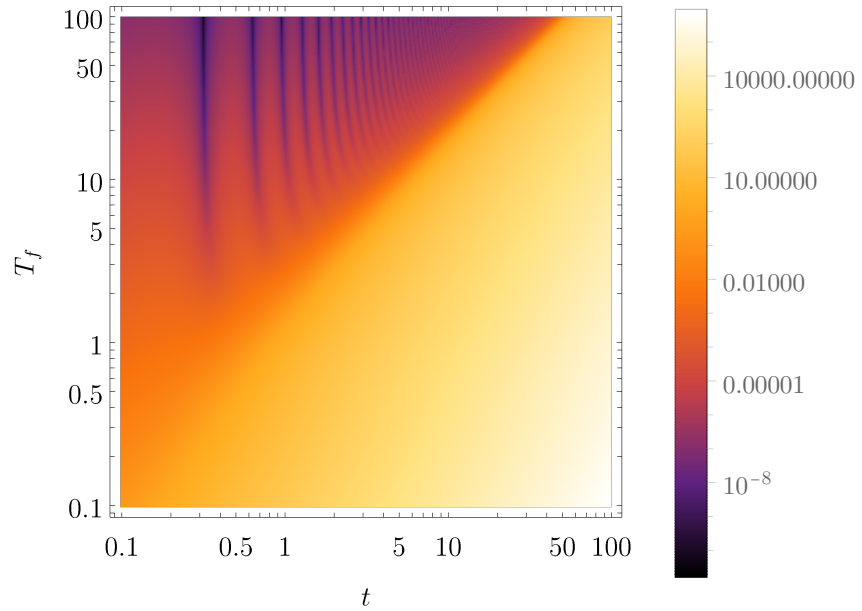


Figure 4.19: Energy variance for $\Delta_{sc} = 0.2$ for linear driving. Note that only $t < T_f$ has physical meaning.

5. Lipkin-Meshkov Glick model

The Lipkin-Meshkov Glick model is a simple model manifesting the quantum phase transitions. The aim of this chapter is to understand the properties of the ground state and see its influence on different driving protocols.

The model is defined by Hamiltonian

$$\hat{H} = \hat{J}_3 + \lambda \hat{V}_1 + \chi \hat{V}_2 + \chi^2 \hat{V}_3, \quad (5.1)$$

where

$$\hat{V}_1 = -\frac{1}{2j} \hat{J}_1^2 \quad (5.2)$$

$$\hat{V}_2 = -\frac{1}{2j} [\hat{J}_1(\hat{J}_3 + j\mathbb{1}) + (\hat{J}_3 + j\mathbb{1})\hat{J}_1] \quad (5.3)$$

$$\hat{V}_3 = -\frac{1}{2j} (\hat{J}_3 + j\mathbb{1})^2. \quad (5.4)$$

Using the Spherical harmonics basis $\{|j, m\rangle\}$ for quantum numbers j as the angular momentum and m its projection on the direction of \hat{J}_3 and defining

$$\hat{J}_{\pm} := \frac{1}{2}(\hat{J}_1 \pm i\hat{J}_2), \quad (5.5)$$

we get the matrix elements

$$\langle j'm' | \hat{J}^2 | jm \rangle = j(j+1)\delta_{j'j}\delta_{m'm} \quad (5.6)$$

$$\langle j'm' | \hat{J}_3 | jm \rangle = m\delta_{j'j}\delta_{m'm} \quad (5.7)$$

$$\langle j'm' | \hat{J}_{\pm} | jm \rangle = \sqrt{(j \mp m)(j \pm m + 1)}\delta_{j'j}\delta_{m'm\pm1}, \quad (5.8)$$

where $\delta_{a'b}$ is Kronecker delta. The Hamiltonian in Eq. 5.1 can be written as

$$\begin{aligned} \hat{H} = & J_3 - \frac{\lambda}{8j}(J_+ + J_-)^2 - \frac{\chi}{4j} [(J_+ + J_-)(J_3 + j\mathbb{1}) + (J_3 + j\mathbb{1})(J_+ + J_-)] \\ & - \frac{\chi^2}{2j} (J_3 + j\mathbb{1})^2, \end{aligned} \quad (5.9)$$

which has pentadiagonal matrix representation. During the whole paper, $j = N/2$ will be used.

5.1 Special cases

Because of pentadiagonal character of the Hamiltonian, the discussion will start at $N = 3$, followed by $N = 5$. Then the limit $N \rightarrow \infty$ will be taken along with the generalization of some characteristics to an arbitrary dimension.

Due to the complexity of our Hamiltonian, it is not possible to prove every statement analytically. Some numerical methods, supported by some basic theorems, are needed.

5.1.1 Case $N = 3$

The lowest dimension behaving similarly to higher N is 3 with the matrix represented Hamiltonian

$$\hat{H} = \begin{pmatrix} -\frac{\lambda+6}{4} & -\frac{\chi}{2\sqrt{3}} & -\frac{\lambda}{2\sqrt{3}} & 0 \\ -\frac{\chi}{2\sqrt{3}} & \frac{(-7\lambda-4\chi^2-6)}{12} & -\chi & -\frac{\lambda}{2\sqrt{3}} \\ -\frac{\lambda}{2\sqrt{3}} & -\chi & \frac{(-7\lambda-16\chi^2+6)}{12} & -\frac{5\chi}{2\sqrt{3}} \\ 0 & -\frac{\lambda}{2\sqrt{3}} & -\frac{5\chi}{2\sqrt{3}} & -\frac{\lambda}{4} - 3\chi^2 + \frac{3}{2} \end{pmatrix}. \quad (5.10)$$

The spectrum of this Hamiltonian can be calculated analytically using some complex functions $D, E, F, G : \mathbb{C} \rightarrow \mathbb{C}$, see Appendix A, as

$$E_0 = \frac{1}{12} \left(G - F - \frac{\sqrt{D - E}}{2} \right) \quad (5.11)$$

$$E_1 = \frac{1}{12} \left(G - F + \frac{\sqrt{D - E}}{2} \right) \quad (5.12)$$

$$E_2 = \frac{1}{12} \left(G + F - \frac{\sqrt{D + E}}{2} \right) \quad (5.13)$$

$$E_3 = \frac{1}{12} \left(G + F + \frac{\sqrt{D + E}}{2} \right). \quad (5.14)$$

Eigenvectors can also be written analytically, but doing it here would be redundant. On sections $\lambda = 1$ and $\chi = 1$, see Figures 5.1 resp. 5.2, it can be seen the general behavior of the spectrum, where the energies get close to each other somewhere around the center of our coordinate system $(\lambda; \chi)$ and then separate monotonously to never meet again. In addition, the spectrum is symmetrical for $\chi \leftrightarrow -\chi$.

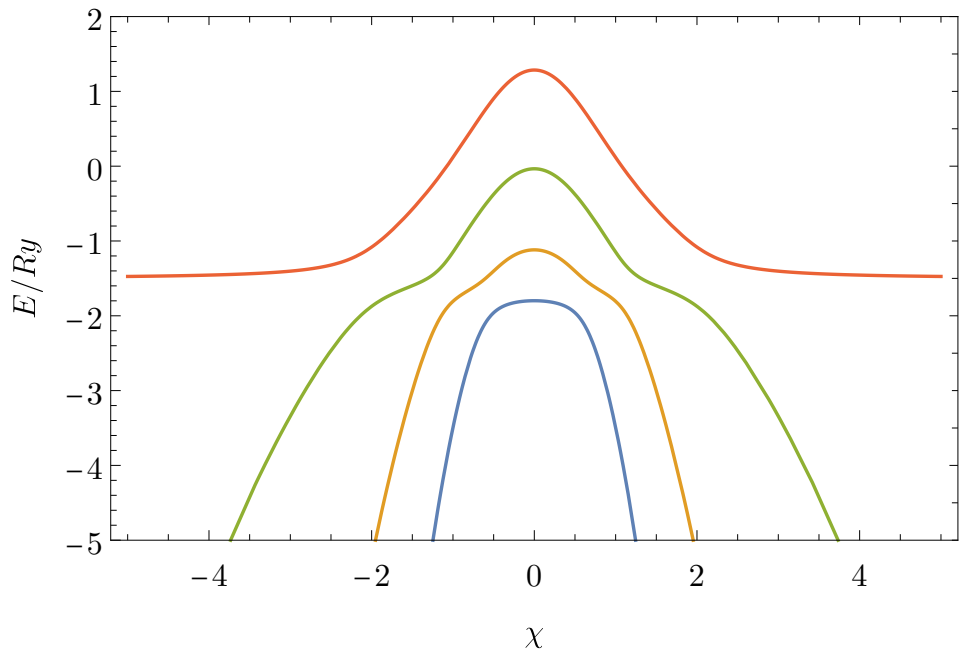


Figure 5.1: Energy for the case $N = 3$, section $\lambda = 1$

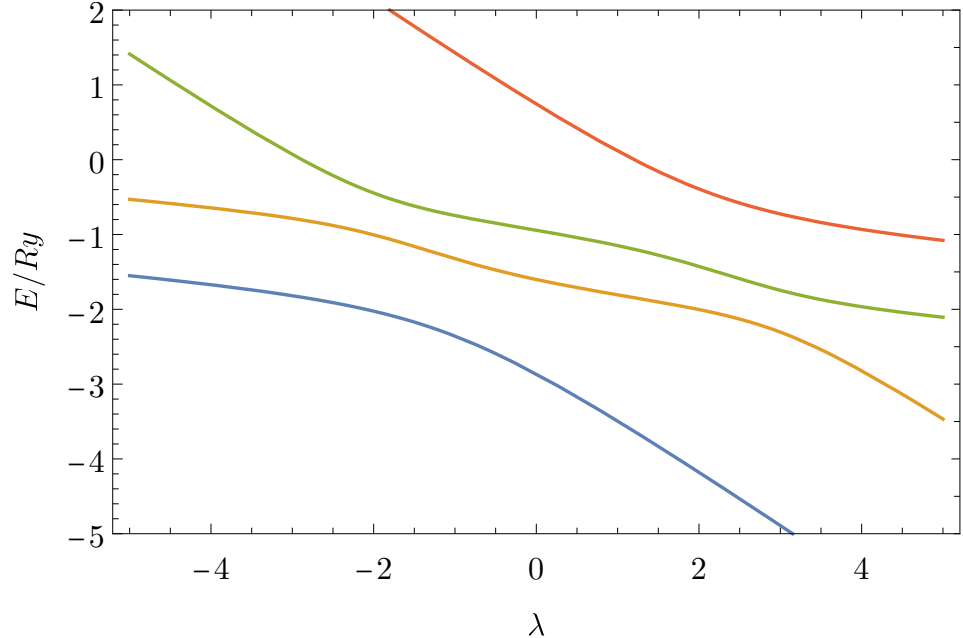


Figure 5.2: Energy for the case $N = 3$, section $\chi = 1$

From the Equations 5.11, 5.12 can be seen that there might exist degeneracy between every two neighboring energy levels¹. Specifically, for $E_0 = E_1$ for $D = E$, which for real values λ , χ has two solutions

$$(\lambda_d, \pm\chi_d) = \left(-\frac{1}{2}; \sqrt{\frac{3}{5}} \right).$$

Point-like characteristics correspond to Theorem 2, which states that Hamiltonian driven by two real parameters can be degenerated only on 0-dimensional manifolds.

If the energy spectrum is degenerate and the metric tensor diverges, see individual elements in Fig. 5.3, its determinant also diverges, as shown in Fig. 5.4, along with Christoffel symbols in Fig. 5.5. Note that the metric tensor determinant is positive definite, thus the manifold is Riemannian. Further on, it reflects the symmetry $\chi \leftrightarrow -\chi$, except for elements g_{12} , Γ_{121} , Γ_{211} , and Γ_{222} , which switch their sign.

¹If the functions D, E, F, G were real numbers, degeneracies would exist between every two neighboring energy levels. Because they are complex, the solution $E_i = E_j$ might not exist. Even though we will see that it's probably not that case and degeneracy exist between every two neighboring energy levels.

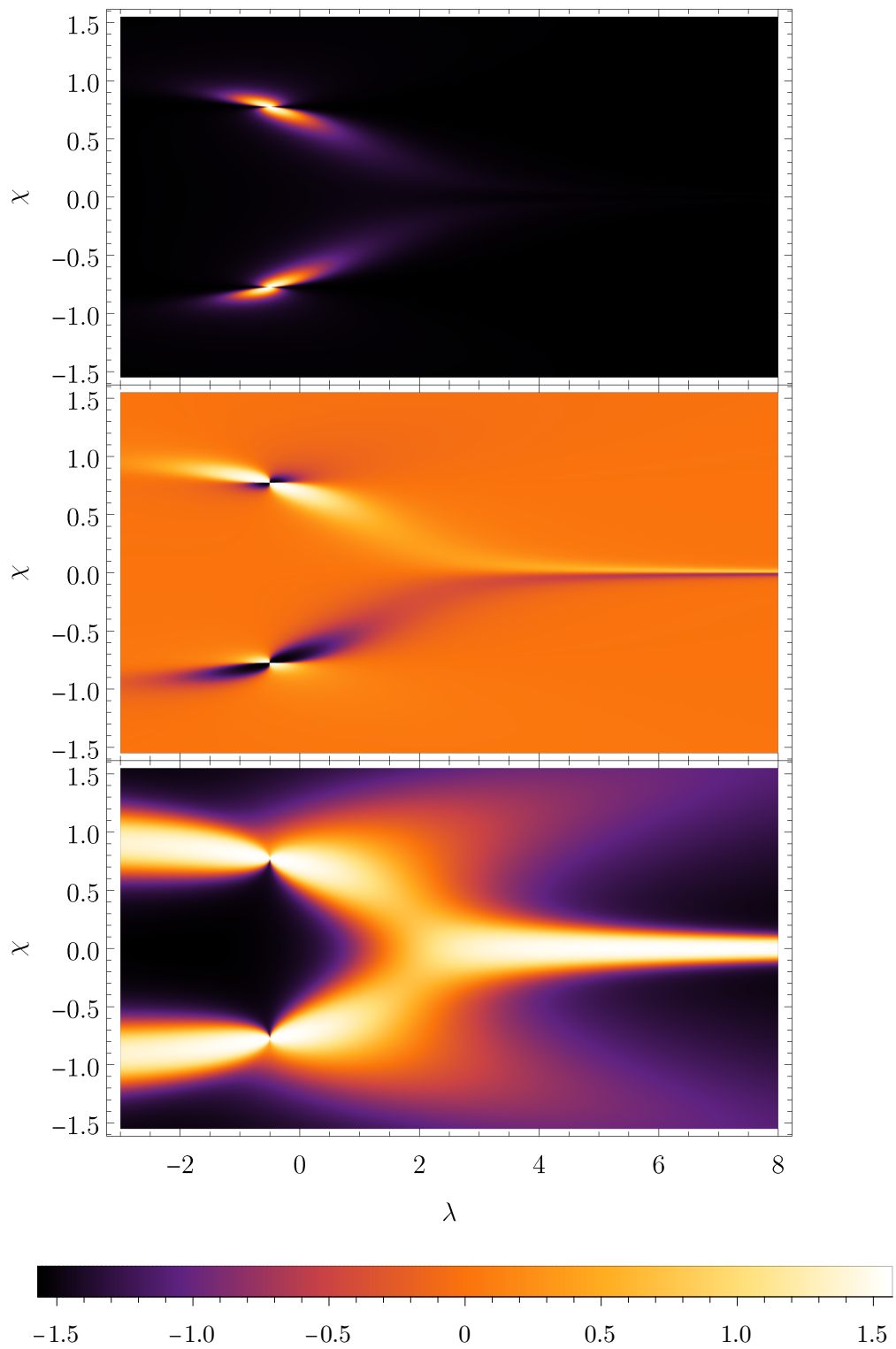


Figure 5.3: Arctangent of the metric tensor elements for the case $N = 3$ in the parametric space. From the top: $\arctan(g_{11})$, $\arctan(g_{12}) = \arctan(g_{21})$, $\arctan(g_{22})$

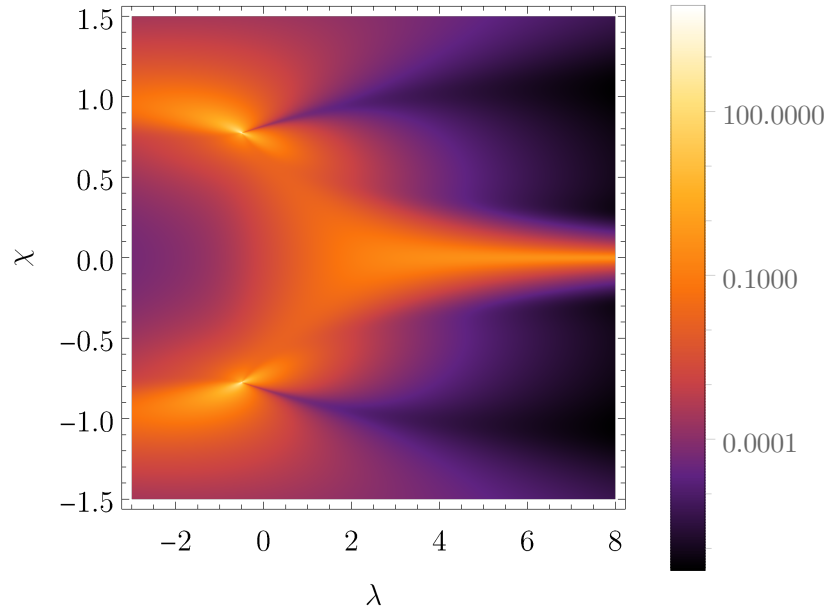


Figure 5.4: Ground state metric tensor determinant in a parametric space for $N = 3$.

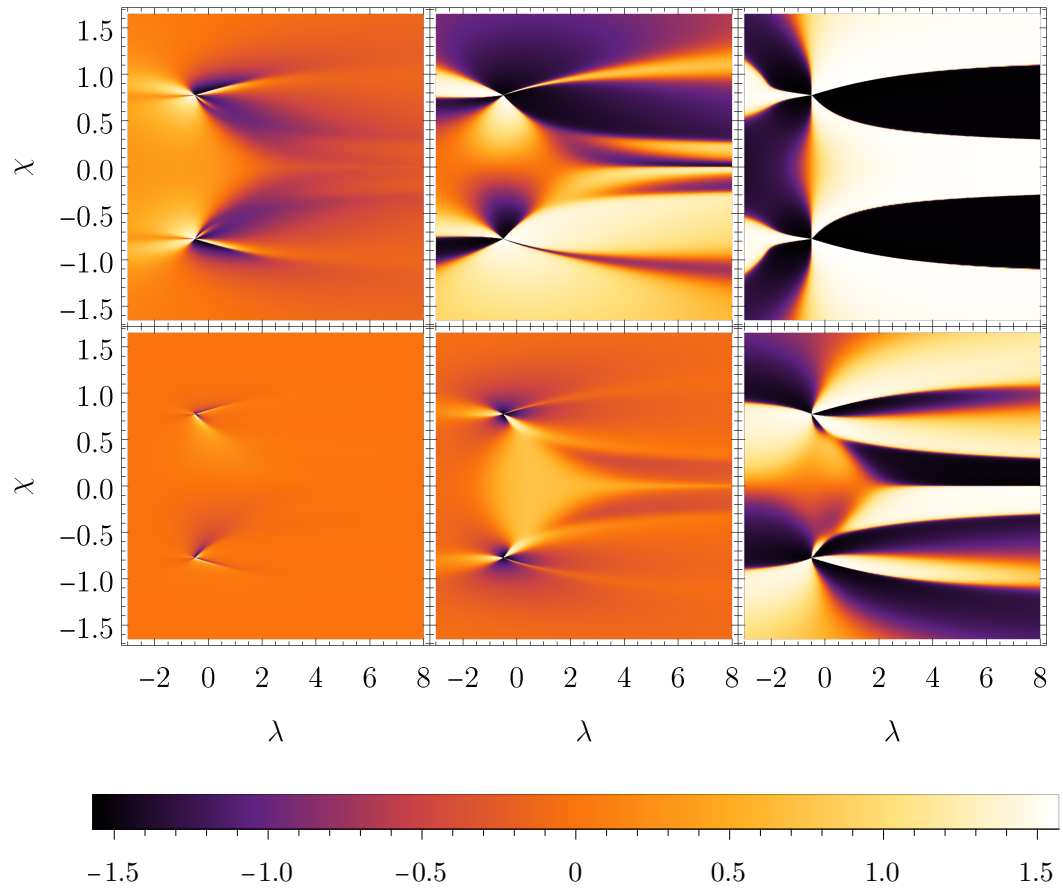


Figure 5.5: Arctangent of the ground state Christoffel symbols for the case $N = 3$. First row from left: $\arctan(\Gamma_{111})$, $\arctan(\Gamma_{121})$, $\arctan(\Gamma_{122})$. Second row from left: $\arctan(\Gamma_{211})$, $\arctan(\Gamma_{221})$, $\arctan(\Gamma_{222})$.

Due to the metric tensor degeneracy, the space is not geodesically maximal. To see that the singularity is not the only *coordinate one*², the Ricci scalar can be calculated, see Fig. 5.6. Divergent Ricci scalar implies the existence of a *physical singularity*. This can be seen from the sections in χ -direction drawn in Fig. 5.7, which at coordinate $(\lambda_d; \chi_d)$ diverges. This implies the singularity is *physical*.

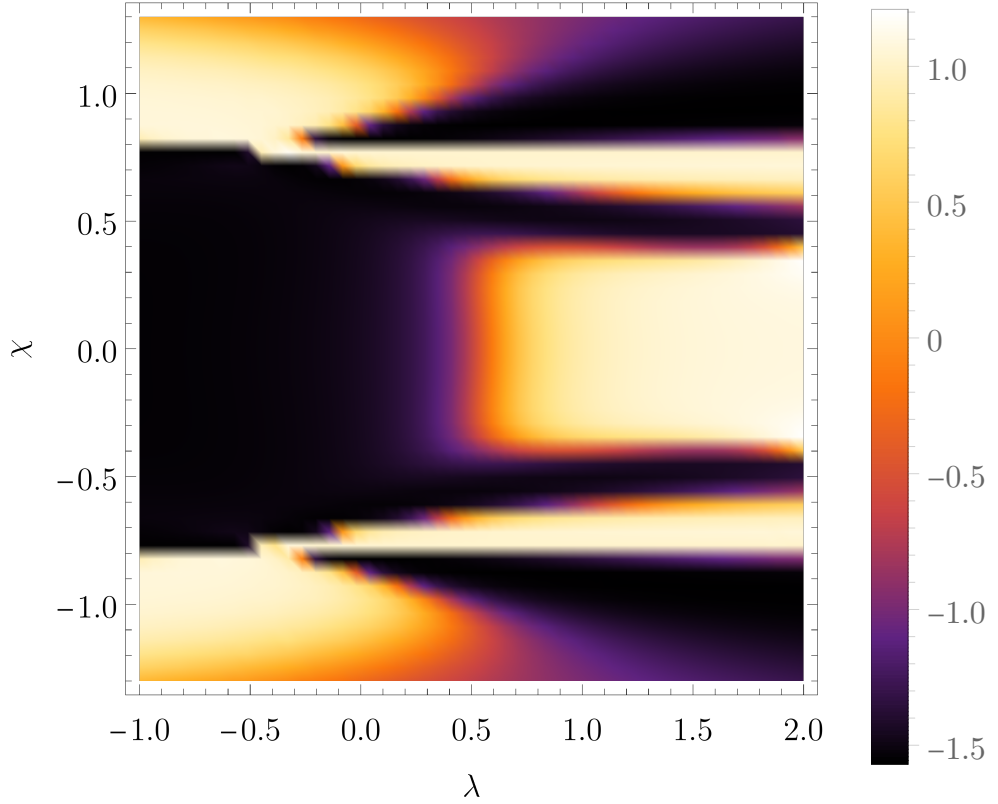


Figure 5.6: Arctangent of Ricci curvature for the case $N = 3$. increase the resolution

²Coordinate singularity is present only in some coordinates. This is different from so-called *physical singularity*, which is present in every choice of the coordinate system.

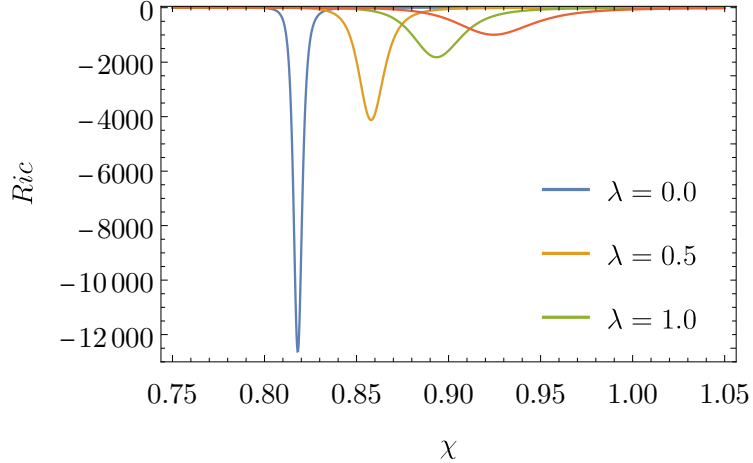


Figure 5.7: Ricci's curvature sections for three different λ .

Some of the system characteristics can be seen from geodesics. *Initial valued Geodesics* are solutions to

$$(\lambda(T_i); \chi(T_i)) =: (\lambda_i; \chi_i) \in \mathbb{R}^2$$

$$\left(\frac{d\lambda(t)}{dt}; \frac{d\chi(t)}{dt} \right) \Big|_{T_i} =: (\lambda'_i; \chi'_i) \in \mathbb{R}_+^2,$$

where T_i is *initial time*, typically 0.

We might also choose *boundary valued geodesics* with fixed initial $(\lambda(0); \chi(0))$ and final position $(\lambda(T_f); \chi(T_f))$. Because the shape of geodesics in parametric space does not depend on the initial derivative, it does not depend on the speed of driving in the parametric space. Initial valued geodesics are therefore more advantageous to calculate, because they have only two free parameters - the initial coordinate $(\lambda; \chi)$. Another reason is purely numeric, because the boundary valued geodesics are calculated by numerous evolutions of initial valued geodesics with response initial parameter tweaking. This makes the calculations slower (in our case they were 10 to 100 times slower).

Results for the geodesics starting at $(\lambda_i; \chi_i) = (0; 0)$, $(\lambda', \chi') = (\cos \theta; \sin \theta)$ can be seen in Fig. 5.8. Other values θ result in a close approach of the geodesics to the singularity, making the calculations numerically unstable. The fact that geodesics lean towards singularities is well known from the theory of General Relativity (GR). The main difference here is that our "test particle" seems to be partially repulsed by the singularity. The analogy with GR would therefore fail because of the nonexistence of negative mass and gravitational dipoles. The better analogy would be electromagnetism, which has a downside in the fact that the geometrical formalism is not used so much in this theory. Comparison of those two intuitive examples can be seen in Fig. 5.9. The geodesic behavior is not caused only by the singularity but also by a large Ricci curvature leaning to the right from it. This means that the distance across this *unreachable gap*, marked by blue line in Fig. 5.8, is also large. This leads to the strong tendency of geodesics to go around the singularity rather than crossing it. The presence of singularities means that our ground state manifold is geodesically incomplete and

according to Theorem 4 there exist some geodesically unreachable coordinates. From this goes the term *unreachable gap*.

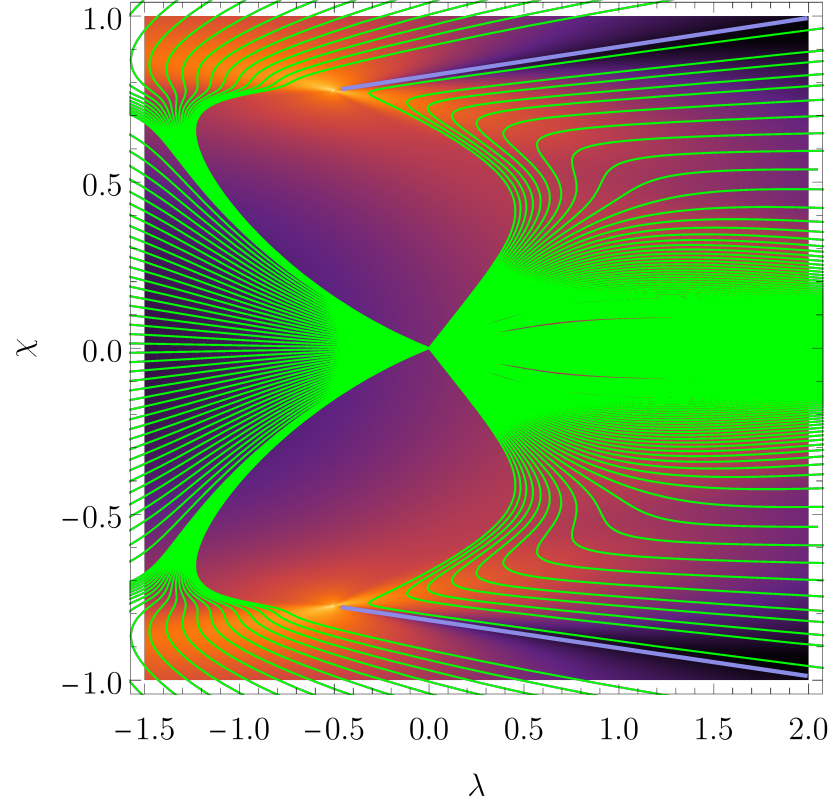


Figure 5.8: **Geodesics** for the case $N = 3$ starting from $(\lambda_i; \chi_i) = (0; 0)$ with $(\lambda'_i; \chi'_i) = (\cos \theta; \sin \theta)$, parametrized by angle $\theta \in [-0.63; 0.63]$, $\theta \in [\pi - 0.225; \pi + 0.225]$, with step $\Delta\theta = 0.01$. **Blue** line marks the high Ricci curvature gap.

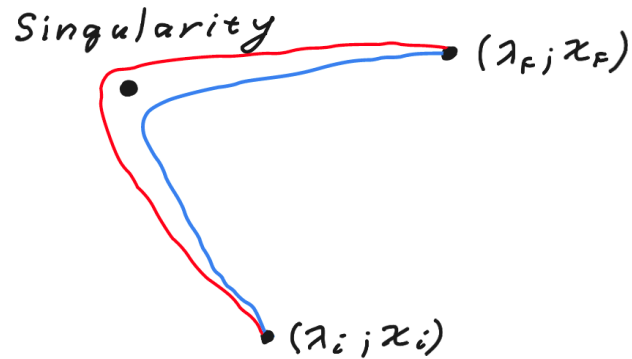


Figure 5.9: Comparing geodesics with **repulsing** (blue) and **attracting** (red) metric tensor divergence in the spherically symmetrical space.

5.1.2 Case $N = 5$

Another special case is $N = 5$. From analysis of the energy levels, we see that there are more degeneracies, see Fig. 5.10. One can see that only $E_0 = E_1$

the degeneracy lies on the separatrix and all others are distributed around. The $\chi \leftrightarrow -\chi$ symmetry holds for all of them.

Another fact, which is good to realize, is how the space itself looks like. This is best seen from the metric tensor determinant, fig. 5.11.

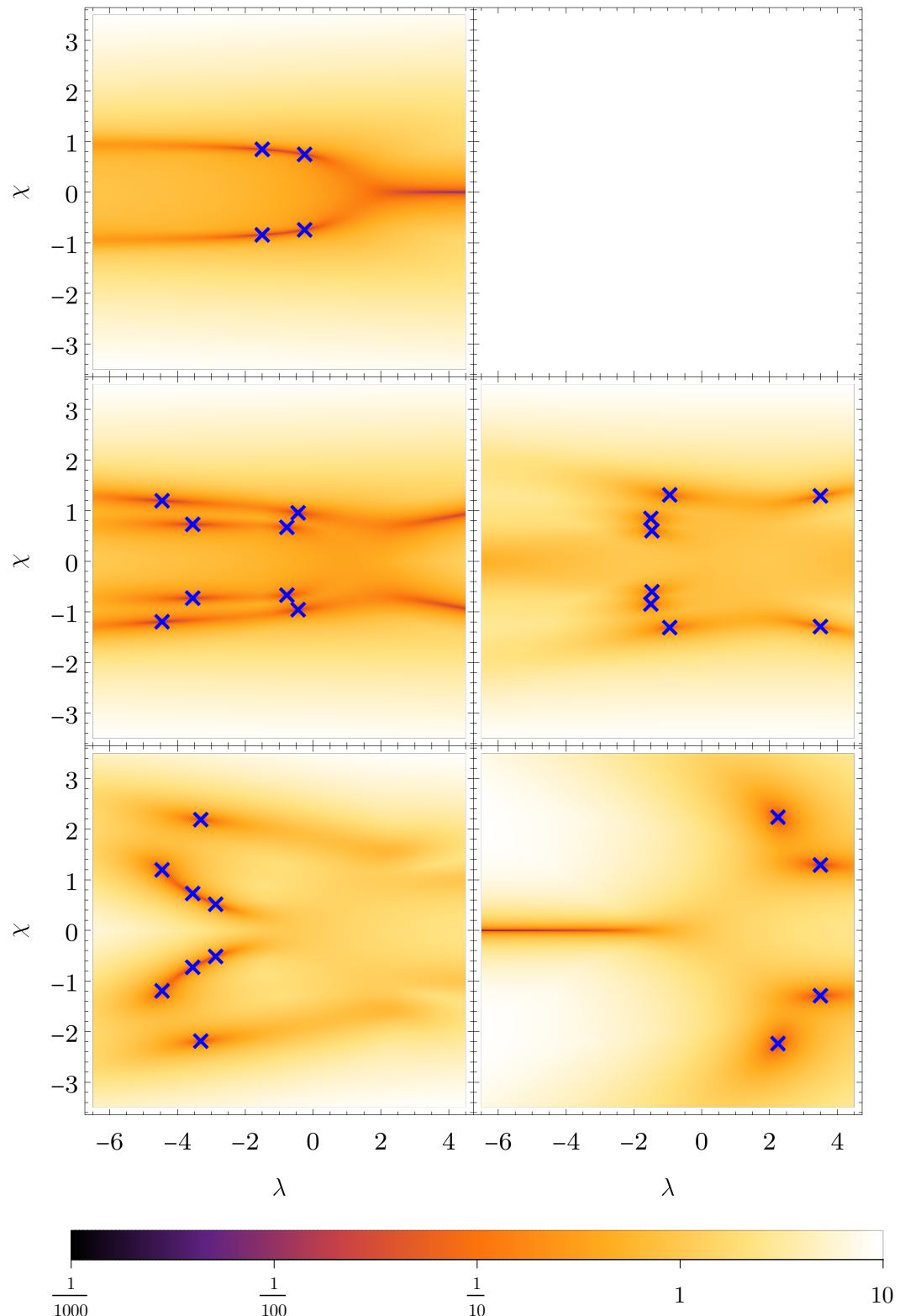


Figure 5.10: Energy differences between neighboring energy levels for $N = 5$. First row: $E_1 - E_0$, second row: $E_2 - E_1$, $E_3 - E_2$, third row: $E_4 - E_3$, $E_5 - E_4$. Spectra degeneracies are marked with blue cross.

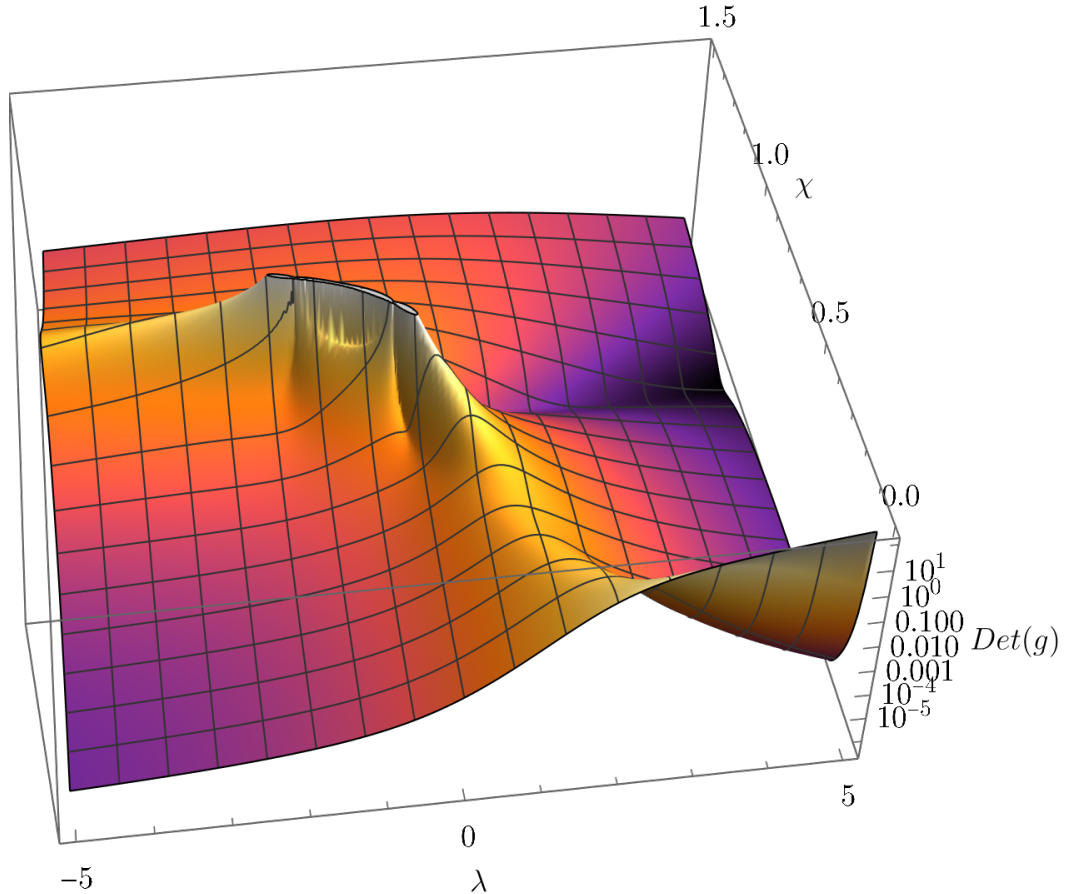


Figure 5.11: Metric tensor determinant for the case $N = 5$.

Geodesics for the case $N = 5$ starting from the point $(0; 0)$ have the characteristics already seen in the case $N = 3$. However, when starting at $(\lambda; \chi) = (1; 0)$, the behavior around the singularity is not the only interesting thing happening. As can be seen in Fig. 5.12, the geodesics tend to deflect themselves from the area with high curvature around the axis $\chi = 0$, which happens even for other initial conditions, just that for $(0; 0)$ it is not so apparent. Small irregularity can be seen in Fig. 5.8 around $(0.5; 0.1)$. This implies that the geodesic equation might have at least two solutions as candidates for the globally shortest path between two points.³

³One might recall the effect of gravitational lensing here. In the presence of any mass in the spacetime, there exists more possible light paths (solutions to the geodesic equation) between two points, differing by the initial condition.

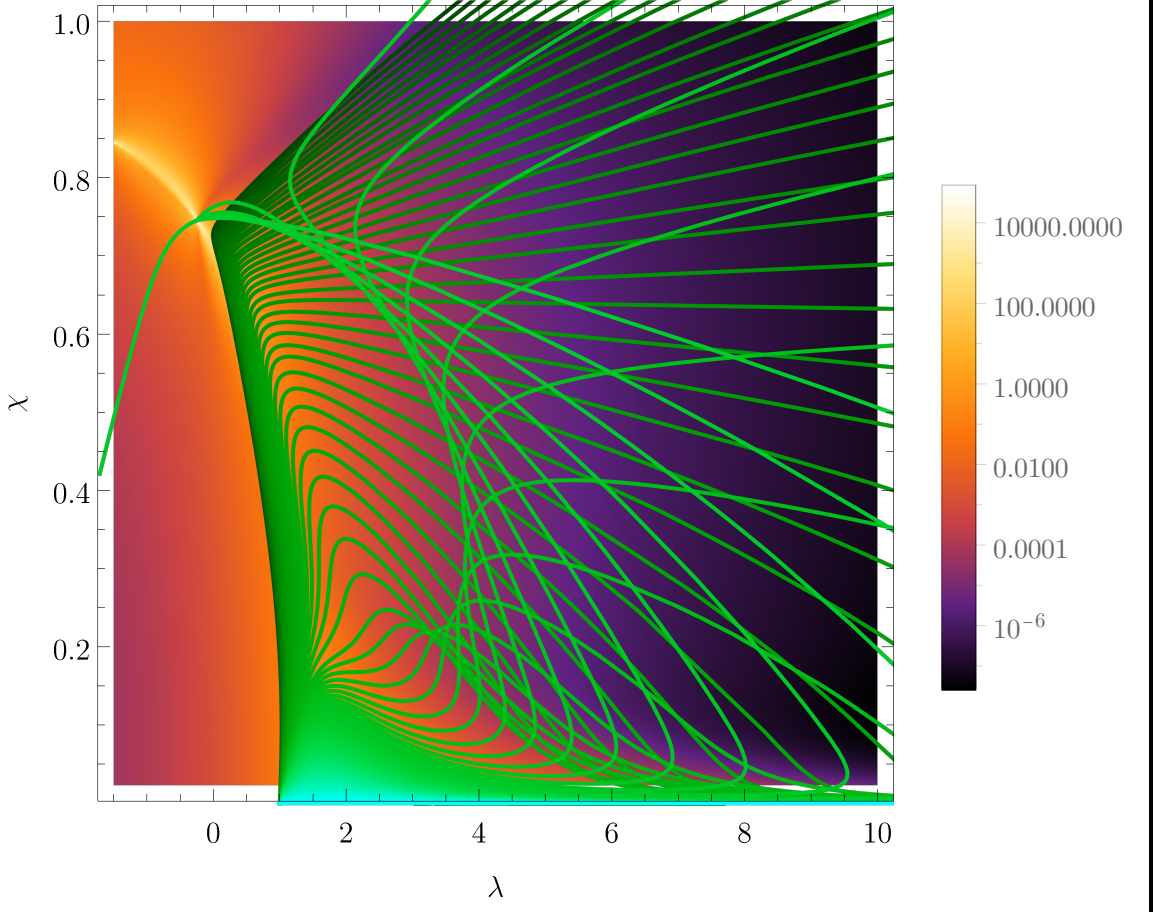


Figure 5.12: Geodesics for the case $N = 5$, starting from the point $(1; 0)$. *The numerics around the singularity breaks down, but the solution is close to the drawn one, i.e. they will pass close to the singularity and continue to the left.*

5.1.3 Limit $N \rightarrow \infty$

The limit $N \rightarrow \infty$ can be applied to the Hamiltonian in Eq. 5.1 using Holstein-Primakoff mapping for bosonic operators

$$\mathcal{H} := \lim_{j \rightarrow \infty} \frac{\hat{H}}{2j}, \quad (5.15)$$

resulting in classical Hamiltonian

$$\begin{aligned} \mathcal{H}(x, p) = & -\frac{1}{2} + \frac{1-\lambda}{2}x^2 + \frac{\lambda-\chi^2}{4}x^4 - \frac{\chi x^3}{2}\sqrt{2-x^2-p^2} - \frac{\chi^2}{4}p^4 \\ & + \frac{p^2}{4} \left[2 + (\lambda - 2\chi^2)x^2 - 2\chi x\sqrt{2-x^2-p^2} \right]. \end{aligned} \quad (5.16)$$

Finding derivatives minima, we get the *separatrix*

$$\chi^2 = \frac{\lambda - 1}{\lambda - 2}, \quad (5.17)$$

which represents the phase transition in the limit $N \rightarrow \infty$. In our case, the transition is of first order everywhere, except in $(\lambda; \chi) = (1; 0)$, where it has order

two. The separatrix is shown in Fig. 5.13 compared to minimum between the ground state and the first excited state $E_1 - E_0$ for $N = 3$ case. With increasing N , it converges to the separatrix line.

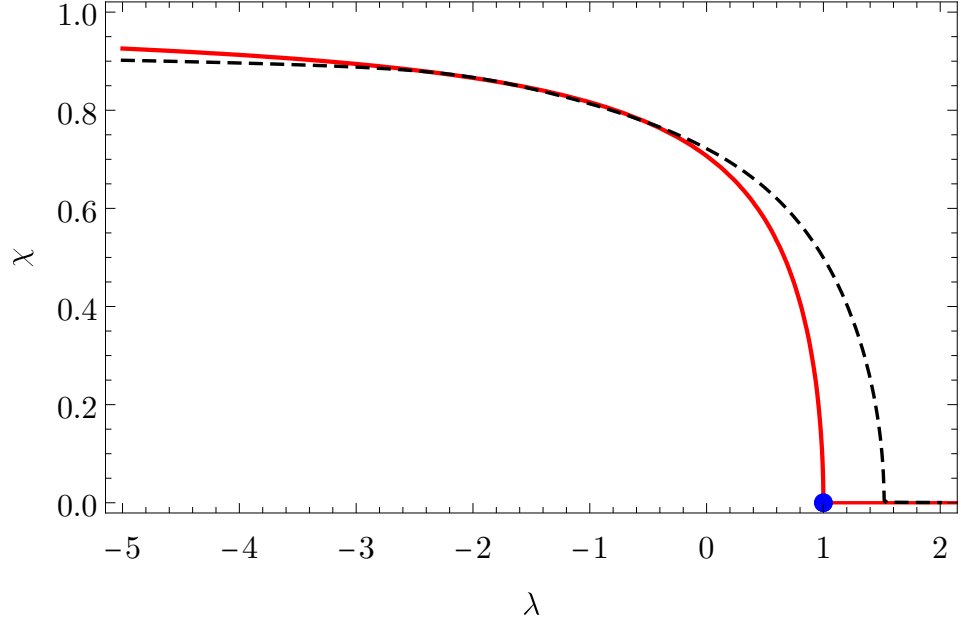


Figure 5.13: First order phase transition, the Separatrix (red), second order transition (blue point) compared to minimum between the ground state and first excited state in $N=3$ case (black, dashed).

5.2 General behavior

For higher dimensions we see the same characteristic behaviour in the energy spectrum sections, see the example in Fig. 5.14, 5.15 for the $N = 10$ case. Between all energy levels there is at least one avoided crossing and between zeroth and the first there are $N - 2$ crossings for N odd and $N - 3$ for N even, which holds up to dimension $N = 10$. Proving this generally is not an easy task, because the singularities might not exist on the real axis.

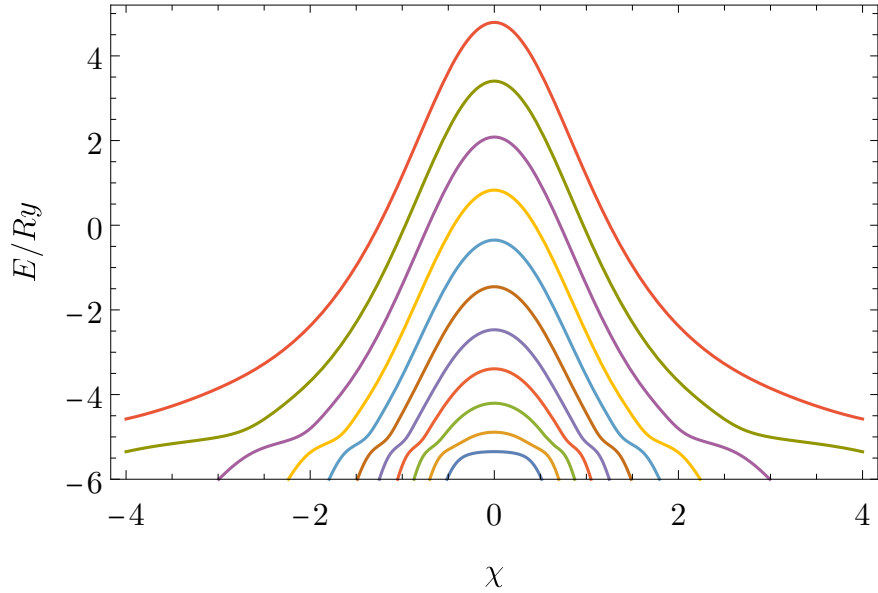


Figure 5.14: Energy spectrum as function of χ , for $\lambda = 1$ and $N = 10$.

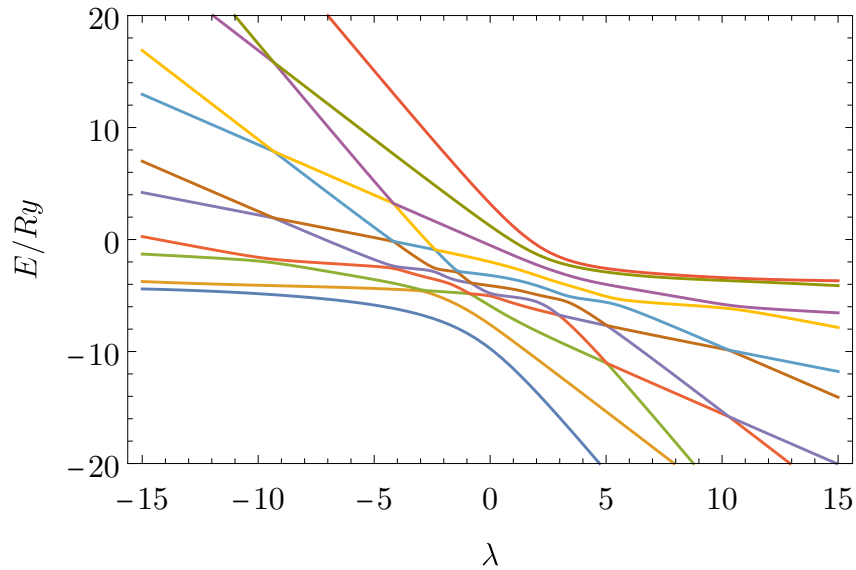


Figure 5.15: Energy spectrum as a function of λ , for $\chi = 1$ and $N = 10$.

Special attention was given to the spectrum degeneracies between the zeroth and the first energy level, because those influence the metric tensor and geodesics. Their exact calculation is numerically costly, and only the first few cases, namely, $N \in \{3, 4, 5, 6, 7\}$, were calculated, see Tab. 5.1.

N	$(\lambda_l; \pm \chi_l)$	$(\lambda_2; \pm \chi_2)$	$(\lambda_r; \pm \chi_r)$
3	$(-\frac{1}{2}; \sqrt{\frac{3}{5}})$		
4	$(-3; \sqrt{\frac{4}{5}})$		$(-\frac{1}{3}; \sqrt{\frac{4}{7}})$
5	$(-\frac{3}{2}; \sqrt{\frac{5}{7}})$		$(-\frac{1}{4}; \sqrt{\frac{5}{9}})$
6	$(-5; \sqrt{\frac{6}{7}})$	$(-1; \sqrt{\frac{2}{3}})$	$(-\frac{1}{5}; \sqrt{\frac{6}{11}})$
7	$(-\frac{5}{2}; \sqrt{\frac{7}{9}})$	$(-\frac{3}{4}; \sqrt{\frac{7}{11}})$	$(-\frac{1}{6}; \sqrt{\frac{7}{13}})$

Table 5.1: Singularities between the zeroth and first energy levels for dimensions 3–7. Subscript $l(r)$ means the most *left(right)-wise* positioned coordinates in the (λ, χ) -plot.

From the singularity behavior in low dimensions, one might see the pattern for (λ_l, χ_l) and (λ_r, χ_r) , i.e., those with minimal, resp maximal λ coordinate is

$$(\lambda_l; \pm \chi_l) = \begin{cases} \left(1 - \frac{N}{2}; \sqrt{\frac{N}{N+2}}\right) & , N \geq 3, N \text{ is odd} \\ \left(1 - N; \sqrt{\frac{N}{N+1}}\right) & , N \geq 3, N \text{ is even} \end{cases} \quad (5.18)$$

$$(\lambda_r; \pm \chi_r) = \left(\frac{1}{1-N}; \sqrt{\frac{N}{2N-1}} \right) \quad , N \geq 3. \quad (5.19)$$

Those were numerically proven to be singularities for cases up to $N = 1000$.

Dimensions 3 to 10 are shown in Fig. 5.16. In addition, the degeneracies between the zeroth and the first energy levels belong to the separatrix described by Eq. 5.17. Due to this, the position of the singularities is constrained to the *second order phase transition line* between points $(\lambda_l, \pm \chi_l)$ and $(\lambda_r, \pm \chi_r)$.

In the limit $N \rightarrow \infty$ they converge to

$$\lim_{N \rightarrow \infty} (\lambda_l; \pm \chi_l) = (-\infty, 1)$$

$$\lim_{N \rightarrow \infty} (\lambda_r; \pm \chi_r) = \left(0, \frac{1}{\sqrt{2}}\right).$$

This means that for $N \rightarrow \infty$, the separatrix is covered by singularities on $\lambda < 0$.

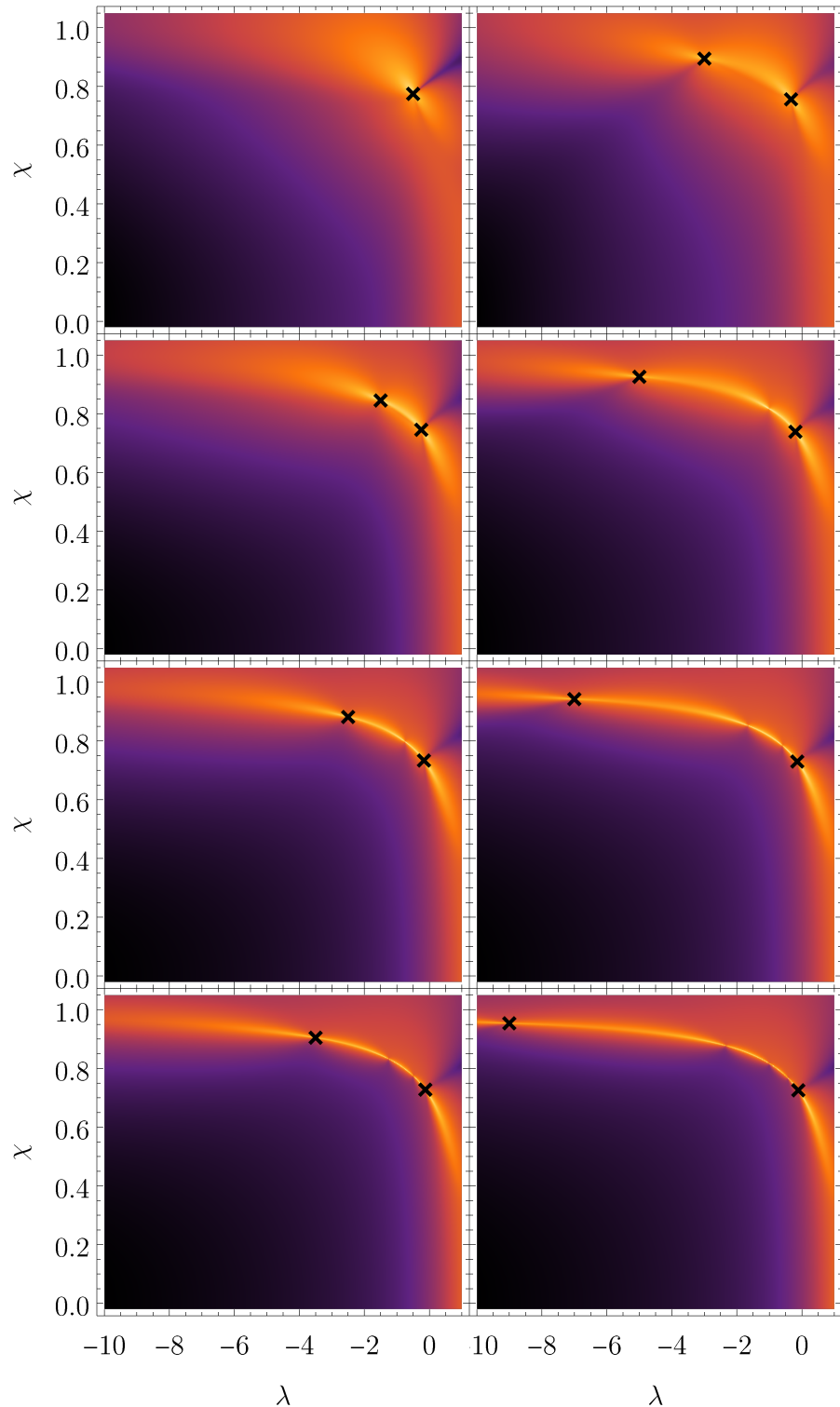


Figure 5.16: Spectrum degeneracies between E_0 and E_1 . Hamiltonian dimensions are 1,3,5,7 in the first column and 2,4,6,8 in the second column. Black crosses mark most left-wise and right-wise singularity and the background corresponds to the metric tensor determinant. Other singularities are also well visible in the determinant.

6. Driving on the ground state manifold

Of special importance in theory of the ground state manifold are geodesics. It is not yet clear what role they have in general, but there are a few known cases in which they play a particular role. As was mentioned in chapter 2.8, one method to achieve low driving fidelity is *path variation*. This means *finding the best possible driving path*. One might say that the ground state manifold geodesics are a good candidate for this path, because they minimize the distance. The problem is that general fidelity driving does not happen on any state manifold and this premise cannot be used. The natural question is: "what types of drivings have minimal fidelity on geodesics?"

Minimizing the distance on state manifolds

Let's have a geodesic $\mathcal{G}(t)$ and some curve $\gamma(t)$ on the ground stat manifold, spanning between points $P_i, P_f \in \mathcal{U}$ during some time T_f , meaning

$$\mathcal{G}(0) = \gamma(0) = P_i \in \mathcal{U}, \quad \mathcal{G}(T_f) = \gamma(T_f) = P_f \in \mathcal{U}.$$

Excitation amplitude during infinitesimal quench is ds , therefore $\sum_i \Delta s_i$ summed along path $\gamma(t)$ is the amplitude of transport along that path. This can be more rigorously expressed by functional

$$s_\gamma = \int_{\gamma(t)} ds = \int_0^{T_f} \sqrt{g_{\mu\nu} \dot{\lambda}^\mu \dot{\lambda}^\nu} dt \quad (6.1)$$

This is the entity, which is minimal if γ is a geodesic. Before moving on, lets quickly review the proof of this statement.

proof: Geodesics minimize the distance on manifold. Functional of distance is

$$s = \int_0^{T_f} \sqrt{g_{\mu\nu} d\lambda^\mu d\lambda^\nu} = \int_0^{T_f} \sqrt{g_{\mu\nu} \frac{d\lambda^\mu}{dt} \frac{d\lambda^\nu}{dt}} dt =: \int_0^{T_f} \mathcal{L}(t, \lambda^\mu, \dot{\lambda}^\mu) dt \quad (6.2)$$

for

$$\mathcal{L} = \sqrt{g_{\mu\nu} \dot{\lambda}^\mu \dot{\lambda}^\nu}. \quad (6.3)$$

Using Euler-Lagrange equations

$$\frac{d\mathcal{L}}{d\lambda^\mu} - \frac{d}{dt} \frac{d\mathcal{L}}{d\dot{\lambda}^\mu} = 0, \quad (6.4)$$

we get for $g_{\mu\nu} = g_{\mu\nu}(\lambda^\mu)$ second order differential equation

$$\ddot{\lambda}^\mu + \Gamma^\mu_{\alpha\beta} \dot{\lambda}^\alpha \dot{\lambda}^\beta = 0 \quad \Gamma^\mu_{\alpha\beta} = \frac{1}{2} g^{\mu\kappa} (g_{\kappa\alpha,\beta} + g_{\kappa\beta,\alpha} - g_{\beta\alpha,\kappa}), \quad (6.5)$$

which is the Geodesic equation. \square

6.1 Minimizing the energy variance

The driving can be restricted to the ground state manifold only in approximation, such that the excited parts of wave-function can be neglected in every step. From Bukov et al. [2019], we have the following theorem.

Theorem 8. *For any fast-forward Hamiltonian¹ $\hat{H}(\lambda(t))$ driven along one dimensional path $\lambda : \mathbb{R} \mapsto \mathbb{R}$ using time t as parametrization, there exist driving speed, for which the fidelity is close to one, $F(t) \approx 1 \forall t \in [0, T_f]$, and the energy fluctuations δE^2 , averaged along the path, are larger than the geodesic length l_λ*

$$\int_0^T \sqrt{\delta E^2(t)} dt =: l_t \geq l_\lambda := \int_{\lambda_i}^{\lambda_f} \sqrt{g_{\lambda\lambda} d\lambda d\lambda} = \int_0^T \sqrt{g_{\lambda\lambda}} \frac{d\lambda}{dt} dt. \quad (6.6)$$

The length l_λ is defined in parametric space (with metric tensor $g_{\lambda\lambda}$) and is generally larger than the distance between wave functions, so called the absolute geodesic, defined with $G_{\mu\nu}$. From its definition, we can see that it corresponds to the metric tensor as we use it.

The energy variance is

$$\delta E^2 := \langle o(t) | \hat{H}(t)^2 | o(t) \rangle - \langle o(t) | \hat{H}(t) | o(t) \rangle^2 = \langle \partial_t(t) | \partial_t o(t) \rangle_c = G_{tt}, \quad (6.7)$$

where in second step the Schrödinger equation was used. The Metric tensor in parametric space is defined as

$$g_{\lambda\lambda} := \langle \partial_\lambda o(t) | \partial_\lambda o(t) \rangle_c \quad (6.8)$$

Proof.

$$\delta E^2 \equiv \langle o(t) | \hat{H}(t)^2 | o(t) \rangle_c = \dot{\lambda}^2 G_{\lambda\lambda} + \mathcal{O}(\dot{\lambda}^4), \quad (6.9)$$

where $\mathcal{O}(\dot{\lambda}^4)$ needs to be positive for any real-valued Hamiltonian. This comes from the fact, that it has instantaneous time-reversal symmetry. \square

The conjecture can be extended to an arbitrary dimensional path. The main problem of this conjecture is the statement *close unit fidelity protocol*. It is not clear how good the approximation need to be. This makes the statement much weaker, because it says: *For any driving, there exist driving speed for which the energy variance will be minimized on geodesics.*

6.2 Transport using quenches

Unifying the ground states $|o(\lambda)\rangle$ over all points $\lambda \in \mathcal{U}$ in the parameter space, we get the ground state manifold. Here the fidelity f and distance s are defined

$$ds^2 = 1 - F = 1 - |\langle o(\lambda + \delta\lambda) | o(\lambda) \rangle|^2. \quad (6.10)$$

The final fidelity of transport on \mathcal{M} is then

$$F = \iint_{\gamma(t)} g_{\mu\nu} d\lambda^\mu d\lambda^\nu = \int_{t_i}^{t_f} \underbrace{\int_{t_i}^\tau g_{\mu\nu} \frac{d\lambda^\mu}{dt} \frac{d\lambda^\nu}{dt} dt d\tau}_{\mathcal{L}(\lambda^\mu, \dot{\lambda}^\mu, \tau)}. \quad (6.11)$$

¹The system is driven to the target state in some fixed time.

Using Euler-Lagrange equations for time-independent $g_{\mu\nu} = g_{\mu\nu}(\lambda^\mu)$, leads to

$$\int_{t_i}^{\tau} \left[g_{\mu\nu,\kappa} \dot{\lambda}^\mu \dot{\lambda}^\nu - \frac{d}{dt} \left[g_{\mu\nu} (\delta_\kappa^\mu \dot{\lambda}^\nu + \dot{\lambda}^\mu \delta_\kappa^\nu) \right] \right] dt = 0, \quad (6.12)$$

which needs to be zero for integration over any subset (t_i, τ) . This can be achieved for any path only if the integrand itself is zero, which happens if the geodesic equation is satisfied.

The fidelity F measures transition probability between two eigenstates, $|\psi_1\rangle$, $|\psi_2\rangle$, of two different Hamiltonians (in our case, of one Hamiltonian with two different values of driving parameter $\boldsymbol{\lambda}_1, \boldsymbol{\lambda}_2$). Those two states belong to the same Fiber space $\mathcal{PH}(\boldsymbol{\lambda}) \times \mathcal{U}$ from which the coefficients (index of energy state; $\boldsymbol{\lambda} \in (\mathbb{Z}, \mathbb{R}^n)$) are taken. Because $\mathcal{PH}(\boldsymbol{\lambda})$ are canonically isomorphic for $\forall \boldsymbol{\lambda} \in \mathcal{U}$, there is no problem in parallel transport from one space to another, which is needed for evaluating the braket $\langle \psi(\boldsymbol{\lambda}_1) | \psi(\boldsymbol{\lambda}_2) \rangle$. This is important notice, because the integration in braket can be performed only if both elements belong to the same space.

The distance minimization runs into some interpretation problems. On one hand, minimization of the distance is equivalent to maximization of the sum of infinitesimal fidelities along the path (we say we *maximize the fidelity along the path*). On the other hand we are using only ground states in every step of the transport, therefore defining the fidelity to be one. There are actually two ways out of this confusion. *Perturbed adiabatic driving* and *Transport using quenches*.

Closed adiabatic driving

In the first case, we imagine at every point of transport, that the fidelity is small enough, that for some small parameters $\delta_i \in \mathbb{C}$, we can write the transport over distance ds in eigenbasis at time $t = 0$, as

$$|o(\boldsymbol{\lambda}_i)\rangle \equiv \begin{pmatrix} Z_0(\boldsymbol{\lambda}_i) \\ 0 \\ \vdots \\ 0 \end{pmatrix} \xrightarrow{\text{transport } ds} |o(\boldsymbol{\lambda}_i + \delta\boldsymbol{\lambda})\rangle \equiv \begin{pmatrix} Z_0(\boldsymbol{\lambda}_i + \delta\boldsymbol{\lambda}) \\ 0 \\ \vdots \\ 0 \end{pmatrix} + \underbrace{\begin{pmatrix} 0 \\ \delta_1(\boldsymbol{\lambda}_i + \delta\boldsymbol{\lambda}) \\ \vdots \\ \delta_n(\boldsymbol{\lambda}_i + \delta\boldsymbol{\lambda}) \end{pmatrix}}_{\Delta(\boldsymbol{\lambda}_i + \delta\boldsymbol{\lambda})},$$

where the last term is neglected, because

$$\langle \Delta(\boldsymbol{\lambda}) | o(\boldsymbol{\lambda} + \delta\boldsymbol{\lambda}) \rangle \approx 0.$$

This might have interesting implication for slow transports, or small distance transports. For slow transports, this condition is hardly fulfilled, because one needs to neglect the sum of many of these terms. For example when some slow thermalization is considered during transport. The easier way would be to reset the state into the ground-state, when the fidelity gets too far from 1. This can be achieved by projecting the state $|\psi(t)\rangle$ to the ground state $|0(t)\rangle$ periodically, such that every time the fidelity is almost one. These small jumps are sometimes called *quenches*. Let's see the mathematics behind this idea.

If we imagine $\delta\boldsymbol{\lambda}$ to be finite (not infinitely small, as the notation suggests), the *transport* means *doing a sequence of quenches and measuring the system after*

every quench. This leads to the *quantum Zeno effect*. In this case it can be shown directly by splitting the distance s on parametric space \mathcal{U} to N equal pieces. The fidelity for N splits will then be

$$F(N) = (1 - \Delta s)^N = \left(1 - \left(\frac{s}{N}\right)^2\right)^N \xrightarrow{N \rightarrow \infty} 1, \quad (6.13)$$

meaning the consequent measurements on the system leads to collapse to the instantaneous eigenstate and the adiabatic condition for transport holds ($F = 1$).

Such measurements can be achieved by fast thermalization of the system. If the finite speed thermalization with $N = T/\tau$ for the mean time between two measurements τ , we get

$$\begin{aligned} \log f(N) &= N \log \left(1 - \left(\frac{s}{N}\right)^2\right) = -\frac{s^2}{N} + o\left(\frac{s^4}{n^3}\right) \\ f(N) &= \exp\left(-s^2 \frac{\tau}{T} - \frac{s^4}{2N^3} \dots\right) = \exp\left(-s^2 \frac{\tau}{T}\right) \left(1 + o\left(\frac{s^4}{N^3}\right)\right) \end{aligned} \quad (6.14)$$

Some notion of the space of our Hamiltonian can be seen by quenching from $(\lambda_i; \chi_i) = (0; 0)$ to $(\lambda; \chi)$ in Figure 6.1.

In Figure 6.2, we can see equidistant points, meaning $\int_a^b ds = \text{const}$ between every two neighboring points on ground state manifold geodesics. One can see that if the system is measured periodically, the quenches jump smaller distances when closer to a point of degeneracy. Decreasing time step Δt has no effect on the relative fidelity of quenches during the evolution but has an effect on their absolute fidelity. As one would expect from quantum Zeno effect, when $\Delta t \rightarrow 0$, the transport becomes adiabatic, and the fidelity at any time will become 1. See that the shape of the curves looks similar in the columns, but their magnitude decreases.

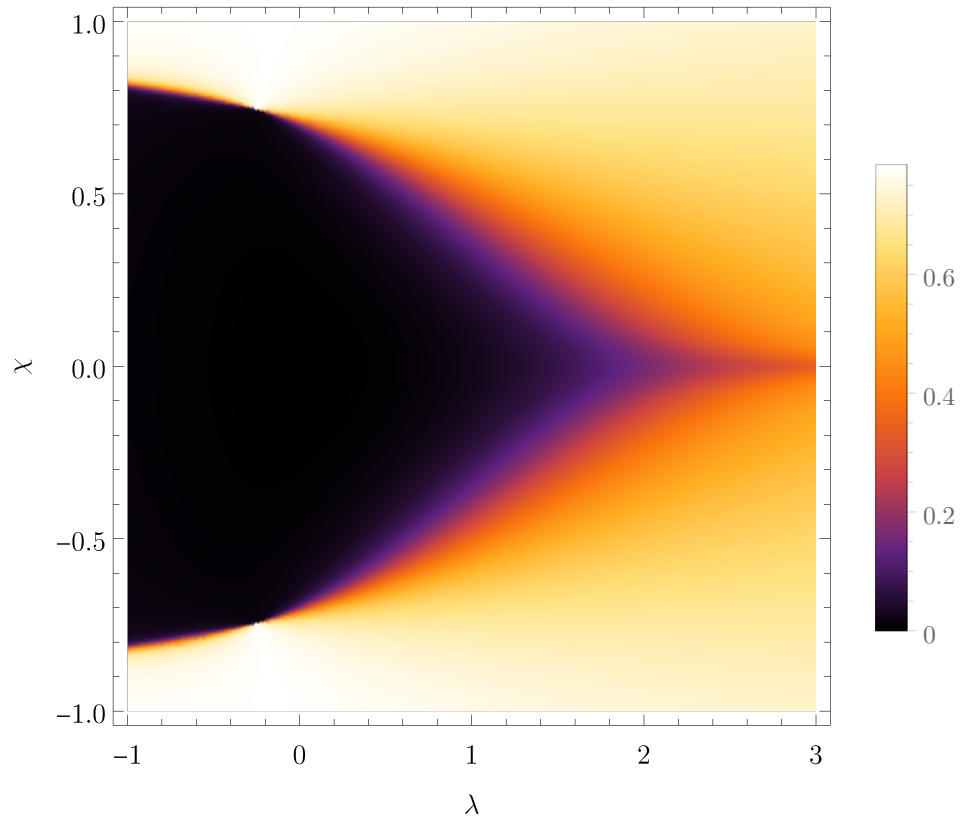


Figure 6.1: Arctangens of the fidelity of quench from $(\lambda_i; \chi_i) = (0; 0)$ to the coordinate $(\lambda; \chi)$.

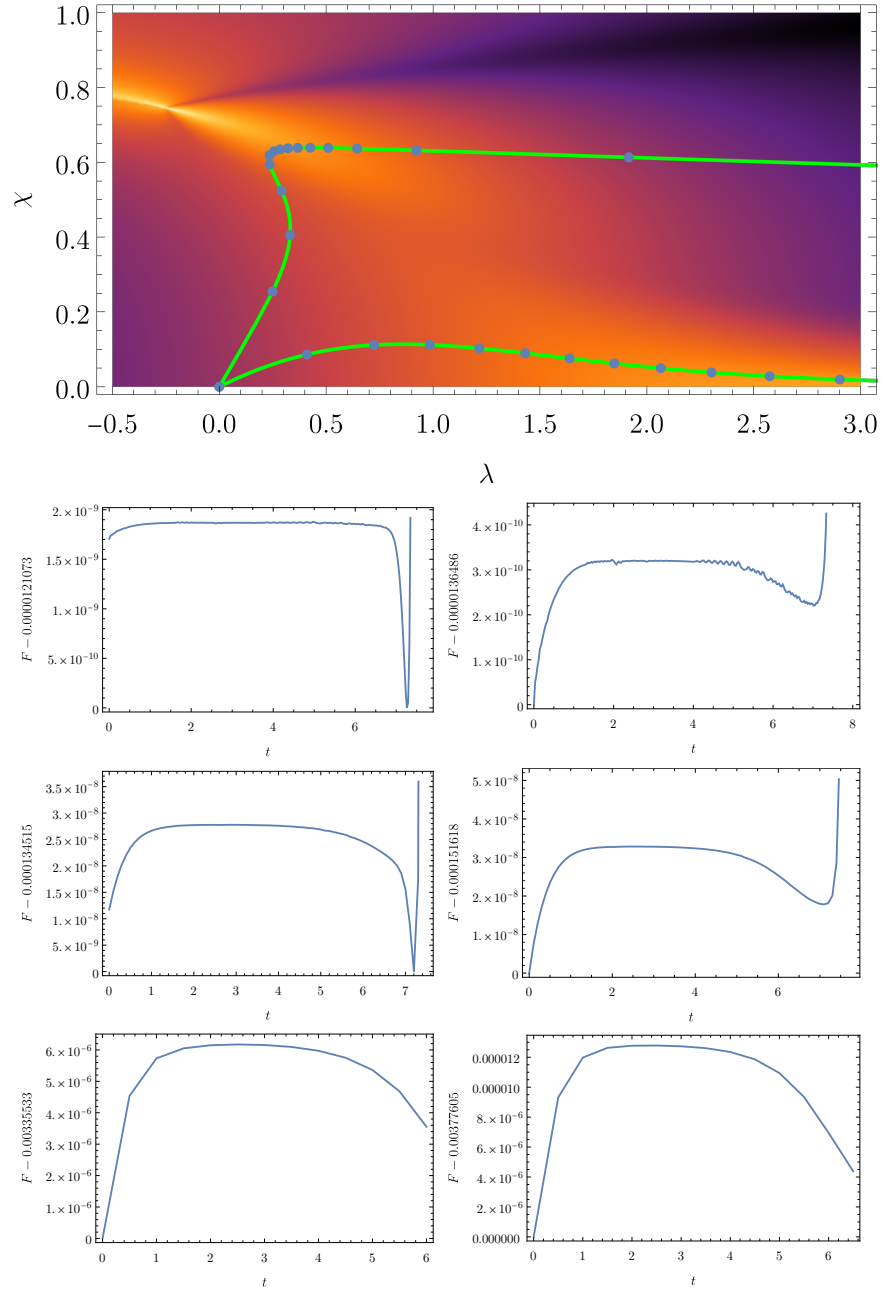


Figure 6.2: Fidelity for sequential quenches along geodesics (see green lines on top). Left (right) column corresponds to lower (upper) geodesic. Time steps from top are $\Delta t \in \{0.03, 0.1, 0.5\}$. Time difference between points in the plot on top is $\Delta t = 0.5$.

Conclusion

geodesics Most stable curves for counterdiabatic driving...this is like: "what if?", I have no idea

check all

Bibliography

- Abhay Ashtekar and Troy A. Schilling. Geometry of quantum mechanics. In *AIP Conference Proceedings*, volume 342, pages 471–478, Cancun (Mexico), 1995. AIP. doi: 10.1063/1.48786. URL <http://aip.scitation.org/doi/abs/10.1063/1.48786>. ISSN: 0094243X.
- Abhay Ashtekar and Troy A. Schilling. Geometrical Formulation of Quantum Mechanics. *arXiv:gr-qc/9706069*, June 1997. URL <http://arxiv.org/abs/gr-qc/9706069>. arXiv: gr-qc/9706069.
- M. V. Berry. Quantal phase factors accompanying adiabatic changes. *Proc. R. Soc. Lond. A*, 392(1802):45–57, March 1984. URL <http://rspa.royalsocietypublishing.org/content/392/1802/45>.
- M V Berry. Transitionless quantum driving. *Journal of Physics A: Mathematical and Theoretical*, 42(36):365303, aug 2009. doi: 10.1088/1751-8113/42/36/365303. URL <https://doi.org/10.1088/1751-8113/42/36/365303>.
- Michael V. Berry. The quantum phase, five years after' in 'Geometric Phases in Physics'. *A Shapere, F Wilczek. (World Scientific) 7-28*, 1989.
- Marin Bukov, Dries Sels, and Anatoli Polkovnikov. Geometric Speed Limit of Accessible Many-Body State Preparation. *Physical Review X*, 9(1):011034, feb 2019. ISSN 2160-3308. doi: 10.1103/PhysRevX.9.011034. URL <https://doi.org/10.1103/PhysRevX.9.011034><https://link.aps.org/doi/10.1103/PhysRevX.9.011034>.
- Ran Cheng. Quantum Geometric Tensor (Fubini-Study Metric) in Simple Quantum System: A pedagogical Introduction. *arXiv:1012.1337 [math-ph, physics:quant-ph]*, April 2013. URL <http://arxiv.org/abs/1012.1337>. arXiv: 1012.1337.
- Marián Fecko. *Differential Geometry and Lie Groups for Physicists*. Cambridge University Press, 2006. doi: 10.1017/CBO9780511755590.
- C. Gorodski. *An introduction to Riemannian geometry*. 2012. URL <https://www.ime.usp.br/~gorodski/teaching/mat5771-2016/gorodski-riem-geom-2012.pdf>. Preliminary version.
- Daniel Gutiérrez-Ruiz, Diego Gonzalez, Jorge Chávez-Carlos, Jorge G. Hirsch, and J. David Vergara. Quantum geometric tensor and quantum phase transitions in the lipkin-meshkov-glick model. *Phys. Rev. B*, 103:174104, May 2021. doi: 10.1103/PhysRevB.103.174104. URL <https://link.aps.org/doi/10.1103/PhysRevB.103.174104>.
- Michael Kolodrubetz, Dries Sels, Pankaj Mehta, and Anatoli Polkovnikov. Geometry and non-adiabatic response in quantum and classical systems. *Physics Reports*, 697:1–87, 2017. ISSN 0370-1573. doi: <https://doi.org/10.1016/j.physrep.2017.07.001>. URL <https://www.sciencedirect.com/science/article/pii/S0370157317301989>. Geometry and non-adiabatic response in quantum and classical systems.

W. Tu Loring. *Differential Geometry*. Springer International Publishing, 2017.
doi: 10.1007/978-3-319-55084-8.

Mathieu Molitor. Exponential families, Kahler geometry and quantum mechanics. *Journal of Geometry and Physics*, 70:54–80, August 2013. ISSN 03930440. doi: 10.1016/j.geomphys.2013.03.015. URL <http://arxiv.org/abs/1203.2056>. arXiv: 1203.2056.

Hiroki Nakamura. *Nonadiabatic transition: concepts, basic theories and applications*. World Scientific, Hackensack, New Jersey, second edition edition, 2012. ISBN 978-981-4329-77-4.

P. Petersen. *Riemannian Geometry*. Springer Verlag, 1998. ISBN 978-0-387-29403-2.

Gerardo Ortiz Rigolin, Gustavo. Beyond the quantum adiabatic approximation: Adiabatic perturbation theory. *Physical Review A* 78, no. 5 (November 18, 2008): 052508, 2008. URL <https://doi.org/10.1103/PhysRevA.78.052508>.

J. R. R. Tolkien. *The Lord of the Rings*. Folio Society, 1977. ISBN 978-0458907502.

List of Figures

1.1	stolen from wiki, redraw in tikz	9
2.1	Base manifold $\mathcal{U} \subset \mathbb{R}^d$ is visualized as a line. From every point λ there is constructed one Hilbert space $\mathcal{H}(\lambda)$ as a fiber. The union of all these fibers is full Hilbert space \mathcal{H}_{full}	12
2.2	For every λ we have the Hilbert space $\mathcal{H}(\lambda)$ containing all states $e^{i\varphi} \psi(\lambda)\rangle$. Choosing the phase φ fixes some projective Hilbert space \mathcal{PH} .	13
2.3	From the full Hilbert space we identified eigenstates. First was caused by the fiber structure and separates different Hilbert spaces $\hat{\mathcal{H}}(\lambda)$. Newly introduced sectioning correspond to eigenstates of individual Hamiltonians and creates Riemannian manifolds \mathcal{M}_s .	14
2.4	Geometrical intuition to transport on fiber manifold sections \mathcal{M}_s .	15
2.5	Parallel transport around some closed curve C . The eigenstate from \mathcal{PM}_s can be transported to another eigenstate in \mathcal{M}_s . The anholonomy represents their difference in a gauge direction.	16
4.1	Driving along the geodesic. λ_i and λ_f are initial resp. final parameters. Density plot shows the difference between Hamiltonian eigenvalues.	35
4.2	Infidelity in time for final time $T_f = 1$ for geodesical driving.	37
4.3	Final infidelity dependence on final time T_f for geodesical driving.	37
4.4	Infidelity dependence on final time in logarithmic scale. We can observe difference in numerical precision of both methods in the height of spikes. As we will see later, the spikes should go to zero, thus analytical formula has better numerical precision.	37
4.5	Rescaled final infidelity $T_s := 2sT_f$ dependence on final time. Red points mark the condition $F = 1$.	38
4.6	Fidelity dependence on time and final time in log-log scale. Note that only $t < T_f$ has physical meaning.	38
4.7	Energy variance for geodesical driving protocol.	39
4.8	Driving along the linear path. $\lambda_i = (-10; 1)$ and $\lambda_f = (10; 1)$ are initial resp. final parameters. Density plot shows the difference between Hamiltonian eigenvalues.	40
4.9	Infidelity in time for three final times $T_f \in \{1, 5, 20\}$ for the linear driving defined in 4.35.	41
4.10	Value of first element of the ground state vector $\alpha \equiv 0(t)\rangle^1$ during linear driving.	42
4.11	Final infidelity as a function of T_f with zoom on transitional part.	43
4.12	Final infidelity as a function of T_f in log-log scale wit linear scaled plot inserted.	44
4.13	Final infidelity as a function of Δ and T_f and its three regimes. Zoomed boundary between them can be seen on 4.14.	44
4.14	Fine structure of the boundary between fast-driving and adiabatic regimes of final infidelity.	45

4.15	Final infidelity as a function of t for fast-driving regime, $T_f = 80 < T_c$	45
4.16	Final infidelity as a function of t for close-adiabatic regime. $T_f = 170 > T_c$	46
4.17	Fidelity as a function of driving final time, approximated by the sum (green) of Landau-Zener (red, dashed) and APT (purple, dashed)	47
4.18	Fidelity dependence for linear driving with $\Delta = 1$. Black line marks $t = T_f$, dashed black line $t = T_f/2$ and purple dashed line is the approximate value of T_c . Blue lines marks driving from Fig. 4.15, 4.16, visualizing the final times of the driving.	48
4.19	Energy variance for $\Delta_{sc} = 0.2$ for linear driving. Note that only $t < T_f$ has physical meaning.	49
5.1	Energy for the case $N = 3$, section $\lambda = 1$	51
5.2	Energy for the case $N = 3$, section $\chi = 1$	52
5.3	Arctangent of the metric tensor elements for the case $N = 3$ in the parametric space. From the top: $\arctan(g_{11})$, $\arctan(g_{12}) = \arctan(g_{21})$, $\arctan(g_{22})$	53
5.4	Ground state metric tensor determinant in a parametric space for $N = 3$.	54
5.5	Arctangent of the ground state Christoffel symbols for the case $N = 3$. First row from left: $\arctan(\Gamma_{111})$, $\arctan(\Gamma_{121})$, $\arctan(\Gamma_{122})$. Second row from left: $\arctan(\Gamma_{211})$, $\arctan(\Gamma_{221})$, $\arctan(\Gamma_{222})$.	54
5.6	Arctangent of Ricci curvature for the case $N = 3$. increase the resolution	55
5.7	Ricci's curvature sections for three different λ .	56
5.8	Geodesics for the case $N = 3$ starting from $(\lambda_i; \chi_i) = (0; 0)$ with $(\lambda'_i; \chi'_i) = (\cos \theta; \sin \theta)$, parametrized by angle $\theta \in [-0.63; 0.63]$, $\theta \in [\pi - 0.225; \pi + 0.225]$, with step $\Delta\theta = 0.01$. Blue line marks the high Ricci curvature gap.	57
5.9	Comparing geodesics with repulsing (blue) and attracting (red) metric tensor divergence in the spherically symmetrical space.	57
5.10	Energy differences between neighboring energy levels for $N = 5$. First row: $E_1 - E_0$, second row: $E_2 - E_1$, $E_3 - E_2$, third row: $E_4 - E_3$, $E_5 - E_4$. Spectra degeneracies are marked with blue cross.	59
5.11	Metric tensor determinant for the case $N = 5$.	60
5.12	Geodesics for the case $N = 5$, starting from the point $(1; 0)$. The numerics around the singularity breaks down, but the solution is close to the drawn one, i.e. they will pass close to the singularity and continue to the left.	61
5.13	First order phase transition, the Separatrix (red), second order transition (blue point) compared to minimum between the ground state and first excited state in $N=3$ case (black, dashed).	62
5.14	Energy spectrum as function of χ , for $\lambda = 1$ and $N = 10$.	63
5.15	Energy spectrum as a function of λ , for $\chi = 1$ and $N = 10$.	63

5.16	Spectrum degeneracies between E_0 and E_1 . Hamiltonian dimensions are 1,3,5,7 in the first column and 2,4,6,8 in the second column. Black crosses mark most left-wise and right-wise singularity and the background corresponds to the metric tensor determinant. Other singularities are also well visible in the determinant.	65
6.1	Arctangens of the fidelity of quench from $(\lambda_i; \chi_i) = (0; 0)$ to the coordinate $(\lambda; \chi)$	70
6.2	Fidelity for sequential quenches along geodesics (see green lines on top). Left (right) column corresponds to lower (upper) geodesic. Time steps from top are $\Delta t \in \{0.03, 0.1, 0.5\}$. Time difference between points in the plot on top is $\Delta t = 0.5$	71

A. Eigenvalues for Lipkin-Meshkov Glick model

Eigenvalues for $N = 3$ case of Lipkin-Meshkov Glick model are

$$E_0 = \frac{1}{12} \left(G - F - \frac{\sqrt{D - E}}{2} \right) \quad (\text{A.1})$$

$$E_1 = \frac{1}{12} \left(G - F + \frac{\sqrt{D - E}}{2} \right) \quad (\text{A.2})$$

$$E_2 = \frac{1}{12} \left(G + F - \frac{\sqrt{D + E}}{2} \right) \quad (\text{A.3})$$

$$E_3 = \frac{1}{12} \left(G + F + \frac{\sqrt{D + E}}{2} \right), \quad (\text{A.4})$$

for

$$\begin{aligned} A = & 16\sqrt[3]{2} \left(64\lambda^6 - 192\lambda^5\chi^2 + 24\lambda^4 (52\chi^4 - 93\chi^2 + 36) \right. \\ & - 8\lambda^3 (29\chi^4 + 414\chi^2 - 513)\chi^2 \\ & + 6\lambda^2 (1225\chi^8 - 10053\chi^6 + 17595\chi^4 - 10557\chi^2 + 1377) \\ & + \left((64\lambda^6 + 864\lambda^4 + 8262\lambda^2 + 3(818\lambda - 27285)\chi^{10} \right. \\ & + 6(\lambda(1225\lambda - 3198) + 27108)\chi^8 \\ & - (2\lambda(\lambda(116\lambda + 30159) - 89073) + 326727)\chi^6 \\ & + 6(\lambda(\lambda(8\lambda(26\lambda - 69) + 17595) - 42660) + 51516)\chi^4 \\ & - 3(2\lambda(\lambda(4\lambda(\lambda(8\lambda + 93) - 171) + 10557) - 16119) + 36207)\chi^2 \quad (\text{A.5}) \\ & \left. + 24013\chi^{12} + 25515 \right)^2 \\ & - \left((16\lambda^4 + 144\lambda^2 + 2(74\lambda - 1185)\chi^6 + 3(4\lambda(16\lambda - 77) + 1329)\chi^4 \right. \\ & - 2(2\lambda(\lambda(8\lambda + 93) - 207) + 1161)\chi^2 + 889\chi^8 + 1053 \left. \right)^{1/2} \\ & + 6\lambda(409\chi^8 - 3198\chi^6 + 29691\chi^4 - 42660\chi^2 + 16119)\chi^2 + 24013\chi^{12} \\ & - 81855\chi^{10} + 162648\chi^8 - 326727\chi^6 + 309096\chi^4 \\ & \left. - 108621\chi^2 + 25515 \right)^{1/3} \end{aligned}$$

$$\begin{aligned} B = & \frac{256\sqrt[3]{2}}{3A} \left(16\lambda^4 + 144\lambda^2 + 2(74\lambda - 1185)\chi^6 + 3(4\lambda(16\lambda - 77) \right. \\ & \left. + 1329)\chi^4 - 2(2\lambda(\lambda(8\lambda + 93) - 207) + 1161)\chi^2 + 889\chi^8 + 1053 \right) \quad (\text{A.6}) \end{aligned}$$

$$C = 4\sqrt{\frac{A}{3\sqrt[3]{2}} + B + \frac{16}{3}(4\lambda^2 - (4\lambda + 33)\chi^2 + 49\chi^4 + 45)} \quad (\text{A.7})$$

$$D = -\frac{A}{3\sqrt[3]{2}} - B - \frac{8}{3} \left(59\lambda^2 + 436\lambda\chi^2 + 392\chi^4 + 132\chi^2 - 180 \right) \\ + 8 \left(5\lambda + 14\chi^2 \right)^2 \quad (A.8)$$

$$E = \frac{9216}{C} \left((\lambda - 1)\chi^4 - 4(\lambda - 1)\chi^2 + \lambda - 2\chi^6 \right) \\ F = \frac{1}{2} \sqrt{\frac{A}{3\sqrt[3]{2}} + B + \frac{16}{3} (4\lambda^2 - (4\lambda + 33)\chi^2 + 49\chi^4 + 45)} \quad (A.9) \\ G = -5\lambda - 14\chi^2$$

B. Attachments

B.1 First Attachment

Mathematica code for metric tensor and geodesics??